INVESTIGATION OF AUTOPHAGY RELATED MARKERS IN BRAIN TISSUE OF EARLY-ONSET TAY - SACHS DISEASE MOUSE MODELS

A Thesis Submitted to
The Graduate School of Engineering and Sciences of
İzmir Institute of Technology
in Partial Fulfillment of the Requirements for the Degree of

MASTER OF SCIENCE

in Molecular Biology and Genetics

by
Nurselin ATEŞ

December 2018
İZMİR

We approve the thesis of **Nurselin ATEŞ**

Examining Committee Members

Prof. Dr. Volkan SEYRANTEPE
Department of Molecular Biology and Genetics, İzmir Institute of Technology

Assist. Prof. Dr. Şükrü GÜLEÇ
Department of Molecular Biology and Genetics, İzmir Institute of Technology

Prof. Dr. Petek BALLAR KIRMIZIBAYRAK
Department of Basic Pharmaceutical Sciences, Ege University

13 December 2018

Prof. Dr. Volkan SEYRANTEPE
Supervisor, Department of Molecular Biology and Genetics,
İzmir Institute of Technology

Prof. Dr. Volkan SEYRANTEPE
Head of Department of Molecular
Biology and Genetics

Prof. Dr. Aysun SOFUOĞLU
Dean of Graduate School of
Engineering and Sciences

ACKNOWLEDGMENTS

I would first like to express my deepest gratitude to my supervisor Prof. Dr. Volkan SEYRANTEPE for his guidance, encouragement, patience, understanding, support and extensive knowledge that helped me throughout my studies and my thesis writing.

I would like to express my special thanks to Prof. Dr. Petek BALLAR KIRMIZIBAYRAK and Assist. Prof. Dr. Şükrü GÜLEÇ for being my committee members and also for their attention and advice. I would also like to thank to Assoc. Dr. Ayten NALBANT for her contribution and advice.

I am thankful to The Scientific and Technological Research Council of Turkey (TUBITAK) (215Z083) for their financial support of this project and for providing me scholarship.

I am also grateful to my co-workers Berkay DAĞALP, Tuğçe ŞENGÜL, Melike CAN and Hande BASIRLI for their support, assistance, sincere help and kindness during the thesis project. I especially thank to Secil AKYILDIZ DEMIR and Zehra Kevser TIMUR who mentored me through my graduate studies. I am also grateful to undergraduate members of Seyrantepe Laboratory.

At last but not least, I am deeply grateful to my father Kemal ATEŞ, my mother Hanife ATEŞ and my sisters Gülşah ATEŞ and İrem ATEŞ for their infinite love, motivation, belief, encouragement and support throughout my life and my education. Without their support, I will not be able to be here.

ABSTRACT

INVESTIGATION OF AUTOPHAGY RELATED MARKERS IN BRAIN TISSUE OF EARLY-ONSET TAY - SACHS DISEASE MOUSE MODELS

Tay-Sachs disease is an autosomal recessively inherited lysosomal storage disorder that mainly affects the central nervous system. It is caused by mutations on the HEXA gene encoding α-subunit of β-Hexosaminidase A enzyme. The enzyme normally catalyses GM2 to GM3 conversion but when it is absent or dysfunctional the GM2 degradation is interrupted. Progressive accumulation of the undegraded GM2 ganglioside in neurons causes neurodegeneration and eventual death for the patient. The *Hexa*$^{-/-}$ mice generated as Tay-Sachs model was nearly normal and a bypass mechanism mediated by a sialidase was discovered. Neu3 sialidase involvement in ganglioside degradation in the Tay-Sachs disease pathology was reported and the *Hexa*$^{-/-}$*Neu3*$^{-/-}$ mice was observed to mimic the neuropathologic and clinical phenotype of the disease. Therefore, it can be used as early-onset-Tay-Sachs disease mouse model. Lysosomal storage diseases have been reported as disorders of autophagy as the lysosomal accumulation expected to affects the autophagical-lysosomal pathway in one way or another. In the concept of our study comparative analysis of *WT, Hexa*$^{-/-}$*,Neu3*$^{-/-}$ and *Hexa*$^{-/-}$ *Neu3*$^{-/-}$ mice provided the information that early-onset Tay-Sachs disease model exhibit impairment in autophagic flux and secondary accumulation of autophagic components. The effect of abnormal GM2 and this secondary accumulation on apoptotic regulators and trigger factors were also investigated. In the light of our study, impairment in autophagic flux, increased oxidative stress and ER-stress are involved in the disease pathology of early-onset Tay-Sachs disease mouse model.

ÖZET

ERKEN BAŞLANGIÇLI TAY-SACHS HASTALIĞI FARE MODELLERİNİN BEYİN DOKUSUNDA OTOFAJİYLE İLİŞKİLİ BELİRTEÇLERİN ARAŞTIRILMASI

Tay-Sachs hastalığı merkezi sinir sistemini etkileyen, ölümle sonuçlanan ve otozomal resesif bir şekilde aktarılan bir lizozomal depo hastalığıdır. GM2 gangliositinin yıkılmasını sağlayan β-Hexosaminidase A enziminin α-subunitini kodlayan HEXA genindeki bozukluk GM2 gangliositinin sinir hücrelerinde birikimine ve hastalık fenotipinin görülmesine sebep olur. Hasta bebekler doğduklarında normal olsalar da ilerleyici GM2 birikimi; sinir hücrelerinde artan ölüme, zihinsel ve motor fonksiyonlarında bozulmaya ve 2-4 yaşlarında da ölüme neden olur. Hastalığın ilk fare modeli olarak oluşturulan *Hexa*$^{-/-}$ fareler, yeterince GM2 birikimi göstermeyip hastalık fenotipini taklit etmemişlerdir. Yakın zamanda erken başlangıçlı Tay-Sachs Hastalığı fare modeli olarak üretilen *Hexa*$^{-/-}$*Neu3*$^{-/-}$ fareler; Tay-Sachs hastalarında olduğu gibi, merkezi sinir sistemlerinde ilerleyici GM2 birikimi göstermiş ve hastalığın diğer patolojik özelliklerini de taklit etmiştir. Lizozomal depo hastalıklarının genel fenotipi olan lizozomlardaki anormal birikim otofajik-lizozomal yolağı da etkilemesi beklendiği ve bazı hastalıklarda gösterildiği için; lizozomal depo hastalıkları otofaji bozuklukları olarak da adlandırılmıştır. Bizim çalışmamız kapsamında *WT, Hexa*$^{-/-}$*, Neu3*$^{-/-}$ ve *Hexa*$^{-/-}$ *Neu3*$^{-/-}$ fareleri kullanılarak yapılan karşılaştırmalı analizler sonucunda; erken başlangıçlı Tay-Sachs hastalığı fare modelinde otofajik akışta bozulma olduğu ve otofajiyle alakalı proteinleril ikincil bir birikmeye sebep olduğu gösterilmiştir. Anormal GM2 ve bu ikincil birikiminin apoptotik düzenleyiciler ve tetikleyici faktörler üzerindeki etkisi de araştırılmıştır. Çalışmamız ışığında; erken başlangıçlı Tay-Sachs hastalığı fare modelinde otofajik akışta bozulma, artan oksidatif ve ER stresinin hastalık patolojisine etkisi olduğu tahmin edilmiştir.

Dedicated to my precious family...

TABLE OF CONTENTS

LIST OF FIGURES

LIST OF TABLES

CHAPTER 1

INTRODUCTION

1.1. Lysosomal Storage Diseases

Lysosomal storage disorders (LSDs) are a group of diseases in which lysosomal homeostasis is disturbed because of inherited gene mutations. The mutations mostly inherited in autosomal recessive manner but some are inherited by X-linked mutations (Platt et al., 2012; Boustany et al., 2013). They primarily caused by mutations in not only a lysosomal enzyme with and acid hydrolysis function but also non-enzymatic lysosomal proteins like transporters or hydrolase activators; deficiency or dysfunctionality of which lead to abnormal accumulation of macromolecular substrates; as they involve in the degradation of the macromolecules. This storage perturbs nervous system, eye, bone, muscle, and reticuloendothelial system; and eventually leads to cell death (Boustany et al., 2013).

Even if the incidence of LSDs is determined approximately 1:5000 live births (Fuller et al., 2006), when undiagnosed or misdiagnosed cases are considered the incidence level would be undoubtedly higher. Common trait of all LSDs is the accumulation of monomer or macromolecules in the organelles involved in the endosomal–autophagic–lysosomal system. Biochemical characterization of these accumulated substances provides determination of defective lysosomal enzymes or nonenzymatic proteins causing the pathology. (Platt, Boland, and van der Spoel 2012)

The symptoms depend on the disease of interest and age of onset of the disease. As some are diagnosed at birth (i.e. infantile GM1 gangliosidosis), others' symptoms may appear in late infancy or childhood. Even if most of the LSDs are appear in childhood, some can be diagnosed at adulthood (i.e. late-onset GM2 Gangliosidosis). The general symptoms include failure in development, visual disorders, organomegaly, morphologic disturbances, seizures and neuromotor regression. These neurological and motor complications progressively increases the morbidity and decreases the quality of life and eventually leads to death in most cases (Du et al. 2001).

Up to now there are 50 known LSDs in humans. Deficiencies of different proteins give rise to specific lysosomal storage diseases and they classified depending on the nature of the storage material (i.e. Sphingolipidosis, Oligosaccharidosis, Mucopolysaccharidoses etc.) (Table 1.1).

Table 1.1. Classification of common lysosomal storage disorders based on the storage molecule.

Classification	Disease	Storage Molecule
Mucopolysaccharidosis	Hurler Syndrome	Dermatan and heparan sulphate
	Sanflippo Syndrome	Heparan sulphate
Oligosaccharidosis	Mannosidosis	Mannose-containing oligosaccharides
	Sialidosis	Sialyloligosaccharides
Sphingolipidosis	Gaucher Disease type 2	Glucocerebrosidase
	Niemann-Pick type A&B	Sphingomyelin
	Krabbe Disease	Galactocerebroside
	GM1 Gangliosidosis	GM1 ganglioside
	GM2 Gangliosidosis	GM2 ganglioside

1.2.Gangliosides

Gangliosides sialic acid containing acidic glycosphingolipids that are component of cell membranes are extensively spread throughout body tissues(Sonnino et al., 2007). They are mainly expressed in nervous tissue and specifically found in plasma membrane of neural cells. Hence they are highly concentrated in grey matter of the brain as they make up 10-12% of neuronal membrane (Palmano et al., 2015). Gangliosides are extends into the extracellular space through their glycan group and embedded to the plasma membrane by their ceramide lipid moiety. They are mostly components of specific membrane microdomains called lipid rafts which are highly concentrated with cholesterol and sphingolipids and participate in regulation of signal transduction pathways depending on the protein and lipid composition of the raft. The interactions between these lipid rafts, gangliosides and membrane proteins involves in important cellular processes like cytokine and adhesion signal transduction and

membrane protein regulation. Their functions involve cell-cell recognition through their specific sialoglycan components, and cell adhesion, motility and growth through glycosynaptic microdomains (Palmano et al. 2015). Through signalling pathways; gangliosides also affects neural development and function, cell-cell recognition. They comprise most of (%75) the conjugated sialic acid in the brain and they provide important level of cell surface glycans in neural cells.

Gangliosides comprise of glycan attached ceramide core through a glycosidic linkage. Depending on the polysaccharaide combination of the glycan chains (glucose, galactose and N-acetylgalactosamine); gangliosides may contain 1 to 7 sialic acid residues and this diversity is characteristic feature of gangliosides. They particularly generated in endoplasmic reticulum and transferred to golgi apparatus for addition of carbohydrate moieties by specific glycosyl transferases. All gangliosides originates from lactosylceramide, except GM4 which is derived from galactosylceramide (Yu et al., 2011). In Figure 1.1. structure of GM2 ganglioside is shown.

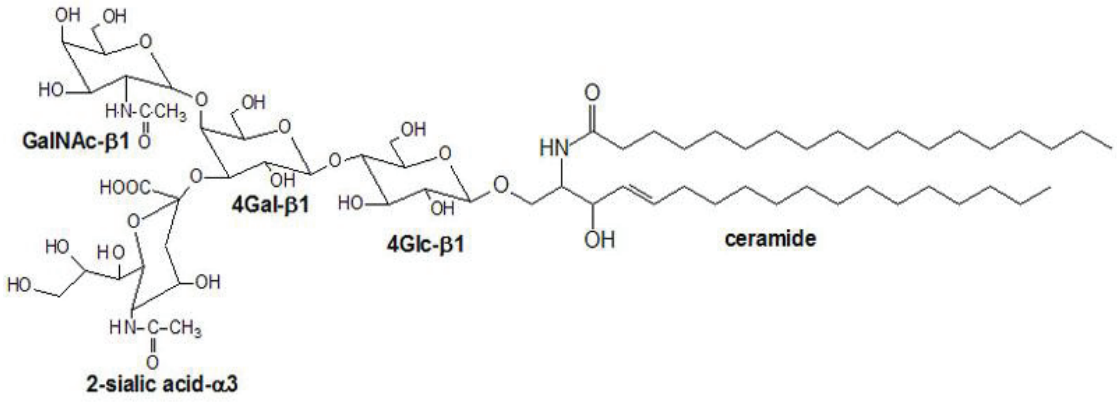

Figure 1.1. Structure of GM2 ganglioside

Brain gangliosides' expression levels and patterns during development are strongly differential (Yu et al., 2011). As the brain development proceeds, the amount of gangliosides and their sialylation degree increase. These complex brain gangliosides are mostly profound in neural cell membrane involving in axon-myelin interaction, Ca^{2+} homeostasis and wide-range of signalling pathways (Schnaar 2010; Ohmi et al. 2012).

1.3. Tay Sachs Disease

GM2 gangliosidosis are a group of severe lysosomal storage disorders that are inherited autosomal recessively and mainly affects the central nervous system of mostly children. The group consists of three different diseases as Tay-Sachs, Sandhoff and GM2-activator deficiency which are caused by mutations in HEXA, HEXB and GM2AP genes respectively. These genes encodes for α and β subunits and activator protein of β-N-acetylhexosaminidase enzyme. The enzyme normally catalyzes GM2 to GM3 conversion by removing N-acetylgalactosamine when all subunits and activator protein are properly functional and are able to form a complex (Gravel et al., 2001). However, when one of them absent or dysfunctional; the GM2 degradation is interrupted. The undegraded GM2 ganglioside is progressively accumulated especially in neurons and causes neurodegeneration at the end. As mentioned, GM2 is an intermediated ganglioside in complex brain ganglioside biosynthesis (Kolter and Sandhoff 1999). GM2, as well as the complex brain gangliosides are mostly abundant in neuronal cells; hence, the GM2 gangliosidosis mostly affects central nervous system of the patients. The babies with the disease are healthy at birth; however, progressive accumulation of GM2 results in increasing death of neurons, disruption in mental and motor functions and eventually death at 2-4 years of age. The three types of GM2 gangliosidosis are clinically similar to each other. Tay-Sachs disease refers to the early-onset type 1 GM2 gangliosidosis and it can also occur at juvenile or chronic form. The highest occurrence rate is among Ashkenazi Jews (Americo et al., 2010). The severity and onset time of the disease depends on the level of residual HEXA enzyme activity (Sandhoff et.al., 1983). The detrimental effect of the disease starts in early pregnancy but the baby with the disease appears healthy until 6 months of age and the development of the baby stalls. By two years of age; recurrent seizures, mental retardation, and loss of motor functions are experienced. As the disease progresses, the child eventually becomes blind, cognitively dysfunctional and paralyzed. Death is observed by the age of four because of the severely affected nervous system.

Tay-Sachs disease is most frequently occurring sphingolipidosis type with the incidence rate 1 in 3500 Ashkenazi Jews and in other population the incidence rate is 1 in 360000 (Rozenberg and Pereira 2001).

There is no available treatment for Tay-Sachs disease yet. Palliative care is the only option for patients. Enzyme replacement therapy and bone marrow transplantation were tried but did not provide beneficial results in infants with Tay-Sachs disease (Kaback 2001). Animal models are used for therapeutic approaches like stem cell transplantation however crossing through blood brain barrier creates an obstacle. Substrate deprivation therapy which has been proved to be effective in Gaucher disease (Cox et al. 2000) is in trial for late-onset Tay-Sachs disease (Platt and Butters 2000). The pharmacological chaperones which provide refolding and correct trafficking of mutant proteins may be beneficial for chronic forms of Tay-Sachs disease (Americo, Filho, and Shapiro 2010). Overall combination of different treatments may hold the most beneficial therapy for Tay-Sachs disease.

1.3.1. Tay Sachs Disease Mouse Model

The mouse models for GM2 gangliosidoses are generated by targeting *Hexa* and *Hexb* genes in mouse (Phaneuf et al. 1996; Yamanaka et al. 1994). HEXB knockout mice mimicked the neuropathological phenotype of the Sandhoff Disease however disruption of HEXA did not cause severe phenotype of early-onset neuropathological phenotype of Tay-Sachs disease. This unexpected result was explained by a bypass pathway in which sialidases in mice are able to remove sialic acid from GM2 and convert it to GA2 which is then degraded by the HexB (Sango et al. 1995; Yuziuk et al. 1998). Hence, $Hexa^{-/-}$ mice cannot be used as a model for human Tay-Sachs disease as it does not display abnormal accumulation of GM2 and other behavioral phenotype. Instead, the $Hexa^{-/-}$ mice exhibit late-onset mild phenotype of Tay-Sachs disease. $Hexa^{-/-}$ mice model exhibit inclusion bodies in lysosomes and GM2 accumulation in neurons but the analysis on brain and liver displayed that the accumulation was below threshold and not toxic. Moreover, it was demonstrated that GA2 ganglioside which is asialyted form of GM2 accumulates in low amounts in $Hexa^{-/-}$ mice model but not in human patients. In $Hexa^{-/-}$ mice model GM2 is catalyzed through metabolic bypass pathway in which it is degraded via GA2 instead of GM3 routed degradation. In the metabolic bypass pathway: removal of sialic acid in GM2 to generate GA2, is mediated by sialidases in mice and the GA2 ganglioside is further catalyzed into ceramide by

HexB enzyme (Phaneuf et al. 1996; Yamanaka et al. 1994). This metabolic bypass pathway provides mice to escape the disease over one year (Igdoura et al., 1999).

Sialidases (a.k.a neurominidases) catalyzes hydrolysis of non-reducing sialic acid linkages in several substrates like glycoproteins, glycolipids or oligosaccharides. In mammals sialidases are found in lysosome (NEU1), cytosol (NEU2), associated to plasma membrane (Neu3) and mitochondrial/-lysosomal/-intracellular membranes (NEU4). They involve in wide range of mechanisms including glycoconjugate metabolism (Monti et al. 2010).

To elucidate the major sialidase that mediates metabolic bypass pathway, firstly *Hexa*$^{-/-}$*Neu4*$^{-/-}$ mice generated; however, it resulted in relatively mild phenotype and NEU4 is determined as modifier gene (Seyrantepe et al. 2010). Then, *Hexa*$^{-/-}$*Neu3*$^{-/-}$ mice generated to identify whether the predominant sialidase catalyzing the bypass pathway is NEU3 or not. Neu3 sialidase was found to be the predominant enzyme mediating the bypass mechanism in mouse pathology of Tay-Sachs disease (Figure 1.2) and *Hexa*$^{-/-}$*Neu3*$^{-/-}$ mice is a useful mouse model for early-onset Tay-Sachs disease.

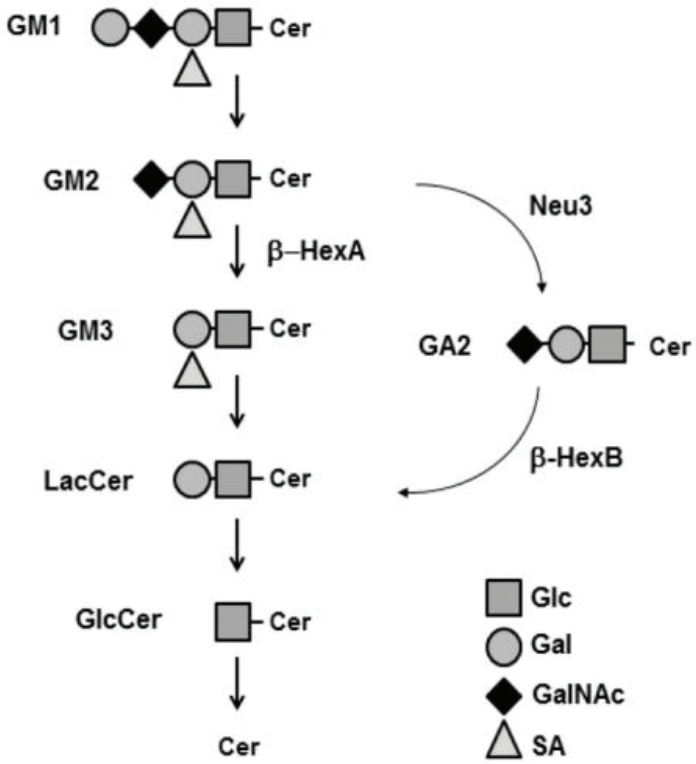

Figure 1.2. Schematic illustration of part of the degradation pathway of glycosphingolipids. NEU3 is determined as primary enzyme mediating

the metabolic bypass in the *Hexa*$^{-/-}$ mouse model (Source: Seyrantepe et al. 2018).

The disruption of both *Hexa* and *Neu3* genes resulted in blockage of ganglioside degradation pathway and abnormal accumulation of GM2 ganglioside in the brain of in *Hexa*$^{-/-}$*Neu3*$^{-/-}$ mice (Figure 1.3). Electron microscopic analysis revealed abnormally increased amount of lysosomes and ring-like structures in neuronal lysosomes of *Hexa*$^{-/-}$ *Neu3*$^{-/-}$ mice resembling human Tay-Sachs phenotype (Figure 1.4). Immunohistochemical analysis of glial fibrillary acidic protein (GFAP) revealed severe astrogliosis in *Hexa*$^{-/-}$*Neu3*$^{-/-}$ mice brain. The *Hexa*$^{-/-}$*Neu3*$^{-/-}$ mice displayed lethal early-onset phenotype of the disease when compared to late-onset mild phenotype (*Hexa*$^{-/-}$). Similar to human Tay-Sachs phenotype; tremors, ataxia and weakened hind limbs were observed in *Hexa*$^{-/-}$*Neu3*$^{-/-}$ mice. Moreover, growth impairment compared to their littermates was reported in in *Hexa*$^{-/-}$*Neu3*$^{-/-}$ mice and is another common feature with human Tay-Sachs patients. Sudden death following progressive neurodegeneration and neurobehavioral abnormalities occurred at high rate in *Hexa*$^{-/-}$*Neu3*$^{-/-}$ mice resembling *Hexb*$^{-/-}$ mice phenotype (Seyrantepe et al. 2018).

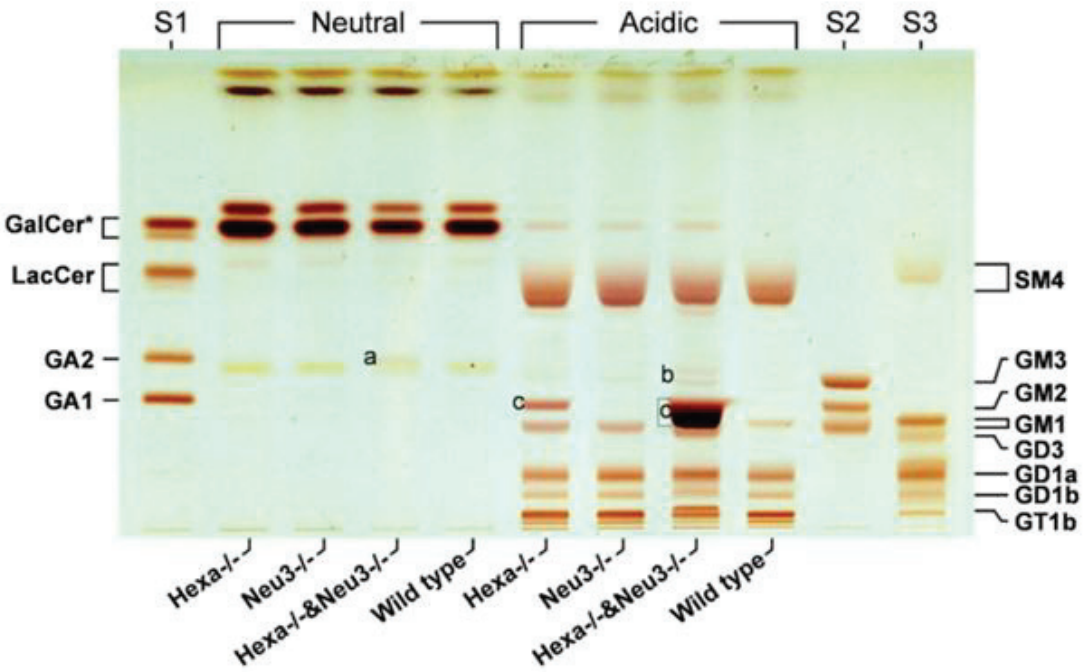

Figure 1.3. GM2 accumulation in the brain of *Hexa*$^{-/-}$*Neu3*$^{-/-}$ mice. (A) GA2, and (B) GM3 also appears in the brains of *Hexa*$^{-/-}$*Neu3*$^{-/-}$ mice. (C) GM2 accumulation in the brains of *Hexa*$^{-/-}$ (mild) and *Hexa*$^{-/-}$*Neu3*$^{-/-}$ (strong) mice (Source: Seyrantepe et al. 2018).

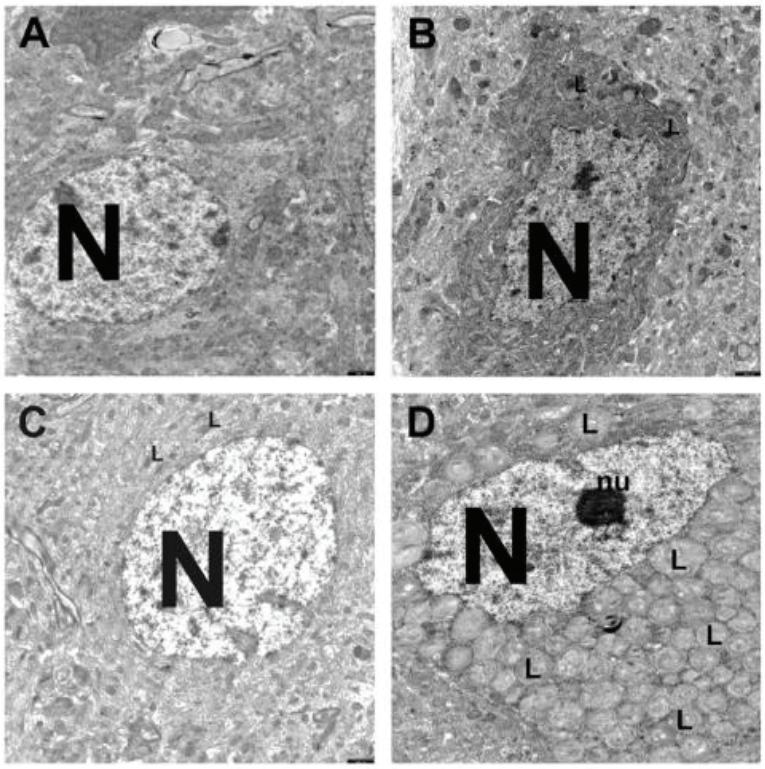

Figure 1.4. Electron microscopic images of neuronal inclusions and increased number of lysosomes in the cortex of (A) *WT*, (B) *Hexa*$^{-/-}$, (C) *Neu3*$^{-/-}$, and (D) *Hexa*$^{-/-}$*Neu3*$^{-/-}$ mice. N: nucleus; L: lysosomes; nu: nucleolus (Source: Seyrantepe et al. 2018).

1.4.Autophagy

Autophagy is the lysosomal degradation of cytoplasmic components and it provides maintaining of cellular homeostasis (Feng et al., 2014). There are three types of autophagy as macroautophagy, microautophagy and chaperone mediated autophagy. 'Autophagy' refers to macroautophagy unless indicated otherwise. In this process autophagic substrates that are to be degraded are sequestered in autophagosome and shuttled to lysosomes to start degradation process. On the contrary, in microautophagy the substances are sequestered by direct invagination there is no need for autophagosome formation. Degraded products are released into cytosol and recycled in new biosynthesis pathway. Autophagy enables recycling of degraded products and also provides response to cellular stress conditions like starvation, accumulation of proteins, or organelle damage (Yang et.al., 2010a; Schneider et.al., 2014).

In autophagy process, firstly the substance that supposed to be degraded engulfed by the phagaphore and double membrane structure called as autophagosome is

formed (Mizushima et al., 2002). The autophagosome then transported to lysosome and fuse with it to form autophagolysosome in which degradation by acidic lysosomal hydrolases takes place (Figure 1.5).

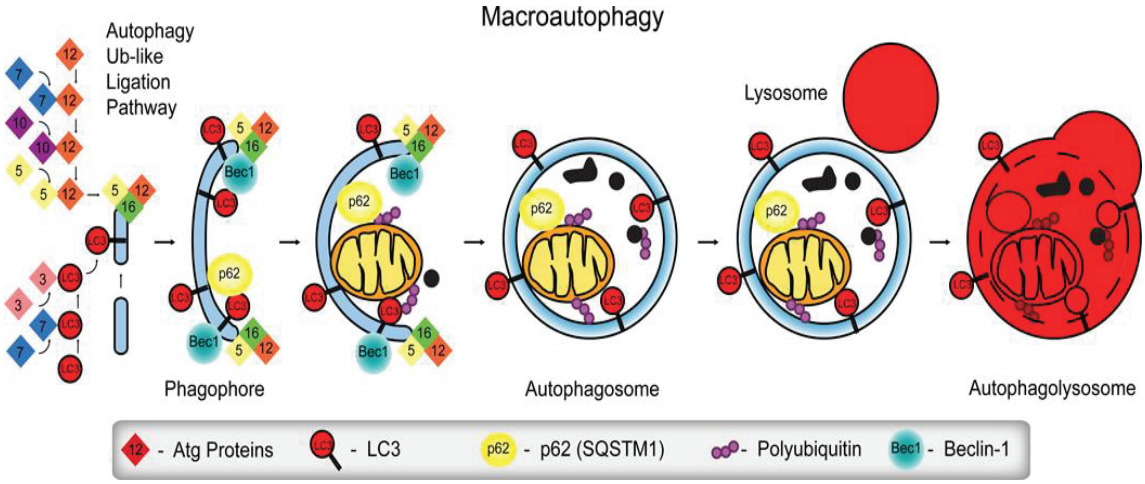

Figure 1.5. Schematic illustration of macroautophagy pathway (Source: Gump and Thorburn 2011).

Autophagy is regulated by autophagy-related (Atg) genes. A subset of these Atg proteins involving in the 'core' molecular machinery are crucial for autophagosome formation These core Atg proteins are consists of (1) Atg1/ULK complex, (2) two ubiquitin-like protein (Atg12 and Atg8/LC3), (3) PI3K/Vps34 complex and (4) two transmembrane proteins Atg9/mAtg9 (Yang et.al., 2010b). These four core protein complexes are recruited to phagaphore assembly site (PAS) where the autophagosome would be formed. Formation of PAS is the initiation step of the machinery, which is followed by expansion of phagaphore and closure of autophagosome and then recycling of the substances.

The autophagic induction depends on the activity of mTORC whose activity is determined by nutrient status. When there is nutrient starvation; mTORC1 is dissociates from ULK complexes and dephosphorylated hence autophagy is inactivated. In contrast, with the nutrient–rich conditions mTORC1 binds to and phosphorylates ULK complex and induces autophagy (Yang et.al., 2010b). Activated ULK1 and Beclin1 are translocated to the phagaphore assembly site and they induce vesicule nucleation. Vesicule nucleation is followed by phagaphore membrane elongation and during this elongation; ATG5 bound ATG12 provides conjugation of phosphotidyletanolamin with MAP1LC3B and then conversion of MAP1LC3B-I to MAP1LC3B-II occurs.

MAP1LC3B-II permanently binds to membranes of phagaphore and autophagosome (Lee et al., 2015).

p62 is a protein that have PB1 domain providing self oligomerization ability and UBA domain enables interaction with ubiquitinated proteins. These features indicate that p62 involves in inclusion formation. It also was also demonstrated that p62 is degraded through autophagical-lysosomal pathway. The autophagic degradation of p62 is mediated by its association with microtubule-associated protein 1 light chain 3 (LC3) which is a protein recruited to phagaphore assembly site and remain attached till the autophagosome is formed (Ichimura and Komatsu 2010). Some of the specific autophagic markers and their functions are listed on Table 1.2.

Table 1.2. Autophagic markers and their functions

Marker	Function
LC3	When autophagy is started the cytoplasmic form of LC3 (LC3I) is recruited to autophagosome and it is converted into LC3 II by site specific proteolysis
Beclin1	It forms the double-membrane structure that engulfs the autophagic material to start the formation of autophagosome.
p62	It is critical for activation of caspase-8; regulates selective autophagy of many substrates. It is degraded with the autophagic material through autophagy.
Lamp2	It is a lysosome-associated protein and is a receptor for chaperone-mediated autophagy.

1.5.Autophagy in Lysosomal Storage Diseases

As mentioned above; autophagy is a process in which damaged organelles are removed and cellular proteins are recycled through autophagical-lysosomal pathway. It functions as a survival response to cellular stresses like starvation (B'Chir et al. 2013). However; over-induction of autophagy can trigger apoptosis (Su et al., 2013). Impairment in autophagic flux has been reported to involve in many neurodegenerative disorders and LSDs including CLN3 disease (Maiuri et al., 2007; Müller et al., 2012).

As lysosome is involved in the most part of the autophagic pathway, autophagy is expected to be associated with LSDs (Raben et al., 2007). This association can be caused by either inhibition or activation of autophagic induction. Dysregulation of autophagy causes accumulation of secondary metabolites like autophagic substrates. Besides the substrates that accumulates because of a block of autophagic flux like polyubiquitinated proteins and p62/SQSTM1; proteins that are involved in autophagosome formation like BECN1 or conversion of cytosolic form of LC3 (LC3-I) to autophagasome-associated form of LC3 (LC3-II) are increased to make an endeavour to counterbalance the impaired autophagy (Pacheco et al., 2007; Settembre et al., 2008).

Up to now autophagical-lysosomal pathway has been investigated in a variety of LSDs. In compliance, a defect in autophagolysosome formation caused by a dysfunction in mTOR pathway is reported in many LSDs (Yu et al., 2010). Accumulation of autophagic substrates caused by autophagic dysfunction in LSDs propose that mechanisms leading to the disease phenotype may be similar to other neurodegenerative disorders like Alzheirmer's disease in which impairment of autophagy and intraneuronal accumulations of protein aggregates are reported (Lieberman et al. 2012).

Impairment of autophagic flux has been reported in the brain of lysosomal storage disease mice models like Sandoff (Keilani et al., 2012) mucopolysaccharidosis type IIIA (MPSIIIA) (Settembre et al., 2008), saposin A (Kose et. al., 2018) and saposin B deficiency (Sun et al., 2013). In these models, increased LC3-II level associated with autophagosome numbers, and accumulated p62 indicating ubiquitin-positive protein aggregates were assessed in mutant mice model brain regions and fibroblast cell lines. Moreover, patient fibroblast belongs to Niemann-Pick Type C (Sarkar et al., 2013) and Gaucher disease showed similar alterations in autophagic flux (Tatti M. et al., 2011).

1.6. Autophagy and Apoptosis Relation

The autophagy and apoptosis mechanisms regulate each other making the other making more or less likely. Under normal conditions autophagy acts in pro-survival mode of action and protects the cell as it provides survival in starvation and other cellular stress conditions; recycles damaged organelles, proteins and aggregates. However, just because it protects the cell from death, it cannot be directly linked to

autophagy. It was reported that autophagy itself can promote death under specific conditions (Kroemer and Levine 2008).

Direct molecular connections between autophagy and apoptosis mechanism has been reported. p62 which a key mediator for selective autophagy is also directly interacts with some apoptotic or antiapoptotic proteins like caspase-8 or TRAF6 (Moscat et.al., 2009). Interaction between caspase-8 and p62 is essential for caspase-8 activation and caspase-8 catalyzes cleavage of p62 upon death receptor activation. Moreover caspase-8 is degraded by autophagy (Gump and Thorburn 2011). Beclin1 is another autophagic regulator involving in apoptosis mechanism. Beclin1 and anti-apoptotic Bcl-2 interact with each other and when the Beclin1 is bound to Bcl-2 it cannot induce autophagy. Autophagy is activated when Beclin1 is released from Bcl-2 by BH3 proteins and consistently with that overexpression of Bcl-2 provides inhibition of autophagy. Furthermore, Beclin1 protein can be cleaved by caspase-3 and in turn autophagy is inhibited in turn (Gump and Thorburn 2011).

Under lysosomal storage disease conditions, the impairment in autophagic flux is common in disease pathology. Accumulation of undegraded substrates in lysosomes inhibits autophagosome-lysosome fusion and this causes inhibition of autophagic flux and secondary accumulation of components involving in autophagy. This secondary accumulation of toxic proteins, dysfunctional mitochondria and/or ER stress results in increased cellular stress and inflammation; eventually leads to apoptotic cell death (Figure 1.6).

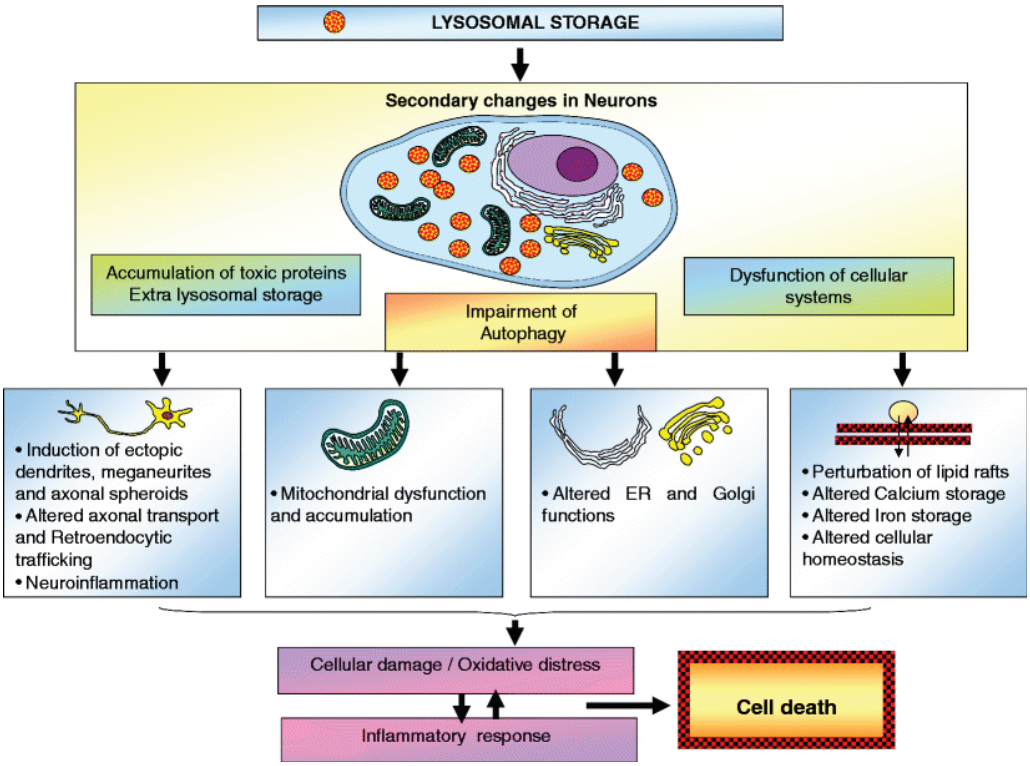

Figure 1.6. The mechanism of neurodegeneration in lysosomal storage conditions (Source: Bellettato et.al., 2010).

1.7.Apoptosis

Apoptosis has been described as a distinctive mode of 'programmed cell death' mechanism. It is strongly regulated and normally occurs during developmental stages and provides homeostasis. Also it is used as a defence mechanism in immunological reactions (Norbury et.al., 2001). The mechanism of apoptosis is highly complex and consists of energy-dependent cascades. There are two main pathways of apoptosis as extrinsic and intrinsic pathway which are also death receptor and mitochondrial pathway respectively. Even if they are different pathways the molecules involving in them influence each other (Igney and Krammer 2002).

Apoptotic cells display various biochemical features like DNA breakdown, protein cleavage, protein cross-linking and phagocytic recognition (Hengartner 2000). In normal conditions caspases are expressed in an inactive proenzyme form and once the apoptosis is induced they are activated and activate other procaspases in return so protease cascade is initiated. This proteolytic cascade amplifies the apoptotic signalling pathway and causes cell death eventually (Elmore 2007). The apoptotic pathway is

initiated by caspase-3 cleavage and ends up with DNA fragmentation, degradation of cytoskeletal and nuclear proteins, apoptotic body formation, production of ligands for phagocytic cell receptors and uptake by phagocytic cell.

The extrinsic pathway is initiated through transmembrane receptor-mediated interactions which involve tumor necrosis factor (TNF) receptor gene superfamily (Locksley et al., 2001). Members of this superfamily has cysteine-rich extracellular domains and cytoplasmic domain called death domain which provides transmission of death signal from cell surface to intracellular signalling pathways (Ashkenazi and Dixit 1998). Up to date; well characterized ligand-death receptor pairs include FasL/FasR, TNF-α/TNFR1, Apo3L/DR3, Apo2L/DR4 and Apo2L/DR5 (Elmore 2007).

The intrinsic pathway triggering apoptosis is initiated through non-receptor mediated stimuli producing intracellular signals. The stimuli can be either negative which is withdrawal of factors causing loss of apoptotic suppression or positive which includes radiation, toxins, hypoxia and free radicals. These stimuli open the mitochondrial permeability transition pore (MPT), cause loss of mitochondrial transmembrane potential and provide release of pro-apoptotic proteins from intermembrane space into cytosol (Saelens et al. 2004). Released pro-apoptotic proteins activate and mediate caspase-dependent mitochondrial pathway. The control and regulation of this pathway is mediated by Bcl-2 family of proteins (Cory and Adams 2002). The proteins of this family regulate mitochondrial membrane permeability may either act as pro- or anti-apoptotic. Anti-apoptotic ones include Bcl-2, Bcl-x, Bcl-XL, Bcl-XS, Bcl-w and pro- apoptotic ones include Bcl-10, Bax, Bak, Bid, Bad, Bim, Bik, and Blk (Elmore 2007). The main mechanism of action of Bcl-2 family proteins is to control whether the cytochrome c is released or not through the regulation of mitochondrial membrane permeability.

As mentioned above; apoptosis is energy dependent programmed cell death process which is required for development, homeostasis and survival of multicellular organisms. Abnormality in apoptotic regulation can result in adverse biological consequences. It can be triggered by several factors including receptor- mediated signals, DNA damage, growth factor withdrawal, ER stress and oxidative stress (Kannan and Jain 2000). Oxidative stress is caused by the imbalance between antioxidant defence mechanism and production of reactive oxygen species (ROS). ROS are normally generated through oxidative phosphorylation mechanism. ROS consist of free radicals (i.e. superoxide anion), hydroxyl radicals and no-radical hydrogen

peroxide. When ROS concentration is low, they are used as secondary messengers in several signal transduction pathways (Suzuki et al., 1996). However, excessive production of ROS causes vital damage to cellular components because they have high chemical reactivity and they can damage DNA, protein, carbohydrates and lipids. There is an antioxidant defence mechanism for these naturally generated ROS. However in the case that ROS overcome these defence mechanisms; the redox homeostasis is disrupted and oxidative stress occurs. Oxidative stress causes cell death by either necrosis or apoptosis. It is reported that disruption of redox homeostasis of cell into more oxidized environment occurs during caspase activation process. Besides several antioxidants blocking apoptosis (McGowan et al. 1996); Bcl-2 which is an anti-apoptotic regulator has antioxidant activity as well. Oxidative stress has been reported to involve several neurodegenerative and lysosomal storage diseases (Kannan et.al., 2000; Donida et al. 2017).

ER-stress is another one of the trigger factors of apoptosis. Endoplasmic reticulum (ER) involves in secretory pathway and provides folding, translocation and post-translational modifications of proteins. When the ER- function is disturbed and ER- stress occurs; unfolded protein response (UPR) is activated to provide the protein homeostasis. The UPR is mediated by three main proteins: IRE1α, PERK and ATF6. Under normal conditions PERK and ATF6 are inactive as they are bound to BiP protein which is a chaperone protein in ER and IRE1α activated by direct binding to unfolded proteins. . When unfolded protein amount increase in ER, BiP is released and mediate folding of unfolded proteins (Gardner and Walter 2011). Activated IRE1α, PERK and ATF6 induces signal transduction pathways that provides alleviation of ER-stress (Sano and Reed 2013). If these UPR-induced pathway are not able to relieve the ER-stress; intrinsic and extrinsic apoptotic pathways are activated. Increased ER-stress inhibits the translation of pro-apoptotic genes like Bcl-2 and induces apoptosis (Sano et.al., 2013). Besides UPR-mediated apoptosis; ER-stress can induce apoptosis by disruption in calcium homeostasis as well (Rizzuto et al. 1998).

Some of the specific apoptotic markers and their functions are listed on Table 1.3. They involve in different mechanisms and their regulation status affects apoptotic pathway in one way or another depending on the marker of interest.

Table 1.3. Apoptotic markers and their functions

Marker	Function
ATF6	Activating transcription factor 6 involves in the unfolded protein response during ER-stress.
Calnexin	It is a calcium-binding ER-associated protein that facilitates protein folding and quality control of protein folding. In ER, it withholds misfolded proteins for degradation.
XBP1	X-box binding protein 1 is a transcription factor that involves in ER stress and unfolded protein response; upon ER-stress it's spliced by activated IRE1.
SOD2	Superoxide dismutase 2 is an enzyme that provides clearance of mitochondrial ROS therefore it has an antiapoptotic role against oxidative stress.
Catalase	It provides catalysis of hydrogen peroxide into water and oxygen and it is the one of the main enzyme that protects the cell from oxidative damage caused by ROS
Ttase1	It is a member of glutaredoxin family and it contributes to antioxidant defence system.
Bcl2	B-cell lymphoma 2 is a member of Bcl-2 family proteins and localized on the outer membrane of mitochondria. It provides inhibition of pro-apoptotic proteins like Bax and Bak.
BclXL	B-cell lymphoma-extra large is a transmembrane protein in mitochondria and inhibits release of cytochrome c and activation of caspases.
Bax	It is member of Bcl-2 family and it mediates opening of mitochondrial voltage-dependent anion channel hence causes loss of membrane potential and release of cytochrome c.
APE1/Ref-1	It has DNA repair and transcriptional regulator activity and control cellular response to oxidative stress.

1.8. Apoptosis in Lysosomal Storage Diseases

Abnormalities in apoptotic regulation has been reported to be a component of several diseases including cancer, AIDS, ischemia, and neurodegenerative disorders like Parkinson's disease, Alzheimer's disease and Huntington's disease.

In LSDs, accumulating substrates acts as ligand for signal transduction receptors and abnormal accumulation of these substrates can disrupt the signalling cascades by altering the regulation of these receptors (Huizing et al. 2008). In chondrocytes of MPS VI or VII animal models pro-inflammatory cytokine secretion and metalloprotease activity are increased and subsequently cartilage degeneration and toll-like receptor 4 (TLR 4) activation by GAGs are reported (Simonaro et al., 2010). Activation of TLR4 upregulates proapoptotic ceramide synthesis hence causes cell death in chondrocytes. Also in Hurler disease abnormal accumulation of heparin sulphate alters the fibroblast growth factor 2 and transforming growth factor β mediated signalling cascades and leads to neurodegeneration and orthopedic pathology (Pan et al. 2005). Moreover apoptosis is also occurs in several types of NCLs including CLN3, CLN5 and CLN8 diseases (Persaud-Sawin et al., 2002; El Haddad et al., 2012).

Increased cell death level was reported in *Hexa*$^{-/-}$*Neu3*$^{-/-}$ mice cerebellum and hippocampus brain sections by terminal deoxynucleotidyl transferase (TdT) dUTP nick-end labeling (TUNEL) assay (Figure 1.7). Increased expression levels of tumor necrosis factor α (TNFα) which has major role in both inflammation and apoptosis, and caspase 4 which involves in ER-stress induced apoptosis were demonstrated in *Hexa*$^{-/-}$*Neu3*$^{-/-}$ mice brain (Seyrantepe et al., 2018).

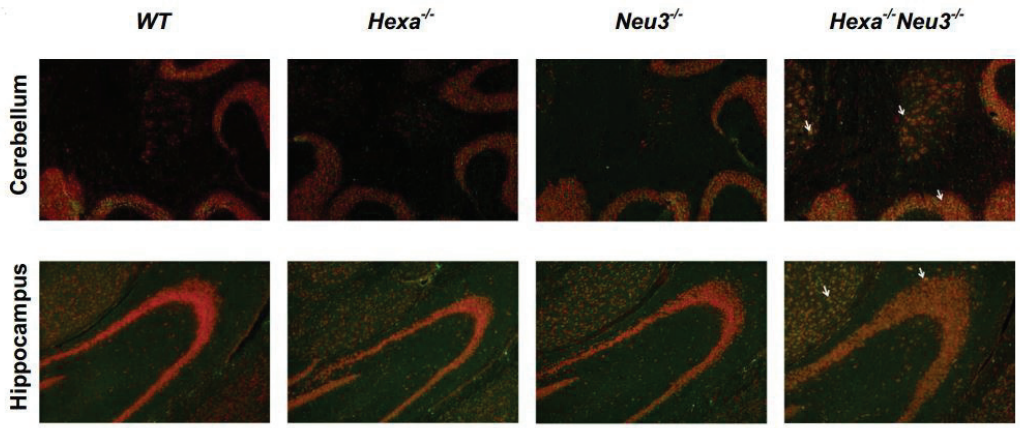

Figure 1.7. Increased cell death was determined by TUNEL assay for the cerebellum and hippocampus of 4.5-month-old *Hexa*$^{-/-}$*Neu3*$^{-/-}$ mice. Numerous TUNEL positive neurons were observed (yellow).

1.9. The Aim of the Study

In this thesis study, our aim was to elucidate the effect of abnormal GM2 accumulation on autophagic pathway in early-onset Tay Sachs disease mouse model. For this purpose the autophagic markers analysed for brain and fibroblast samples obtained from *WT*, *Hexa*$^{-/-}$, *Neu3*$^{-/-}$ and *Hexa*$^{-/-}$*Neu3*$^{-/-}$ mice. It was also aimed to reveal whether there is an alteration in apoptotic regulators or oxidative stress level in the concept of early-onset Tay-Sachs disease mouse model pathology. All together this study allow us to have better understanding of the disease pathology as it provides information about the cellular mechanisms that might interfere in the pathological abnormalities of early-onset Tay-Sachs disease mouse model.

CHAPTER 2

MATERIALS AND METHODS

2.1. Mouse Genotyping

Genotypes of mice were determined by PCR of isolated DNA from tails. Mouse tails were incubated overnight in shaking incubator at 55°C / 70rpm in 500 µl lysis buffer (10% Tris-HCl pH:7.6, 2.5% 0.2M EDTA, 20% SDS, 4% 5M NaCl) and 12 ul proteinase K (25 µg/µl, Sigma). Following day the samples were centrifuged at 14000 rpm for 10 minutes. Supernatant were collected into new tube and same volume of isopropanol (100%) were added on every sample. Upon isopropanol addition; DNA was collected and put into 70% ethanol in new Eppendorf tube. 1 min centrifugation at 14000 rpm was performed in order to precipitate DNA and remove ethanol. After supernatant removal; remaining ethanol was air dried. 100ul ultrapure water was added on dried DNA samples and incubated 1 hour at 55°C to provide DNA dissolution. After concentration of DNAs were measured by using NanoDrop spectrophotometer (ND-1000); PCRs for Hexa and Neu3 gene amplification were performed by using 100ng genomic DNA in 25ul reaction mixture: (25µl reaction mix containing 50pmol of each primer (Table2.1) , 10mM of dNTP mix, 1.5 units Taq polymerase (GeneAid), 1.5mM MgCl2, 10mM Tris-HCl and 50mM KCl buffer containing 10% DMSO. Conditions for PCR are; 1 cycle 30 seconds at 95˚C; 30 cycles 30 seconds at 95˚C, 45 seconds at 60˚C, 45 seconds at 72˚C; and 1 cycle 5 minutes at 72˚C).

Table 2.1. Primer sequences used for genotyping of *Hexa* and *Neu3* alleles

Gene	Primer	Primer Sequence
Neu3	Neu3 Forward	5'-CTCTTCTTCATTGCCGTGCT-3'
	Neo Forward	5'-GCCGAATATCATGGTGGAAA-3'
	Neu3 Reverse	5'-GACAAGGAGAGCCTCTGGTG-3'
HexA	HexA Forward	5'-GGCCAGATACAATCATACAG-3'
	PKG Forward	5'-CACCAAAGAAGGGAGCCGGT-3'
	HexA Reverse	5'-CTGTCCACATACTCTCCCCACAT-3'

2.2. Tissue Handling

Brain samples of 2,5- and 4,5-month-old *WT*, *Hexa*$^{-/-}$, *Neu3*$^{-/-}$ and *Hexa*$^{-/-}$*Neu3*$^{-/-}$ mice were collected by either dissection or fixation.

2.2.1. Brain Dissection

Age matched single and double knockout mice (2.5- and 4.5-month-old) were sacrificed by using CO_2 cabinet. The brains were dissected into two halves of cortex, cerebellum, thalamus and hippocampus regions (Figure 2.1) by using dissector blade. All tissue samples were quick frozen in liquid nitrogen and stored in -80^{o}C until required.

2.2.2. Fixation

In order to be able to perform immunohistochemical analysis, the brains required to be fixated by applying transcardiac perfusion. Ksilazol and basilazin were used to anesthetise the mice by intraperitonal injection. Once the mice faded of, they immobilized lying on their back and securely fixed by tape. An incision was made through abdomen and thoracic cavity was opened by cutting through rib cage. When the heart is exposed the needle was inserted to the left ventricle and the position of the needle was secured. Right atrium was cut by a sharp scissors and ~10ml 0.9% NaCl solution (pH 7.4) was flowed through circulation system. After the mice drained from blood, NaCl was switched to freshly prepared 4% paraformaldehayde in 1XPBS and circulated until all of the organs were fixed (~10ml). Then mice were decapitated and the brains were excised. The brains were incubated in 4%paraformaldehyde solution at +4^{o}C overnight. Then the samples were put through sucrose gradient in which they were incubated 2 hours in each of 10%, 20% and 30% sucrose in 1X PBS solution(pH 7.6) at +4^{o}C. In 30% sucrose, samples were incubated overnight. After that incubation, the brains were embedded in OCT (optimal cutting temperature) containing cryomolds and they were slowly frozen in dry ice containing buckets. Tissues were stored at -80^{o}C. By using Leica Cryostat, 10μm coronal sections of each brain were sectioned and collected

on adhesive-coated slides. These slides were also stored at -80°C for further immunohistochemical analysis (Schneider Gasser et al. 2006; Risher et al. 2014).

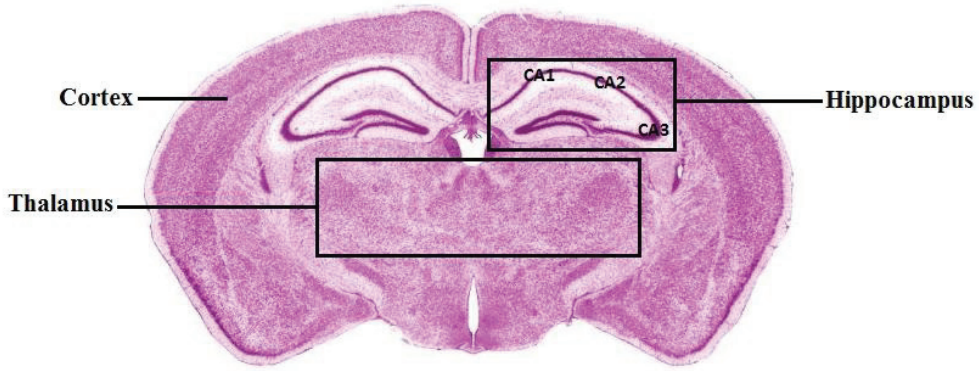

Figure 2.1. Cortex, thalamus and hippocampus of mouse brain in coronal section.

2.3. Real Time PCR

Real time PCR protocol was applied by following RNA isolation, cDNA synthesis and RT-PCR procedures.

2.3.1. RNA Isolation

50 mg of each brain region (cortex, cerebellum, thalamus and hippocampus) were measured and put into 500µl GeneZol (GeneAid) containing 2ml Eppendorf tube and homogenized with RNase free beads by using tissue homogenizator (Retsch MM100). After homogeniztaion samples were incubated at room temperature for 5 minutes and transferred into 1.5 ml Eppendorf tubes. 100µL chloroform was added on each sample and the tubes were shaken robustly for 10 seconds. In order to provide phase separation the samples were centrifuged at 15000xg for 15 minutes at +4°C. After centrifugation, the colourless aqueous upper level containing RNA were transferred into new 1.5 ml Eppendorf tube and one volume of isopropanol (~200-300µl) was added on each sample. After inverting the tube several times they were incubated for 10 minutes at room temperature and then they were centrifuged for 10 minutes at 15000xg at +4°C to provide tight RNA pellet formation. Supernatants were carefully discarded and 1ml 70% ethanol was added on each sample to wash the RNA. After brief vortex, samples were centrifuged for 5 minutes at 15000xg at +4°C. Supernatants were carefully

removed and the RNA pellets were air-dried at 55°C for 5 minutes. In order to resuspend the RNAs 20µl RNase free water was added on each sample and they were incubated in water bath at 50°C for 10 minutes to provide dissolving of RNA pellet in water. Finally concentrations of RNAs were measured by using NanoDrop Spectrophotometer (ND-1000).

2.3.2. cDNA Synthesis

Isolated RNA's were converted into cDNAs by using High-Capacity cDNA Reverse Transcription Kit (Applied Biosystems). 50ng/ul cDNA producing reaction mix was prepared according to manufacturer's instruction. The concentration of RNAs were measured by using NanoDrop. The reaction mix was composed of 1 X RT buffer, 4 mM dNTP mix, 1X RT Random primers, 50 units MultiScribe Reverse Transcriptase were mixed with calculated volume of water and RNA depending on the RNA concentration level of each sample. Total volume of the mixture was arranged to be 20 ul. The reaction was conducted with the conditions: 1 cycle 10 minutes at 25˚C; 1 cycles 120 minutes at 37˚C, 1 cycle 5 minutes at 85˚C.

Normal PCR amplifying GAPDH gene was performed in order to determine whether the cDNA synthesis was successful or not. 25ul reaction mixture containing 0.8 mM of GAPDH gene primers, 10 mM of each dNTPs, 1X reaction buffer with MgCl2 and 1.75 units AmpONE Taq DNA polymerase (GeneAll) were prepared for each cDNA (50ng). The reaction was carried out with the conditions: 1 cycle 2 minutes at 95˚C; 30 cycles 20 seconds at 95˚C, 15 seconds at 65˚C, 22 seconds at 72˚C; and 1 cycle 3 minutes at 72˚C. The reaction products were run on the agarose gel (1%) at 90 volt for 30 minutes.

2.3.3. RT-PCR

The relative expression levels of the genes and primer sequences presented on the Table 2.1 were measured by using Roche LightCycler® 96 System with Roche LightCycler 480 SYBR Green I Master Mix. The reaction mixture was optimized to 20µl reaction mix containing 0.4 uM each primer (Table 2.2) and 1X Roche LightCycler 480 SYBR Green I Master Mix and 50ng cDNA. The reaction was

performed under conditions: 1 cycle 10 minutes at 95˚C; 45 cycles 20 seconds at 95˚C, 15 seconds at 60˚C, 22 seconds at 72˚C by using. For each sample triplicate reactions were prepared and average of the three results were used as gene expression level of sample of interest. The gene expression level was normalized to GAPDH gene expression level and gene expression ratio was obtained for each sample. Two-way ANOVA on GraphPad Prism was used for statistical analysis.

Table 2.2. Primer sequences and RT-PCR product length of the genes to be analyzed

Gene	Primer Sequences	PCR Product
Beclin1	F:5'-GAGGAGCAGTGGACAAAAGC-3' R:5'-CAAACATCCCCTAAGGAGCA-3'	112bp
LAMP2	F:5'- TAACATCAACCCTGCCACAA-3' R:5'- AAGCTGAGCCATTAGCCAAA-3'	176 bp
p62	F:5'- TGTGGAACATGGAGGGAAGAG -3' R:5'- TGTGCCTGTGCTGGAACTTTC -3'	67 bp
ATF6	F:5'- TGGAAGTGGGAAGATCGGGA -3' R:5'- AGGACAGAGAAACAAGCTCGG -3'	354 bp
Calnexin	F:5'- ATTGCCAACCCCAAGTGTGA -3' R:5'- TCCAGCATCTGCAGCACTAC -3'	362 bp
XBP1	F:5'- TCCGCAGCACTCAGACTATG -3' R:5'- GACTCTCTGTCTCAGAGGGGA -3'	360 bp
SOD2	F:5'- GTGTCTGTGGGAGTCCAAGG -3' R:5'- CCCCAGTCATAGTGCTGCAA -3'	339 bp
Catalase	F:5'- TTCGTCCCGAGTCTCTCCAT -3' R:5'- GAGGCCAAACCTTGGTCAGA -3'	351 bp
Ttase1	F:5'- CTGCAAGATCCAGTCTGGGAA -3' R:5'- CTCTGCCTGCCACCCCTTTTAT -3'	322 bp
Bcl2	F:5'- CGCAGAGATGTCCAGTCAGC -3' R:5'- TATGCACCCAGAGTGATGCAG -3'	369 bp

(cont. on next page)

Tablo 2.2. (cont.)

BclXL	F:5'- TCAGCCACCATTGCTACCAG -3' R:5'- GTCTGAGGCCACACACATCA -3'	356 bp
Bax	F:5'- AGGATGCGTCCACCAAGAA-3' R:5'- CTTGGATCCAGACAAGCAGC -3'	306 bp
GAPDH	F:5'- CCCCTTCATTGACCTCAACTAC-3' R:5'- ATGCATTGCTGACAATCTTGAG-3'	347 bp

2.4. Immunohistochemistry

The frozen brain samples for each genotype were cut into 10um cryosections by using Leica Cryostat (CM1850-UV). The sections were mounted onto HistoBond slides and stored at -80^{o}C for further use. When IHC was performed; the slides were kept waiting on ice for 30 minutes and then they were washed with 1X PBS for 10 minutes. In order to provide permeability of cell membranes; the slides were incubated in 100% acetone for 10 minutes then they were washed twice with 1X PBS for 5 minutes. To avoid nonspecific binding; the slides were incubated in blocking solution (10% goat-serum, 4%BSA, 0.3M Glycine in 1X PBS) for 1 hour. After that, primary antibody solution which was LC3 (8µg/µl,MAB8558) and LAMP1 (1:500, ab24170) involving blocking solution were prepared and added on each brain sample on the slides. The incubation conditions for primary antibody were optimized to as follows: overnight (16 hours) at +4^{o}C. Following this incubation the slides were washed three times with 1X PBS for 5 minutes. Secondary antibodies (ab175476, Alexa Fluor®-568 and ab150077 Alexa Fluor®-488) were dissolved in blocking solution and added on slides. After 1 hour incubation with secondary antibody solution, the slides were washed four times with 1XPBS for 5 minutes. The slides were mounted by using Fluoroshield mounting medium DAPI (abcam) and images were obtained by fluorescent microscope (Olympus BX53). Co-localization analysis of red and green fluorescence was applied by using ImageJ.

2.5. Immunocytochemistry

Fibroblasts generated from the mice with each genoptype were used for this analysis. The cells were grown on microslides on 24 well-plate for 24 hours. After washing three times with 1XPBS for 5 minutes; the cells were incubated in 4% paraformaldehyde for 1 hour to provide fixation of cells on the slides. The slides were washed three times with 1XPBS once again and blocking was applied by 1 hour incubation at room temperature with the solution consisting of 10%goat serum, 4%BSA 0.3M Glycine and 0.3%TritonX in 1XPBS. After that the cells were incubated with 5%TritonX in 1XPBS for 30 minutes to provide permeability of the cells. Then the cells were treated overnight at 4^{o}C with the primary antibodies (LC3: 8 µg/µl, 'MAB8558', LAMP: 1/500, 'ab24170' and APE1/Ref-1: 1/200, 'ab137708') dissolved in blocking solution. Following day; the cells were washed three times with 1XPBS and incubated in humidity chamber for 1 hour at room temperature with secondary antibody solution which includes 1/500 of each antibody (ab175476, Alexa Fluor®-568 and ab150077 Alexa Fluor®-488) in blocking solution. For APE1/Ref-1 immunostaining only 1/500 ab150077 Alexa Fluor®-488 was used as secondary antibody. After that the cells were washed three times with 1XPBS-T (0.05% Tween20) and they were mounted on slides with Fluoroshield mounting medium DAPI (abcam). Images were obtained by using fluorescent microscope (Olympus BX53). Co-localization analysis of red and green fluorescence was applied by using ImageJ.

2.6. Western Blot

Western blot protocol was applied by following protein isolation, Bradford assay and SDS-PAGE gel electrophoresis.

2.6.1. Protein Isolation

In order to obtain protein lysates of cortex, cerebellum, hippocampus and thalamus region of WT, Hexa-/-, Neu3-/- and Hexa-/-Neu3-/- mice; brain regions were homogenized with mini homogenizator in protein lysis buffer (1% TritonX100, 50mMHepes, 150mM NaCl, 10%Glycerol, 50mM Tris-Base, 1%PMSF, 1% protease

inhibitor). For cortex and cerebellum 500µl and for thalamus and hippocampus 100µl protein lysis buffer was used to homogenize the tissues. Once the tissues were homogenized thoroughly, the samples were incubated on ice for 1 hour while they were vortexed every 10 minutes. After that; the samples were centrifuged for 15 minutes at 0^{o}C 14000rpm. Supernatants including isolated proteins were collected into new Eppendorf tubes.

2.6.2. Bradford Assay

Isolated proteins were diluted with 1:100 ratio (2ul protein+198ul dh2o). In order to create a standart curve to be able to calculate protein concentrations of the samples, BSA solutions with different concentrations (100,80,40,20...) were prepared. 50ul diluted proteins and BSA solutions were added to the 96well plate and 200ul Bradford Reagent (Sigma) was added onto each sample on 96 well plate. After 10 minutes incubation in dark, the absorbance levels of the samples were measured at 595nm by using microplate reader (BioRad). By using the absorbance level of serially diluted BSA solutions; standart curve graph was plotted and equation was calculated. By using this equation, concentrations of each sample were calculated and the volume required to have same amount of protein (20ug) were determined.

2.6.3. SDS-PAGE Gel Electrophoresis

Table 2.3. Ingredients for resolving and stacking gel preparation of SDS-PAGE gel electrophoresis

Resolving Gel (10%)	**Stacking Gel(5%)**
3 ml Lower buffer (1.5 M Tris-HCl)	1.5 ml Upper Buffer (1M Tris-HCl)
4 ml Acrylamide (30%)	1 ml Acrylamide (30%)
5 ml Water	3.5 ml Water
60µl SDS (10%)	60µl SDS (10%)
60µl APS (10%)	60µl APS (10%)
6 µl TEMED	6 µl TEMED

Resolving gel was prepared as shown in the Table2.2 and poured into the gap between glass plates which were clamped by casting frames. After the gel was polymerized, stacking gel which was also prepared according to the Table2.2 was poured on top of resolving gel and the well-forming comb was inserted into the stacking gel solution. When the stacking gel was completely gelated, the comb was removed; the glass was taken out from casting frames and set into the cell buffer dam. Running buffer (0.25M Tris-Base, 1.92M Glycine, 1%SDS) was poured into the inner chamber and overflowed to outer chamber until the buffer level reaches to required level. Protein samples were prepared by adding the calculated amount of protein and water after Bradford assay and 4:1 loading buffer (40% Glycerol, 240mM Tris-HCl pH 6.8, 8%SDS, 0.04%Bromophenol Blue, 5% β-mercaptoethanol). The protein samples were boiled at 95^{o}C and loaded into the wells. The proteins were separated by SDS-PAGE at 80V for ~2 hours. Then the proteins were transferred onto the nitrocellulose membrane (BioRad) by placing transfer sandwich in transfer chamber containing transfer buffer (48mM Tris-Base, 39mM Glycine, 20%Methanol, pH 9.2) and running at 0.25A for 1hour. After that the blot was blocked by soaking in 5%milk in PBS-T(0.005%Tween20) for 1hour with shaking at room temperature. After rinsing the milk, the blots were incubated overnight at +4^{o}C in primary antibodies of APE1/Ref-1 (1:1000, abcam, ab137708), β-actin (1:1000, cell signalling, 4970) in red solution (5%BSA, 0.02% NaAzide, Phenol Red, in PBS-T pH 7.5). The blots were washed three times for 10 minutes with PBS-T solution followed by incubation with HRP-conjugated secondary antibody (Jackson ImmunoResearch Lab) for 1 hour at room temperature. Then the blots were washed three times again and the proteins were visualized by using LuminataTM Forte Western HRP Substrate (Millipore) on a digital imaging system (Fusion SL, Vilber).

2.7. Flow Cytometry

Intercellular ROS level was measured by using 2'7' –dichlorodihydrofluorescein diacetate (H_2DCFDA) (Sigma). H_2DCFDA is nonpolar compound; when it enters to intracellular environment it is converted to non-fluorescent polar by-product H2DCF by cellular esterases. In the presence of intracellular ROS; H2DCF is oxidized to highly fluorescent 2'7' dichlorofluorescein (DCF). From *WT*, *Hexa*$^{-/-}$, *Neu3*$^{-/-}$ and *Hexa*$^{-/-}$*Neu3*$^{-}$

$^{/-}$ fibroblast cell lines; positive control (H_2O_2 and H_2DCFDA-treated), negative control (non-treated) and sample groups (H_2DCFDA treated) were formed. Positive control group was treated with 100uM H2O2 containing serum free media for 1 hour at 37^{o}C. After washing cells with 1XPBS; both positive control and sample group cells were treated with 5uM H2DCFDA containing serum free media for 30 min. Negative control group were treated with only serum free media for 30 min. After incubation the cells were washed with 1XPBS and tripsinyzed. The trypsin were neutralized with %10 FBS in 1XPBS and the cells were harvested. Harvested cells were centrifuged for 5 min at 1500rpm and supernatant were discarded. After washing with 1XPBS the cells were recentrifuged for 5 min at 1500rpm and supernatant were discarded again. The cells were resuspended in 600ul 1XPBS and triplicate samples (200ul each) were formed for each sample. Then all of the samples were scan on FACScan analyzer.

CHAPTER 3

RESULTS

3.1. Mouse Genotyping

In order to detect wild type and mutant allele of *Hexa* and *Neu3* genes, separate PCRs were performed and depending on the amplified bands the mice were labelled either +/+, +/- or -/- for the genes *Hexa* (Figure3.1.A) and *Neu3* (Figure3.1.B).

3.2. Autophagic Analysis

To understand the whether there is an alteration in autophagic flux in Tay-Sachs mouse model, the autophagic markers: Beclin1, p62 and LAMP2 are analyzed by RT-PCR, immunohistochemistry and immunocytochemistry.

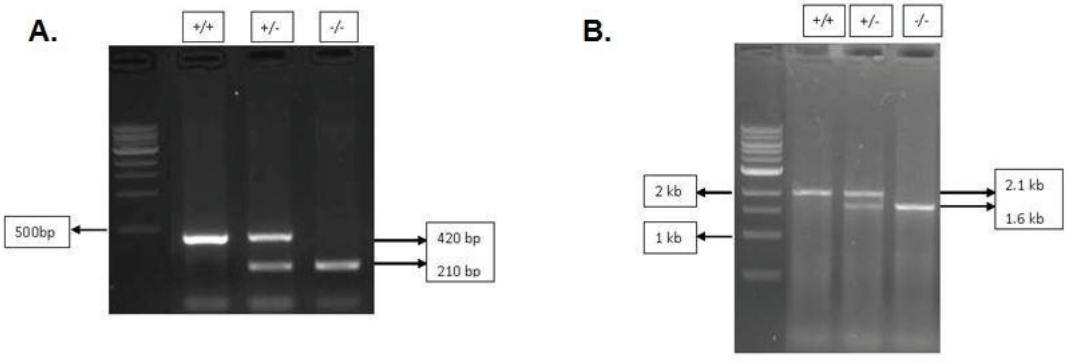

Figure 3.1. Gel images of PCR analysis for genotyping of mice for *Hexa* (A) and *Neu3* (B) by using tail genomic DNA. (A) 210 bp and 420 bp fragments represent mutant allele and wild type allele of *Hexa,* respectively.(B) 1.6 kb and 2.1

kb fragments represent mutant allele and wild type allele of *Neu3,* respectively.

3.2.1. Real Time PCR

RT-PCR analysis was performed to observe the possible changes in gene expression levels of markers in autophagic pathway. Gene expression levels of autophagic markers in cortex cerebellum, hippocampus and thalamus region of *WT*, *Hexa*$^{-/-}$, *Neu3*$^{-/-}$ and *Hexa*$^{-/-}$*Neu3*$^{-/-}$ mice was measured.

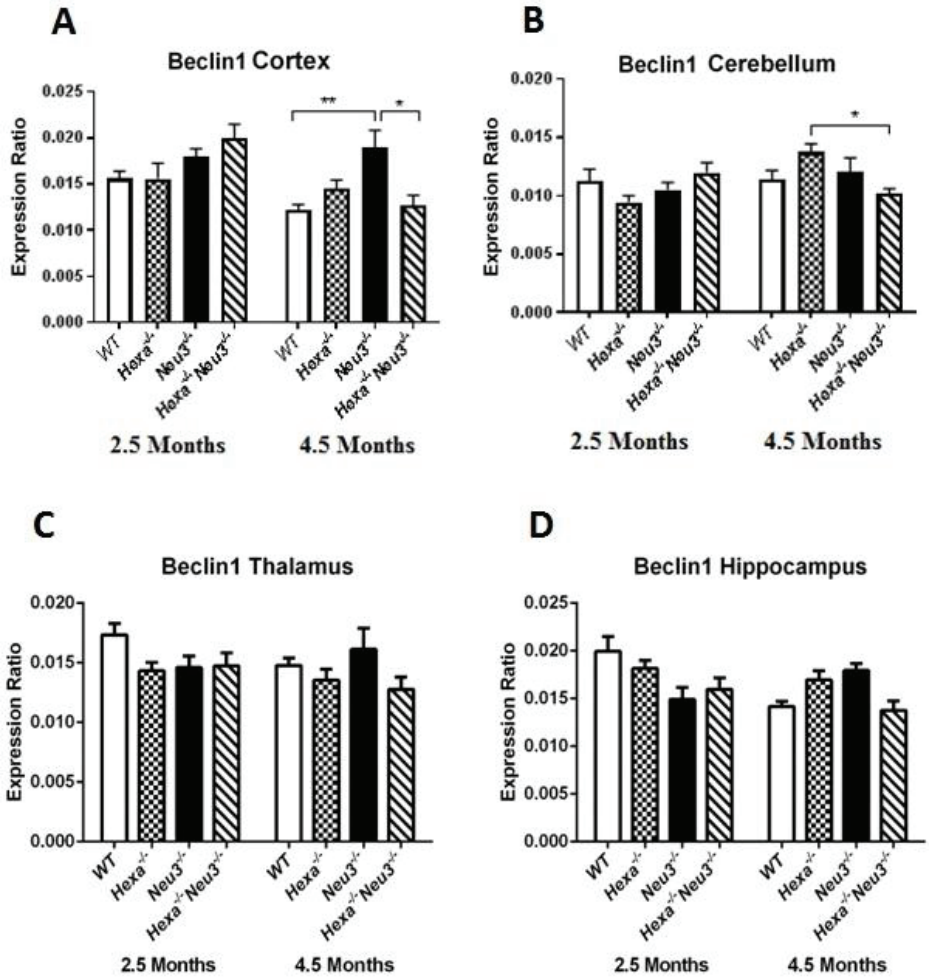

Figure 3.2. Beclin1 gene expression levels of cortex (A), cerebellum (B), thalamus (C) and hippocampus (D) tissues of 2.5- and 4.5-month-old *WT, Hexa*$^{-/-}$*, Neu3*$^{-/-}$ and *Hexa*$^{-/-}$*Neu3*$^{-/-}$ mice. (n=3;*p<0,05,**p<0,01) Expression ratios were calculated by ΔCT method and 2-way-ANOVA analysis was used to determine *p-values* via GraphPad.

Expression of Beclin1 was slightly increased in cortex of 2.5-month-old *Hexa*$^{-/-}$ *Neu3*$^{-/-}$ compared to its littermates and significantly increased in 4.5-month-old *Neu3*$^{-/-}$ when compared to *WT* and *Hexa*$^{-/-}$*Neu3*$^{-/-}$ counterparts (Figure 3.2.A). While no significant difference was observed in thalamus and hippocampus regions; significantly decreased Beclin1 was observed in cerebellum of *Hexa*$^{-/-}$*Neu3*$^{-/-}$ mice when compared to its *Hexa*$^{-/-}$ littermates (Figure 3.2. B, C and D).

In the expression analysis of p62; significant increase was demonstrated in cerebellum of 4.5-month-old *Hexa*$^{-/-}$*Neu3*$^{-/-}$ when compared to its littermates, however; for cortex, thalamus and hippocampus region no significant difference was observed in p62 expression ratio (Figure 3.3. A, B, C and D).

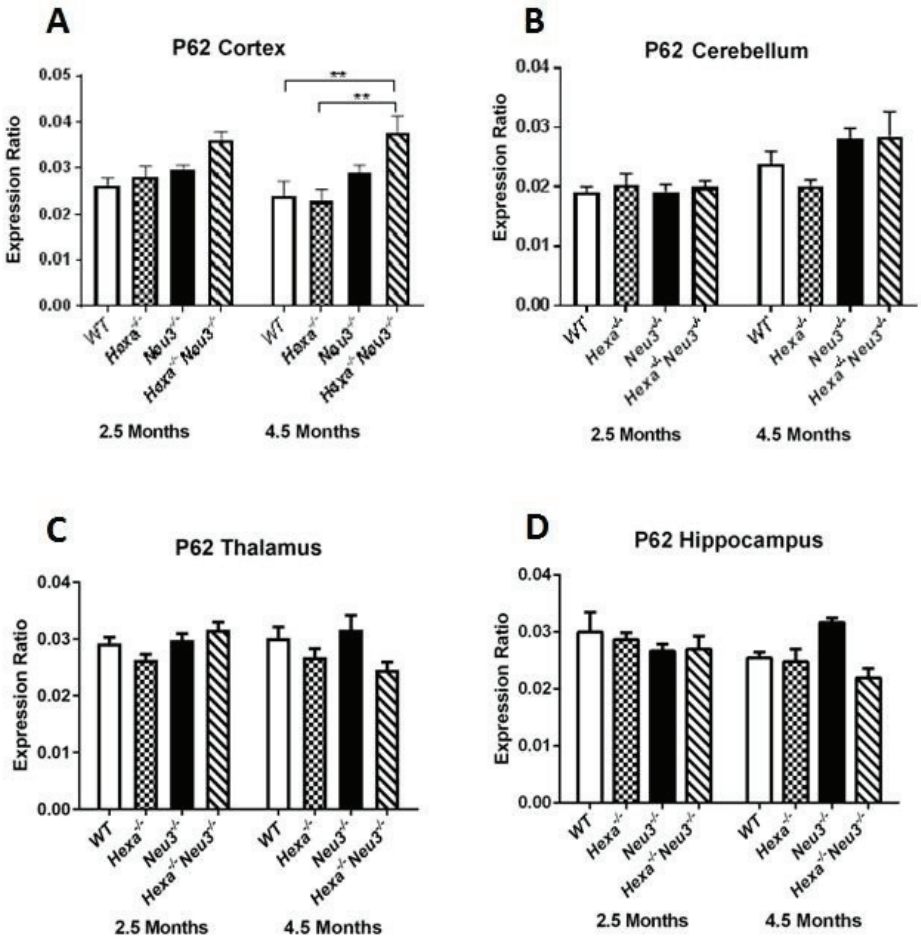

Figure 3.3. p62 gene expression levels of cortex (A), cerebellum(B), thalamus(C) and hippocampus (D) tissues of 2.5- and 4.5-month-old *WT, Hexa*$^{-/-}$*, Neu3*$^{-/-}$ and *Hexa*$^{-/-}$*Neu3*$^{-/-}$ mice. (n=3; **p<0,01) Expression ratios were calculated by ΔCT method and 2-way-ANOVA analysis was used to determine *p-values* via GraphPad.

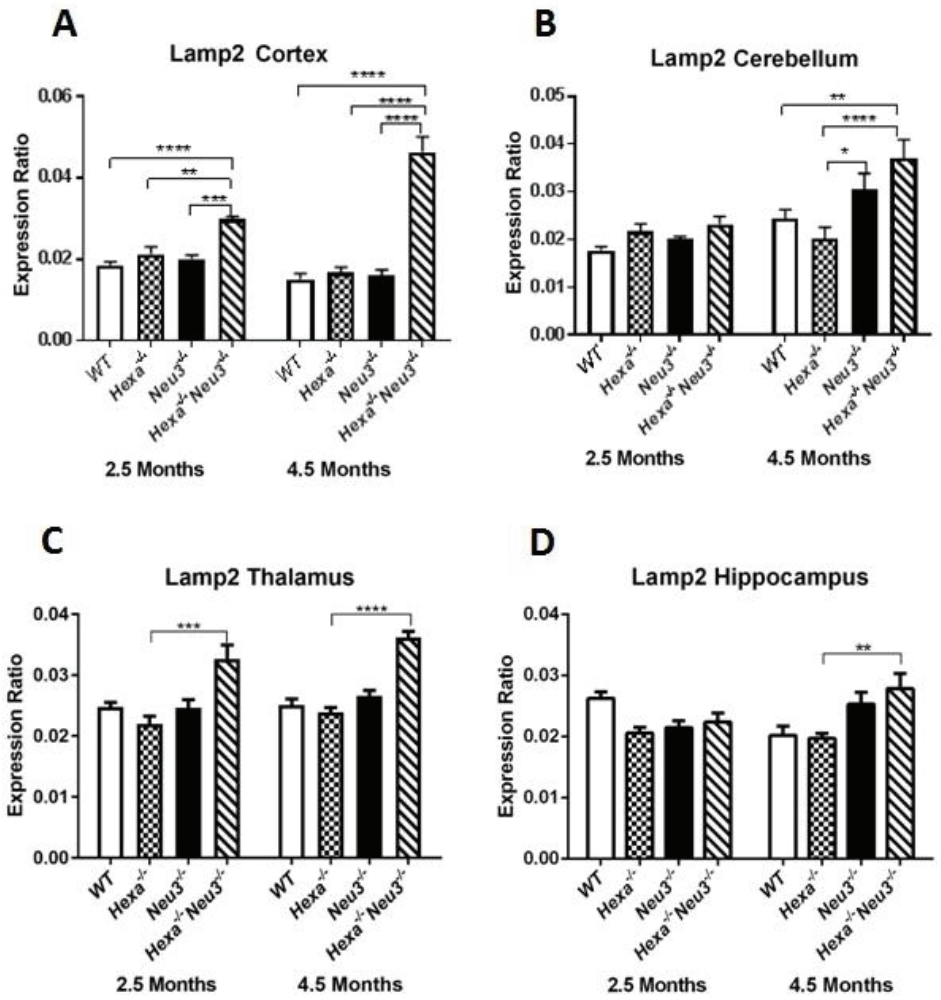

Figure 3.4. LAMP2 gene expression levels of cortex (A), cerebellum(B), thalamus(C) and hippocampus tissues of 2.5- and 4.5-month-old *WT, Hexa*$^{-/-}$*, Neu3*$^{-/-}$ and *Hexa*$^{-/-}$*Neu3*$^{-/-}$ mice. n=3;*p<0,05,**p<0,01,***p<0,001,****p<0,0001) Expression ratios were calculated by ΔCT method and 2-way-ANOVA analysis was used to determine p-values via GraphPad.

LAMP2 expression levels showed significant changes in all the analyzed brain regions. In cortex of both 2.5- and 4.5-month-old *Hexa*$^{-/-}$*Neu3*$^{-/-}$ mice, displayed significantly increased LAMP2 expression ratio when compared to their counterparts (Figure 3.4.A). The expression analysis for cerebellum showed that in 4.5-month-old *Hexa*$^{-/-}$*Neu3*$^{-/-}$ has significantly increased LAMP2 expression when compared to its 4.5-month-old counterparts, however; there was no significant change between 2.5-month-old group(Figure 3.4.B). In both thalamus and hippocampus LAMP2 expression was significantly higher in 4.5-month-old *Hexa*$^{-/-}$*Neu3*$^{-/-}$ mice when compared to that of their *Hexa*$^{-/-}$ counterparts; significant increment was also displayed in thalamus of 2.5-month-old *Hexa*$^{-/-}$*Neu3*$^{-/-}$ mice when compared to their *Hexa*$^{-/-}$ littermates (Figure 3.4.C and D).

3.2.2. Immunohistochemistry

In order to determine whether there is an impairment in autophagic flux and accumulation of secondary substrates; immunohistochemical analysis were performed for LC3, LAMP1 and p62 proteins. In cortex region; the co-localization intensity was significantly higher in *Hexa*$^{-/-}$*Neu3*$^{-/-}$ mice when compared to *WT* and *Hexa*$^{-/-}$ group (Figure 3.5). Significantly increased co-localization intensity level was also observed in cerebellum of *Hexa*$^{-/-}$*Neu3*$^{-/-}$ mice compared to *Hexa*$^{-/-}$ and *Neu3*$^{-/-}$ single knockout ones. On the other hand, in cerebellum of *Neu3*$^{-/-}$, significantly decreased co-localization intensity compared to *WT* was demonstrated as well (Figure 3.6).

A similar case with cortex was observed in thalamus of *Hexa*$^{-/-}$*Neu3*$^{-/-}$ where the co-localization intensity level was significantly higher compared to that of *WT* (Figure 3.7).

Significantly increased co-localization of LC3 and LAMP1 in all of the hippocampal CA1, CA2 and CA3 regions of 4.5-month-old *Hexa*$^{-/-}$*Neu3*$^{-/-}$ mice when compared to *WT*. For CA1 and CA2 regions it was also significantly increased compared to *Hexa*$^{-/-}$ and *Neu3*$^{-/-}$ mice (Figure 3.8, Figure 3.9).

The immunohistochemical analysis on brain regions of *Hexa*$^{-/-}$ and *Hexa*$^{-/-}$*Neu3*$^{-/-}$ mice resulted in significantly increased level of p62 accumulation in cortex and cerebellum regions of *Hexa*$^{-/-}$*Neu3*$^{-/-}$ mice compared to *Hexa*$^{-/-}$ (Figure 3.10.C and 3.10.D).

In hippocampal CA1, CA2 and CA3 regions; significantly increased p62 accumulation was also observed for *Hexa*$^{-/-}$*Neu3*$^{-/-}$ mice when compared to *Hexa*$^{-/-}$ (Figure 3.11.C and D).

Even if slightly increased level is observable for thalamus region of *Hexa*$^{-/-}$*Neu3*$^{-/-}$ mice; p62 accumulation did not display significant change in double knockout mice when compared to *Hexa*$^{-/-}$ (Figure 3.12.C). However in pons significantly elevated p62 accumulation was observed for *Hexa*$^{-/-}$*Neu3*$^{-/-}$ mice compared to *Hexa*$^{-/-}$ (Figure 3.12.D).

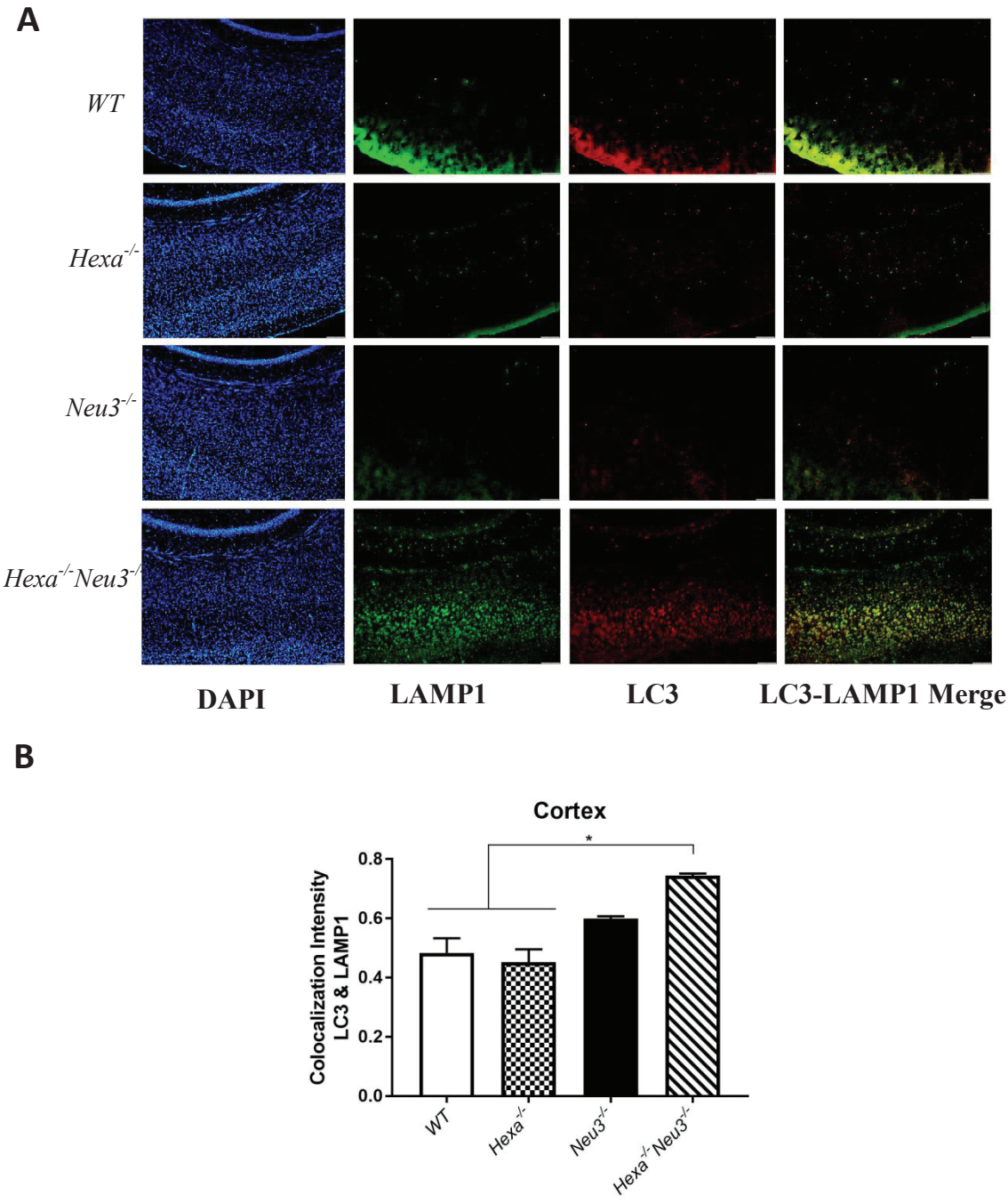

Figure 3.5. (A)Immunostaining of LC3 and LAMP1 in 4.5-month-old *WT, Hexa*$^{-/-}$, *Neu3*$^{-/-}$ and *Hexa*$^{-/-}$*Neu3*$^{-/-}$ mice brain coronal sections, cortex region. Images were taken at 10X magnification and under same light intensity differing only for filter type. (B) Co-localization intensity of LC3 and LAMP1 measured via ImageJ. One-way-ANOVA was used to determine *p-values.* (*p<0,05,**p<0,01,***p<0,001,****p<0,0001)

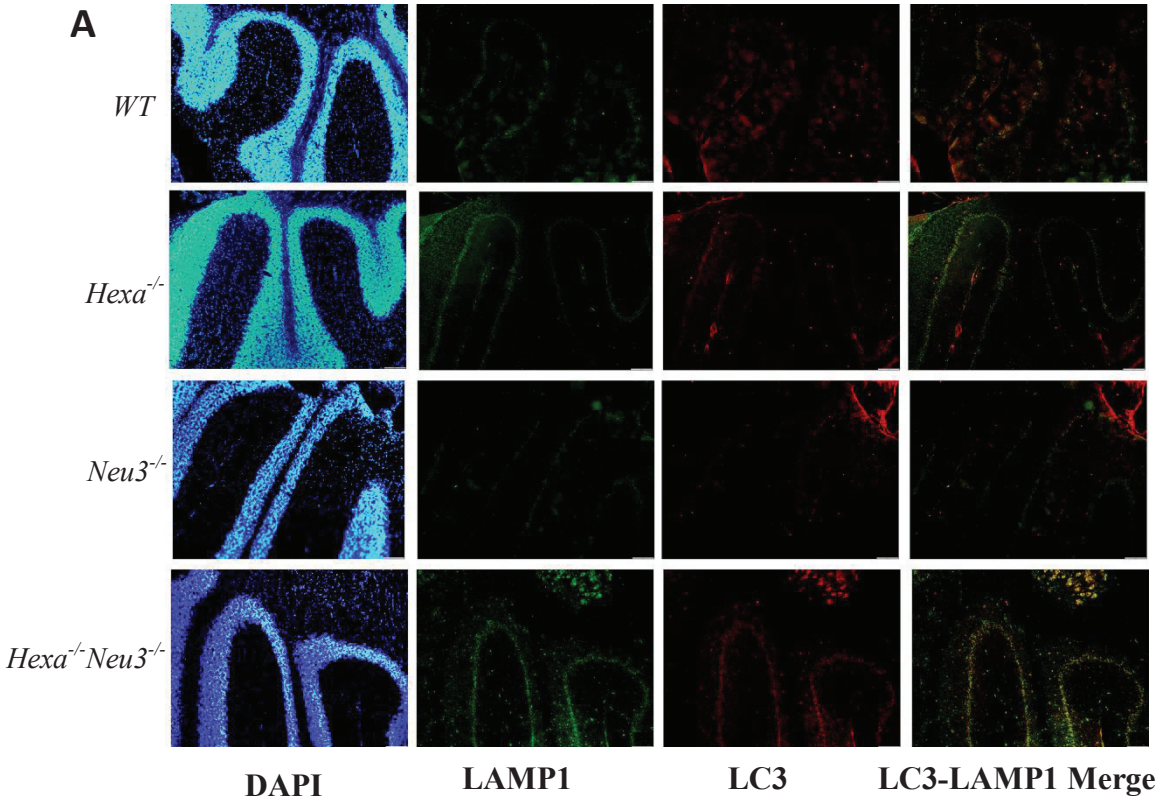

Figure 3.6. (A)Immunostaining of LC3 and LAMP1 in 4.5-month-old *WT, Hexa*$^{-/-}$, *Neu3*$^{-/-}$ and *Hexa*$^{-/-}$*Neu3*$^{-/-}$ mice brain coronal sections, cerebellum region. Images were taken at 10X magnification and under same light intensity differing only for filter type. (B) Co-localization intensity of LC3 and LAMP1 measured via ImageJ. One-way-ANOVA was used to determine *p-values.* (*p<0,05, **p<0,01, ***p<0,001, ****p<0,0001)

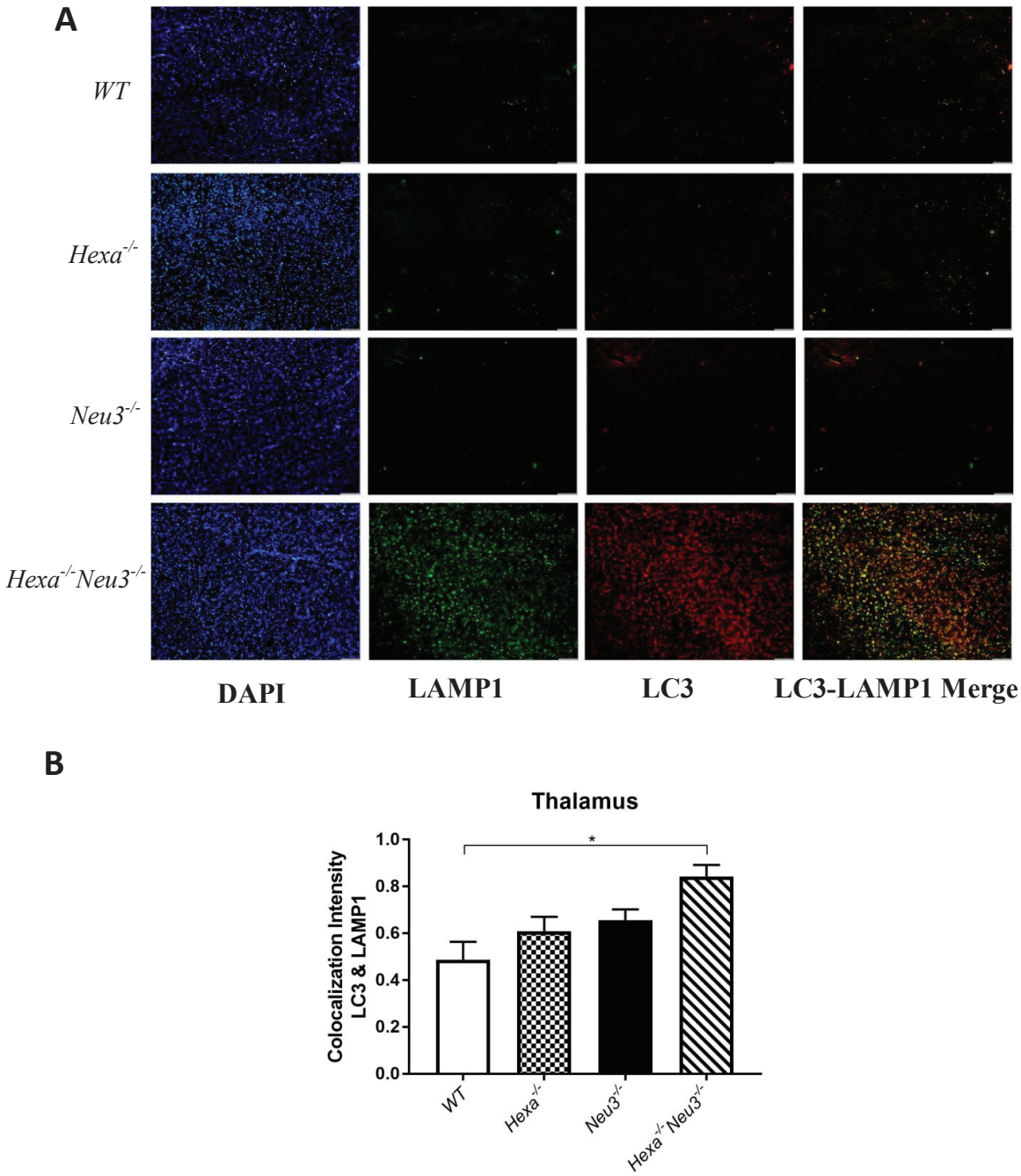

Figure 3.7. (A) Immunostaining of LC3 and LAMP1 in 4.5-month-old *WT, Hexa*$^{-/-}$*, Neu3*$^{-/-}$ and *Hexa*$^{-/-}$*Neu3*$^{-/-}$ mice brain coronal sections, thalamus region. Images were taken at 10X magnification and under same light intensity differing only for filter type. (B) Co-localization intensity of LC3 and LAMP1 measured via ImageJ. One-way-ANOVA was used to determine *p-values.* (*p<0,05, **p<0,01, ***p<0,001, ****p<0,0001)

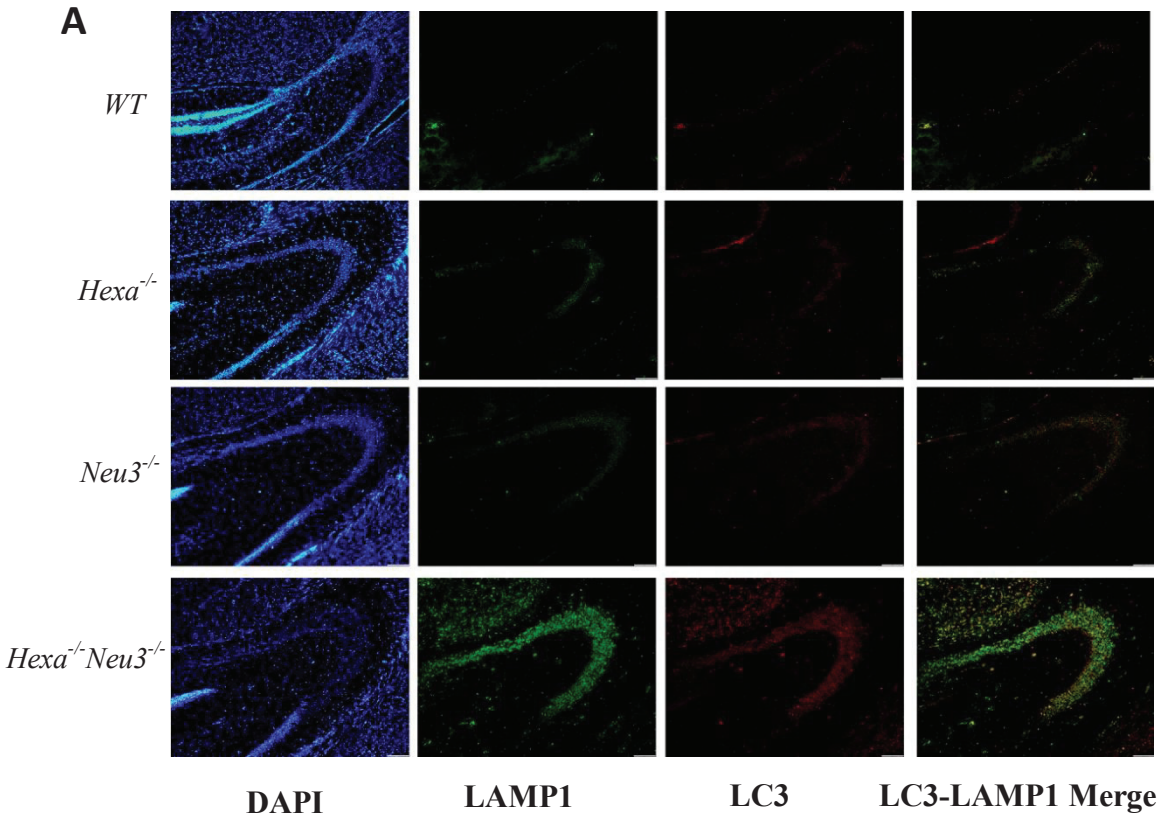

Figure 3.8. (A) Immunostaining of LC3 and LAMP1 in 4.5-month-old *WT, Hexa*$^{-/-}$*, Neu3*$^{-/-}$ and *Hexa*$^{-/-}$*Neu3*$^{-/-}$ mice brain coronal sections, hippocampal CA3 region. Images were taken at 10X magnification and under same light intensity differing only for filter type. (B) Co-localization intensity of LC3 and LAMP1 measured via ImageJ. One-way-ANOVA was used to determine *p- values.* (*p<0,05 ,**p<0,01, ***p<0,001, ****p<0,0001)

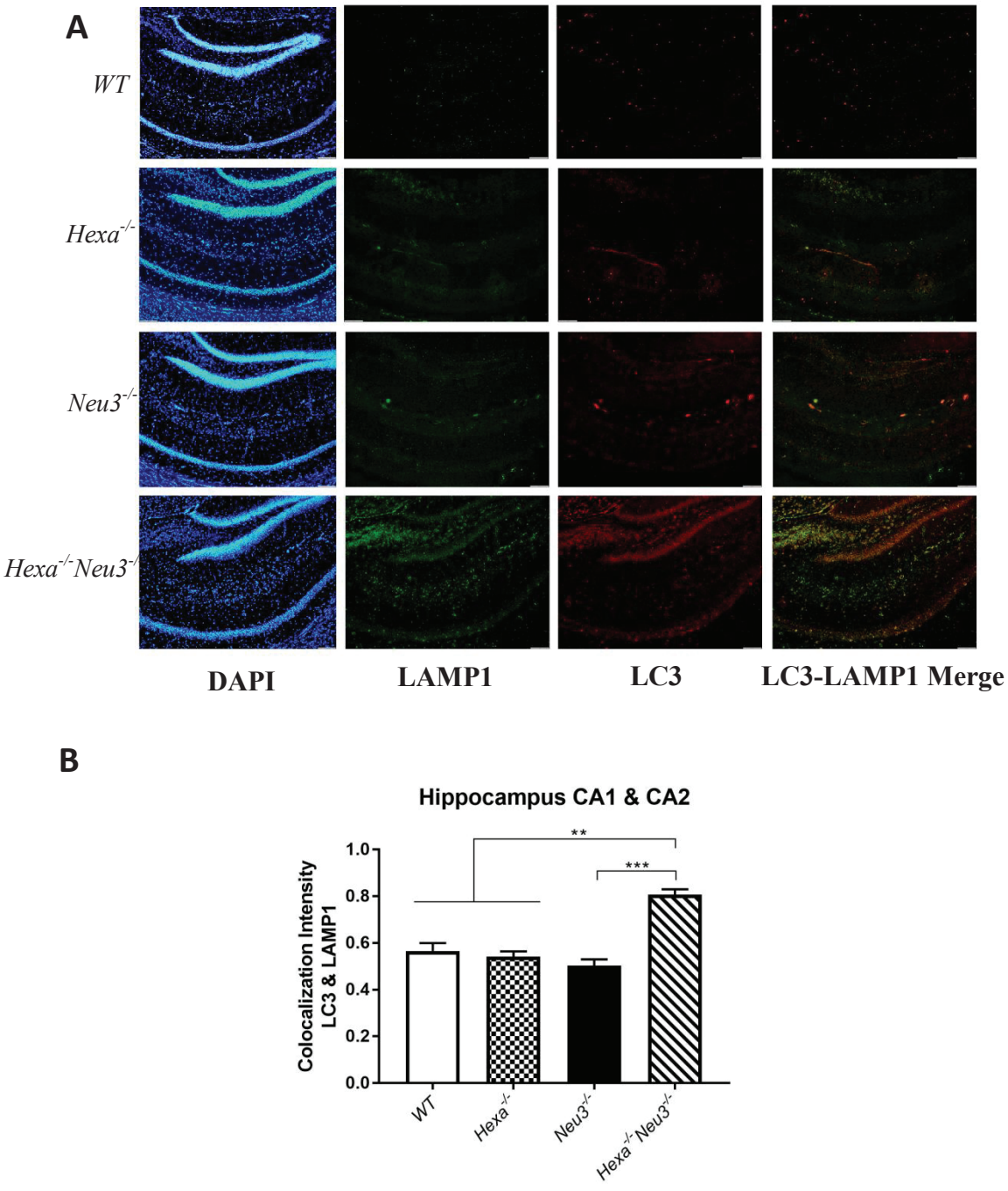

Figure 3.9. (A) Immunostaining of LC3 and LAMP1 in 4.5-month-old *WT, Hexa*$^{-/-}$, *Neu3*$^{-/-}$ and *Hexa*$^{-/-}$*Neu3*$^{-/-}$ mice brain coronal sections, hippocampal CA1 and CA2 regions. Images were taken at 10X magnification and under same light intensity differing only for filter type. (B) Co-localization intensity of LC3 and LAMP1 measured via ImageJ. One-way-ANOVA was used to determine *p- values.* (*p<0,05, **p<0,01, ***p<0,001, ****p<0,0001)

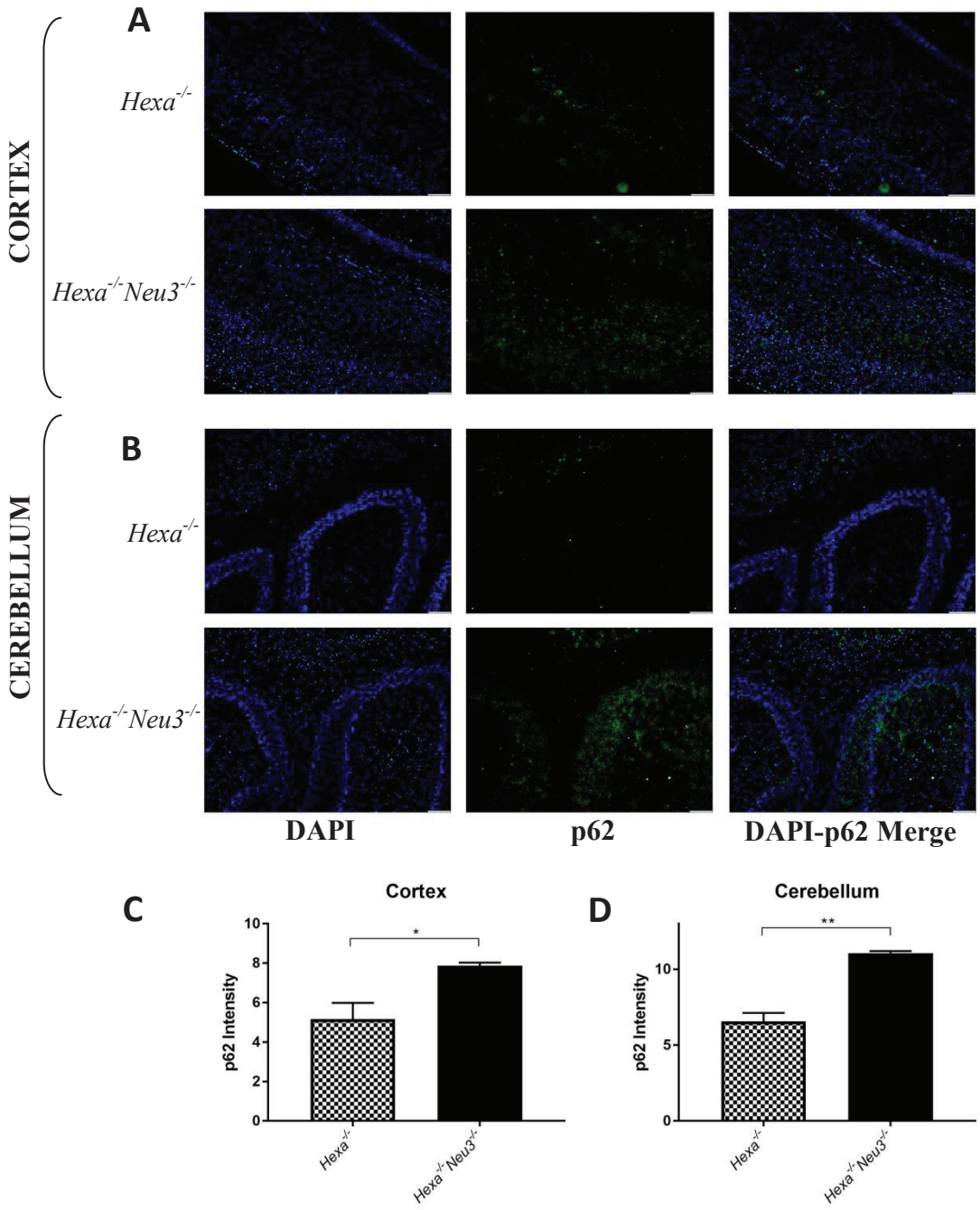

Figure 3.10. Immunostaining of p62 in 4.5-month-old *Hexa*$^{-/-}$ and *Hexa*$^{-/-}$*Neu3*$^{-/-}$ mice brain coronal sections, cortex (A) and cerebellum (B) regions. Images were taken at 10X magnification and under same light intensity differing only for filter type. Intensity of p62 fluorescence in cortex (C) and cerebellum (D) regions were measured via ImageJ. Unpaired t-test was used to determine *p- values*. (*p<0,05, **p<0,01, ***p<0,001, ****p<0,0001)

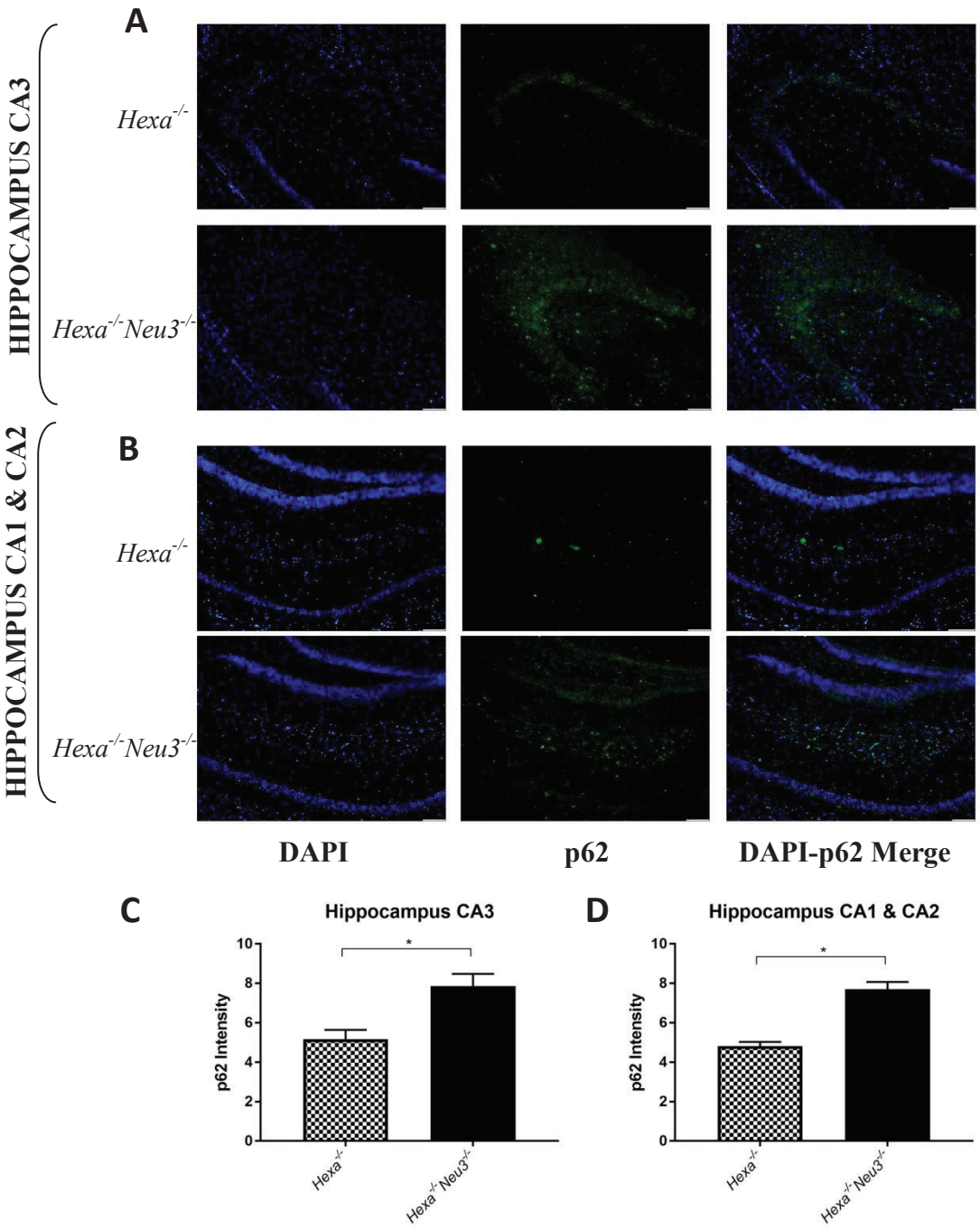

Figure 3.11. Immunostaining of p62 in 4.5-month-old *Hexa*$^{-/-}$ and *Hexa*$^{-/-}$*Neu3*$^{-/-}$ mice brain coronal sections, hippocampal CA3 (A) and CA1&CA2 (B) regions. Images were taken at 10X magnification and under same light intensity differing only for filter type. Intensity of p62 fluorescence in hippocampal CA3 (C) and CA1&CA2 (D) regions were measured via ImageJ. Unpaired t-test was used to determine *p- values*. (*p<0,05, **p<0,01, ***p<0,001, ****p<0,0001)

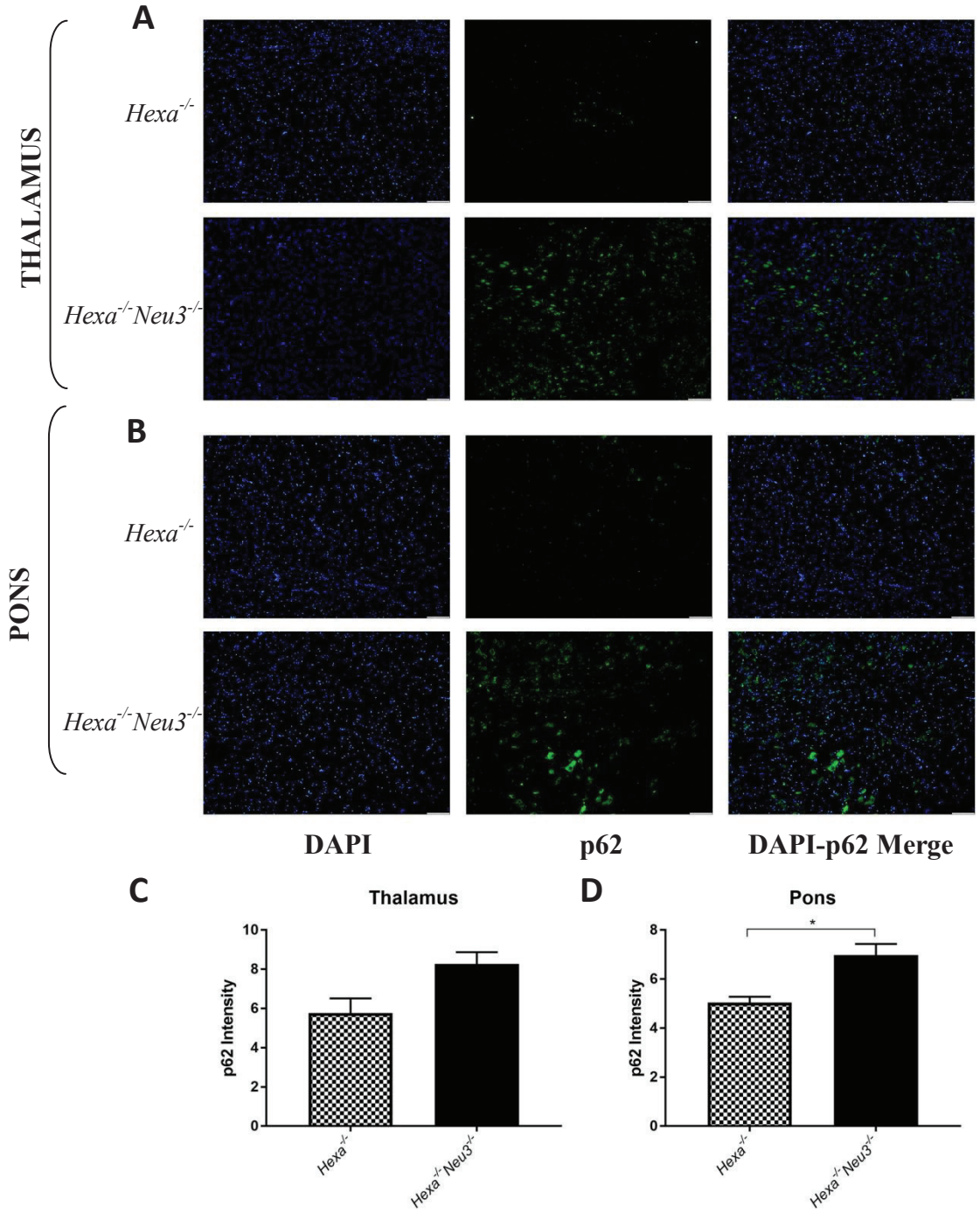

Figure 3.12. Immunostaining of p62 in 4.5-month-old *Hexa*$^{-/-}$ and *Hexa*$^{-/-}$*Neu3*$^{-/-}$ mice brain coronal sections, thalamus (A) and pons (B) regions. Images were taken at 10X magnification and under same light intensity differing only for filter type. Intensity of p62 fluorescence in thalamus (C) and pons (D) regions were measured via ImageJ. Unpaired t-test was used to determine *p- values*. (*p<0,05,**p<0,01,***p<0,001,****p<0,0001)

3.2.3. Immunocytochemistry

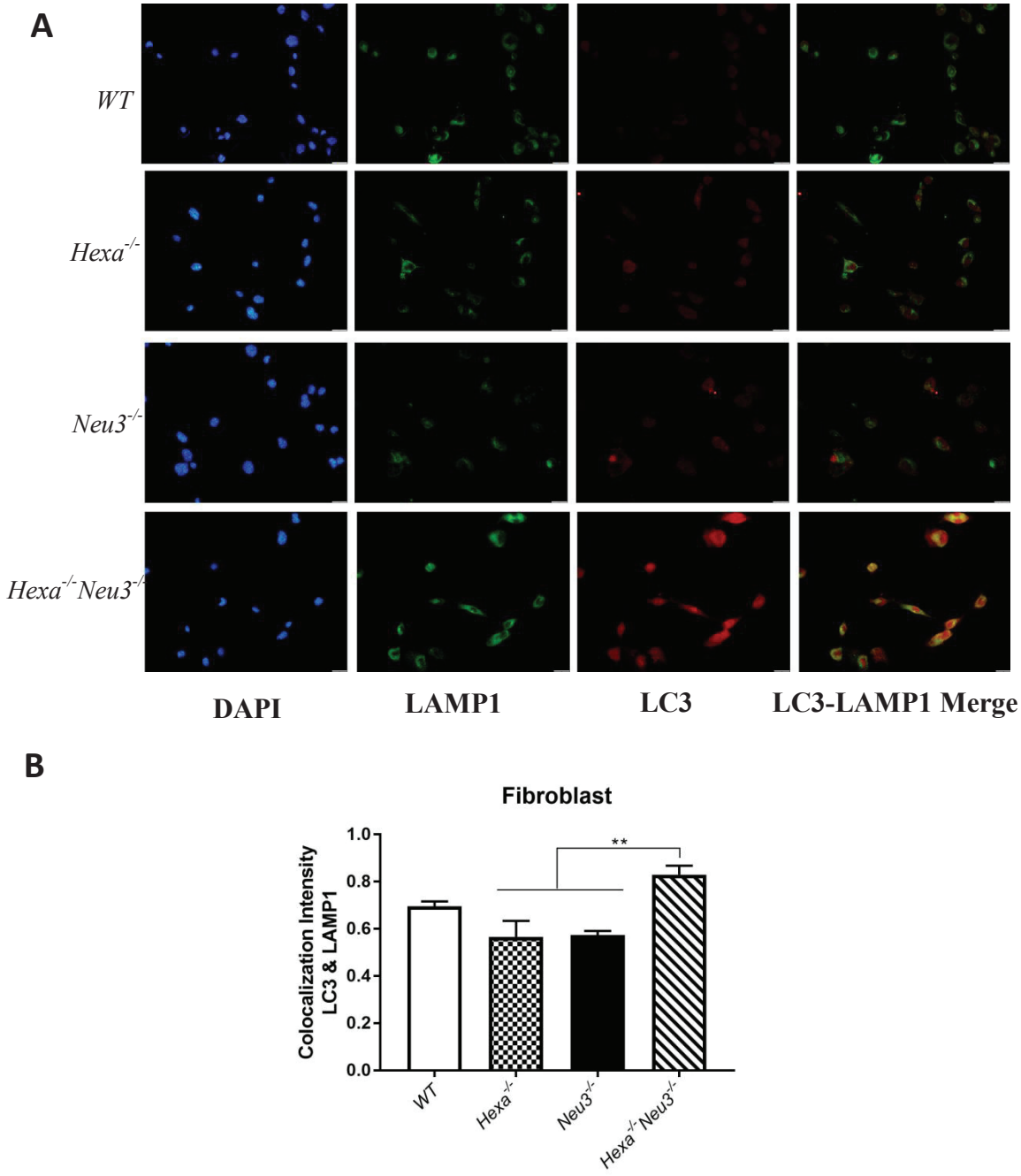

Figure 3.13. (A)Immunostaining of LC3 in *WT, Hexa*$^{-/-}$*, Neu3*$^{-/-}$ and *Hexa*$^{-/-}$*Neu3*$^{-/-}$ fibroblasts. Images were taken at 10X magnification and under same light intensity differing only for filter type. (B) Co-localization intensity of LC3 and LAMP1 measured via ImageJ. One-way-ANOVA was used to determine *p- values.* (*p<0,05,**p<0,01,***p<0,001,****p<0,0001)

Immunocytochemical analysis for LC3 and LAMP1 was performed in fibroblast samples of *WT*, *Hexa*$^{-/-}$, *Neu3*$^{-/-}$ and *Hexa*$^{-/-}$*Neu3*$^{-/-}$ mice as well. The results indicated that, LC3 and LAMP1 co-localization is significantly elevated for fibroblasts from

Hexa$^{-/-}$*Neu3*$^{-/-}$ mice when compared to that of *Hexa*$^{-/-}$ and *Neu3*$^{-/-}$ fibroblasts (Figure 3.13).

3.3. ER-Stress – Oxidative Stress and Apoptosis Related Analysis

In order to understand the whether there is an alteration in oxidative stress and ER-stress related apoptotic mechanism in Tay-Sachs disease mouse model, the markers listed in Table 1.3 are analyzed by RT-PCR, flow cytometry, western blot and immunocytochemistry.

3.3.1. Real Time PCR

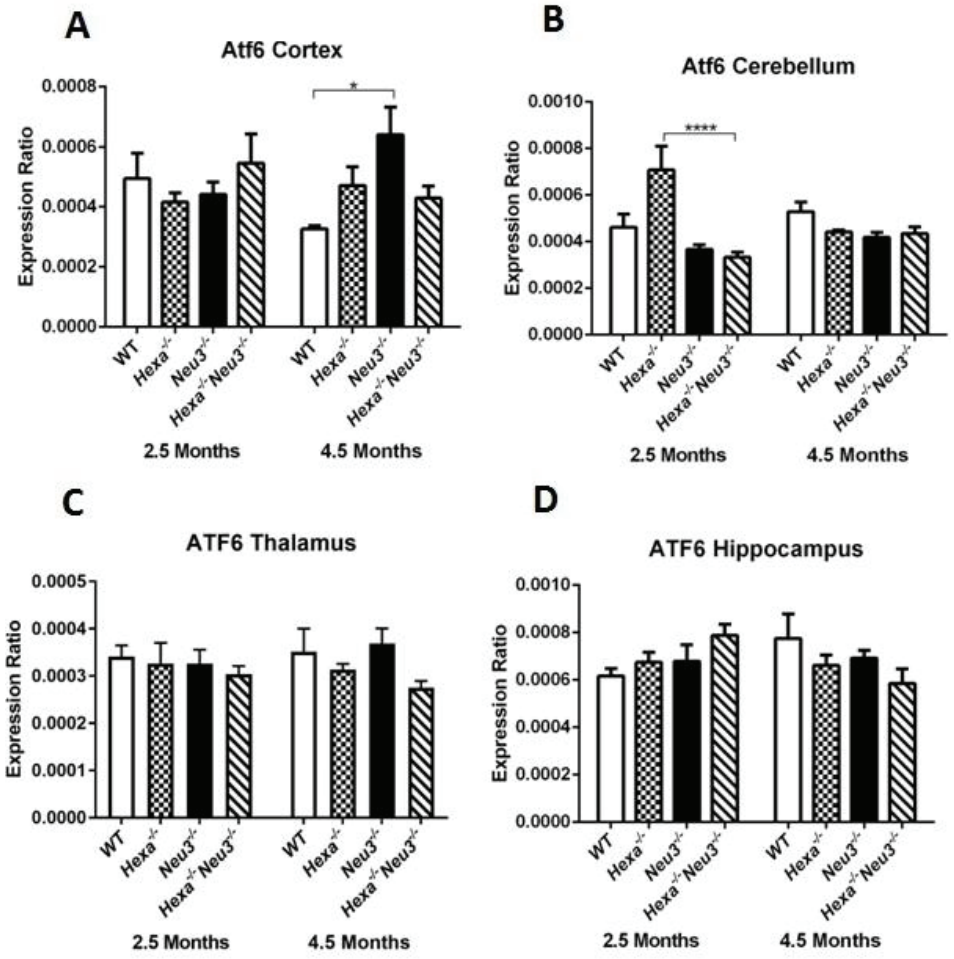

Figure 3.14. ATF6 gene expression levels of cortex (A), cerebellum(B), thalamus(C) and hippocampus (D) tissues of 2.5- and 4.5-month-old *WT, Hexa*$^{-/-}$*, Neu3*$^{-/-}$ and *Hexa*$^{-/-}$*Neu3*$^{-/-}$ mice. (n=3; *p<0,05, **p<0,01, ***p<0,001, ****p<0,0001) Expression ratios were calculated by ΔCT method and 2-way-ANOVA analysis was used to determine p-values via GraphPad.

Expression analysis of ATF6, Calnexin and XBP1 markers were performed to have a better understanding of ER-stress in early-onset Tay - Sachs disease model on RNA level. In cortex of 4.5-month-old *Neu3*$^{-/-}$ mice significantly increased ATF6 expression was observed when compared to its *WT* littermates (Figure 3.14.A) and in cerebellum of 2.5-month-old *Hexa*$^{-/-}$*Neu3*$^{-/-}$ mice significantly decreased ATF6 expression was displayed when compared to its *Hexa*$^{-/-}$ counterparts (Figure 3.14.B). However, no significant difference was observed in ATF6 expression for thalamus and hippocampus regions (Figure 3.14.C and D).

As for Calnexin, in cerebellum of 4.5-month-old *Hexa*$^{-/-}$*Neu3*$^{-/-}$ mice significantly increased Calnexin expression when compared to 2.5-month-old *Hexa*$^{-/-}$ *Neu3*$^{-/-}$mice (Figure 3.15.B). On the other hand there was no significant difference for Calnexin expression in other brain regions except for the slight increase in 2.5- and 4.5-month-old *Hexa*$^{-/-}$*Neu3*$^{-/-}$ mice compared with that of *WT* (Figure 3.15.A, C and D).

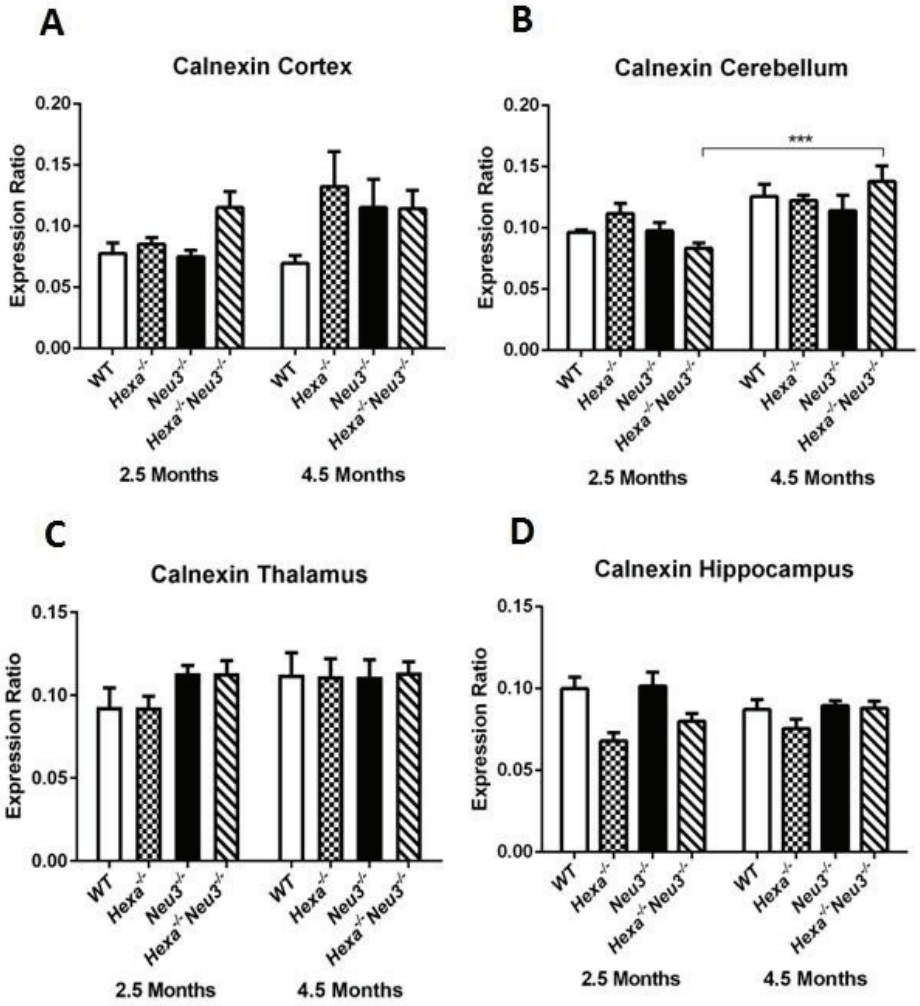

Figure 3.15. Calnexin gene expression levels of cortex (A), cerebellum(B), thalamus(C) and hippocampus (D) tissues of 2.5- and 4.5-month-old *WT, Hexa*$^{-/-}$*, Neu3*$^{-/-}$ and *Hexa*$^{-/-}$*Neu3*$^{-/-}$ mice. (n=3; *p<0,05, **p<0,01, ***p<0,001, ****p<0,0001). Expression ratios were calculated by ΔCT method and 2-way-ANOVA analysis was used to determine p-values via GraphPad.

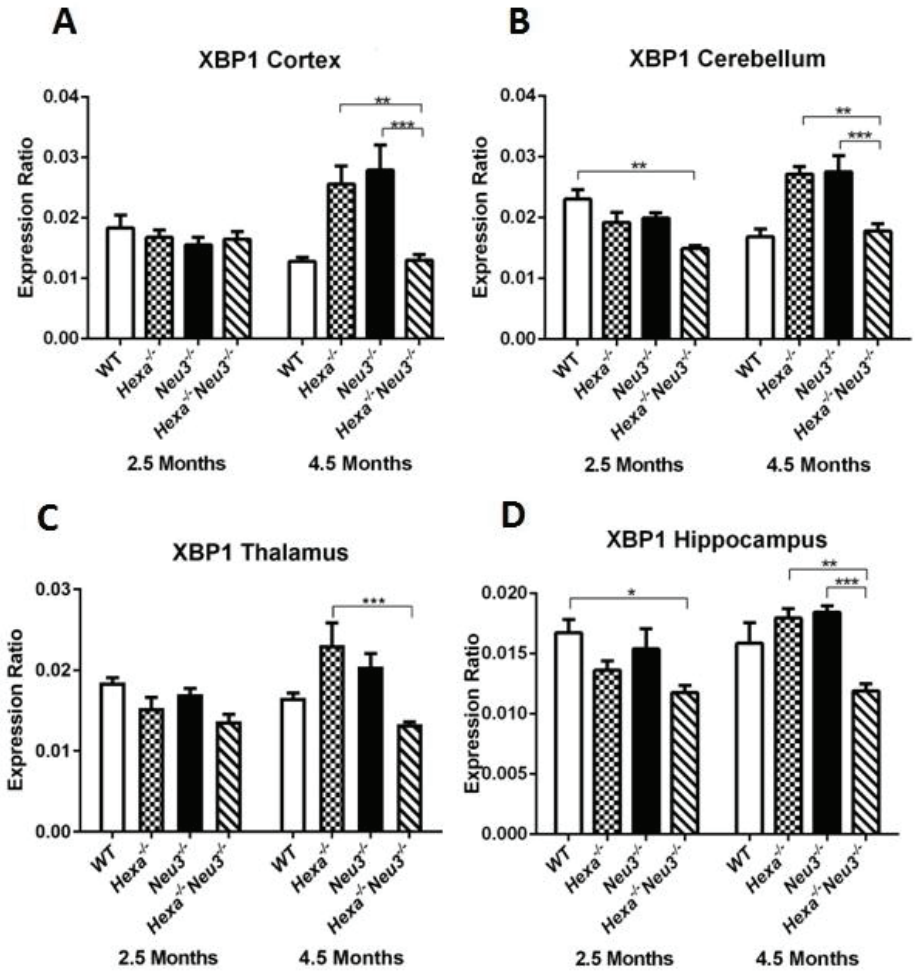

Figure 3.16. XBP1 gene expression levels of cortex (A), cerebellum(B), thalamus(C) and hippocampus (D) tissues of 2.5- and 4.5-month-old *WT, Hexa*$^{-/-}$*, Neu3*$^{-/-}$ and *Hexa*$^{-/-}$*Neu3*$^{-/-}$ mice. (n=3; *p<0,05, **p<0,01, ***p<0,001,****p<0,0001). Expression ratios were calculated by ΔCT method and 2-way-ANOVA analysis was used to determine p-values via GraphPad.

XBP1 expression was significantly decreased in all of the brain regions of 4.5-month-old *Hexa*$^{-/-}$*Neu3*$^{-/-}$ mice compared to *Hexa*$^{-/-}$ littermates. The significantly decreased XBP1 expression in 4.5-month old *Hexa*$^{-/-}$*Neu3*$^{-/-}$ mice comparing to *Neu3*$^{-/-}$ counterparts was also observed in all brain regions except for thalamus. In hippocampus and cerebellum of 2.5-month-old *Hexa*$^{-/-}$*Neu3*$^{-/-}$ mice significantly decreased XBP1 expression was detected when compared to their *WT* littermates (Figure 3.16.A, B, C and D)

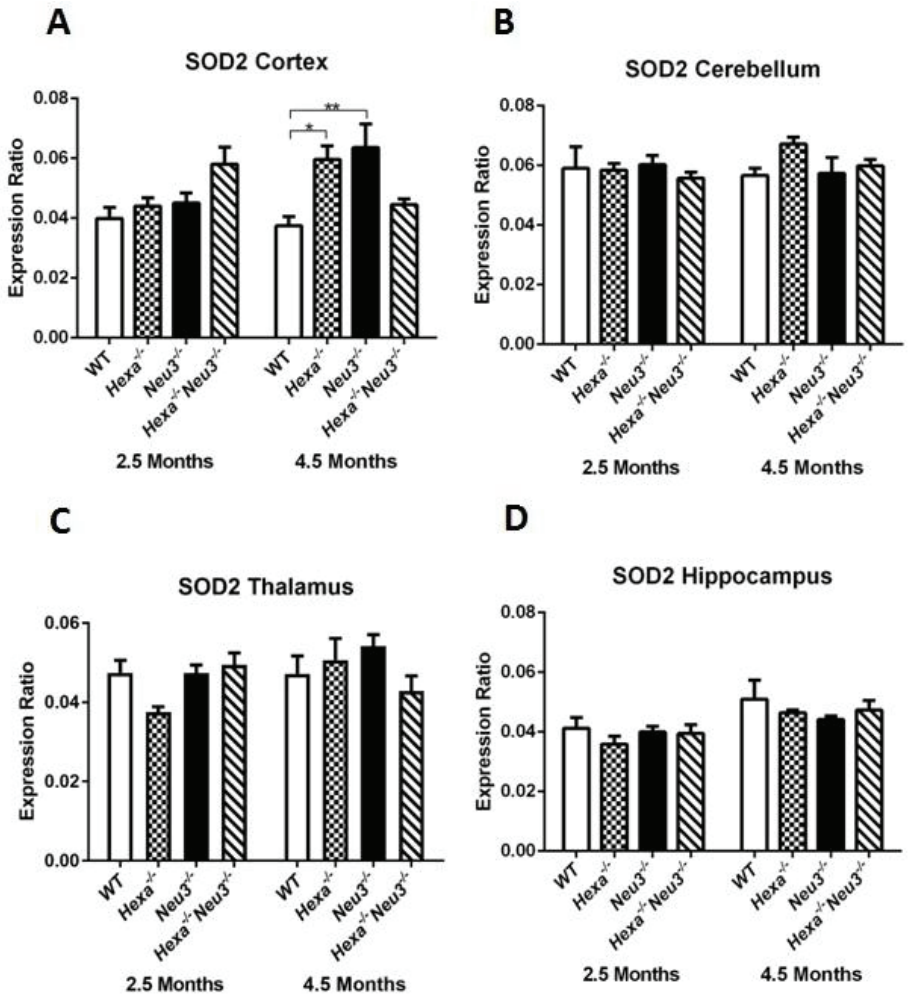

Figure 3.17. SOD2 gene expression levels of cortex (A), cerebellum(B), thalamus(C) and hippocampus (D) tissues of 2.5- and 4.5-month-old *WT, Hexa*$^{-/-}$*, Neu3*$^{-/-}$ and *Hexa*$^{-/-}$*Neu3*$^{-/-}$ mice. (n=3; *p<0,05 ,**p<0,01, ***p<0,001, ****p<0,0001). Expression ratios were calculated by ΔCT method and 2-way-ANOVA analysis was used to determine p-values via GraphPad.

SOD2, Catalase and Ttase1 are oxidative stress markers and their expression was measured in order to understand whether there is a change oxidative stress mechanism on RNA level. SOD2 expression did not exhibit significant change except for cortex of 4.5-month-old *Hexa*$^{-/-}$ and *Neu3*$^{-/-}$ mice when compared to their *WT* littermates (Figure 3.17.A, B, C and D).

In the expression analysis for Catalase gene, there was also no significant change in any of the brain regions except for thalamus of 2.5-month-old *Hexa*$^{-/-}$*Neu3*$^{-/-}$ mice in which it is significantly increased compared to its *Hexa*$^{-/-}$ littermates.(Figure 3.18. A, B,C and D)

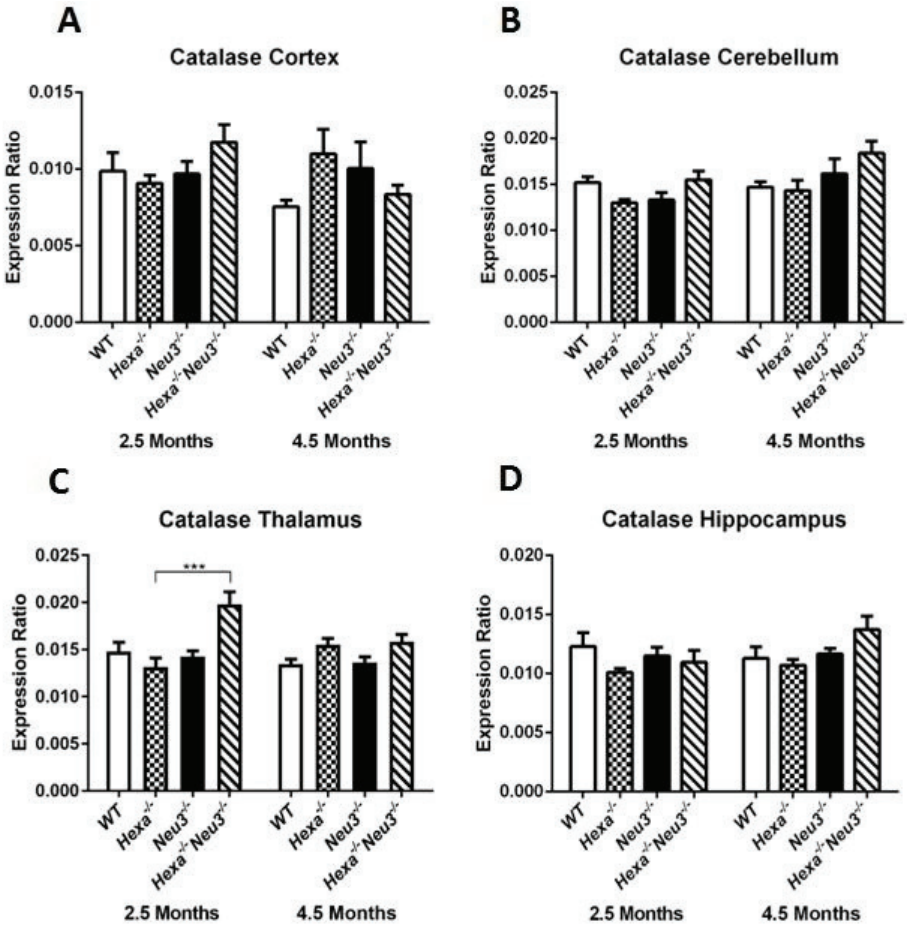

Figure 3.18. Catalase gene expression levels of cortex (A), cerebellum(B), thalamus(C) and hippocampus (D) tissues of 2.5- and 4.5-month-old *WT, Hexa*$^{-/-}$*, Neu3*$^{-/-}$ and *Hexa*$^{-/-}$*Neu3*$^{-/-}$ mice. (n=3; *p<0,05, **p<0,01, ***p<0,001, ****p<0,0001). Expression ratios were calculated by ΔCT method and 2-way-ANOVA analysis was used to determine p-values via GraphPad.

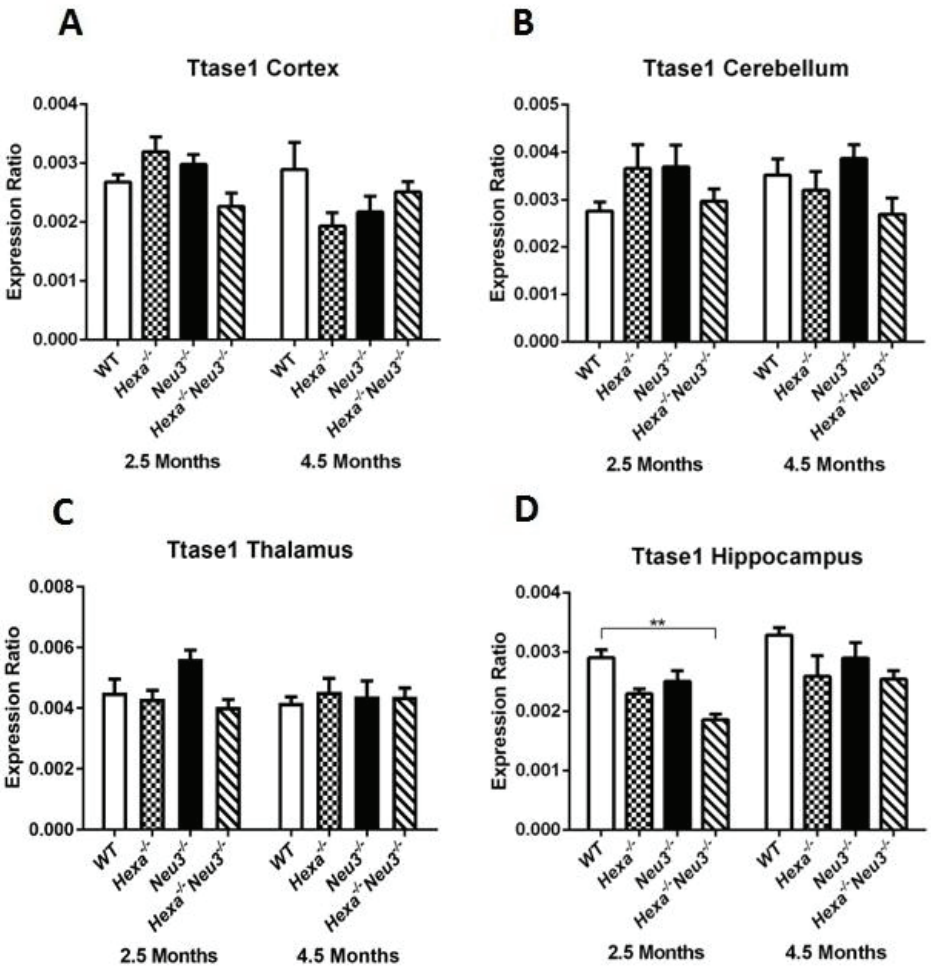

Figure 3.19. Ttase1gene expression levels of cortex (A), cerebellum(B), thalamus(C) and hippocampus(D) tissues of 2.5- and 4.5-month-old *WT, Hexa*$^{-/-}$*, Neu3*$^{-/-}$ and *Hexa*$^{-/-}$*Neu3*$^{-/-}$ mice. (n=3; *p<0,05, **p<0,01, ***p<0,001, ****p<0,0001). Expression ratios were calculated by ΔCT method and 2-way-ANOVA analysis was used to determine p-values via GraphPad.

For Ttase1 expression significant decrease was observed for 2.5-month-old *Hexa*$^{-/-}$*Neu3*$^{-/-}$ mice compared to that of *WT* counterparts. Moreover; even if it is not significant, slight decrease in Ttase1 expression was also displayed for cerebellum and hippocampus of 4.5-month old *Hexa*$^{-/-}$*Neu3*$^{-/-}$ when compared to their other littermates (Figure 3.19. A, B, C and D).

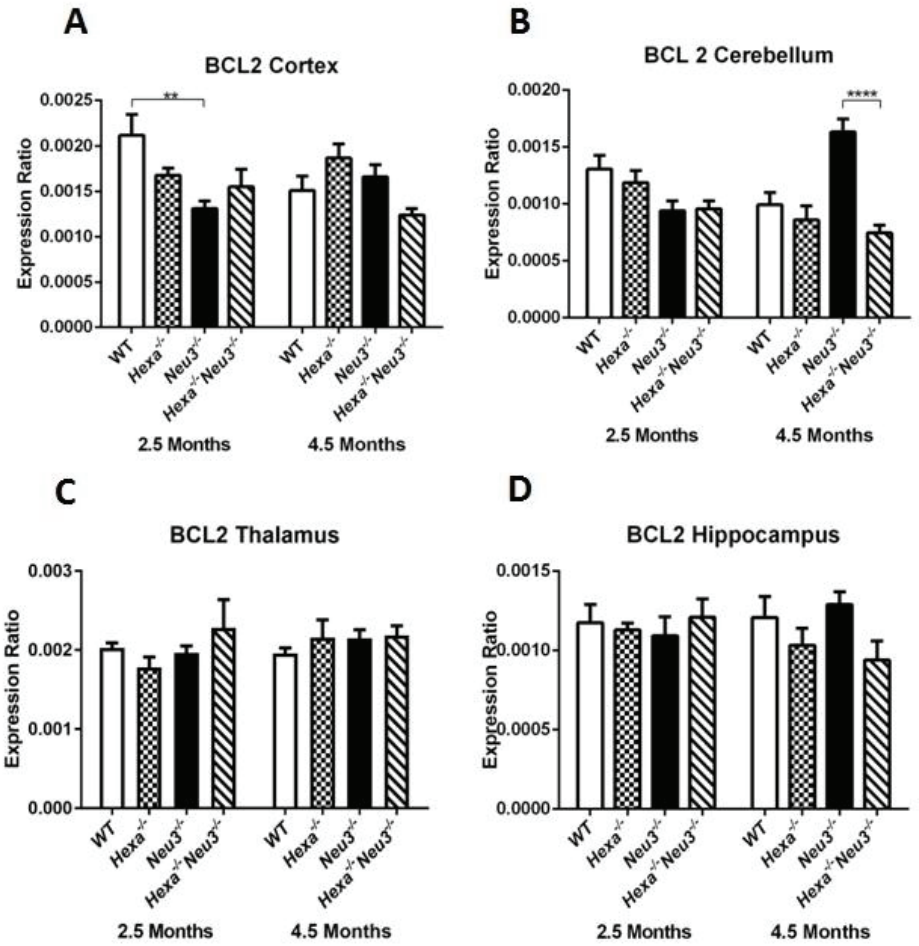

Figure 3.20. BCL2 gene expression levels of cortex (A), cerebellum(B), thalamus(C) and hippocampus(D) tissues of 2.5- and 4.5-month-old *WT, Hexa*$^{-/-}$*, Neu3*$^{-/-}$ and *Hexa*$^{-/-}$*Neu3*$^{-/-}$ mice. (n=3; *p<0,05, **p<0,01, ***p<0,001, ****p<0,0001). Expression ratios were calculated by ΔCT method and 2-way-ANOVA analysis was used to determine p-values via GraphPad.

BCL2, BCL XL and Bax involves in apoptotic regulation and their expressions were also analyzed by RT-PCR. In cortex of 2.5-month-old *Neu3*$^{-/-}$ BCL2 expression was significantly decreased when compared to *WT* counterparts. Significant increase in BCL2 expression in cerebellum of 4.5-month-old *Neu3*$^{-/-}$ was also detected comparing to its other littermates. For hippocampus and thalamus no significant change was observed but slight increase in BCL2 expression in 4.5-month-old *Hexa*$^{-/-}$*Neu3*$^{-/-}$ was also observed when compared to *WT* and *Neu3*$^{-/-}$ counterparts (Figure 3.20. A, B, C and D).

BCL XL and Bax expression did not exhibit significant changes for any of the brain regions and age groups. (Figure 3.21 and Figure 3.22)

.

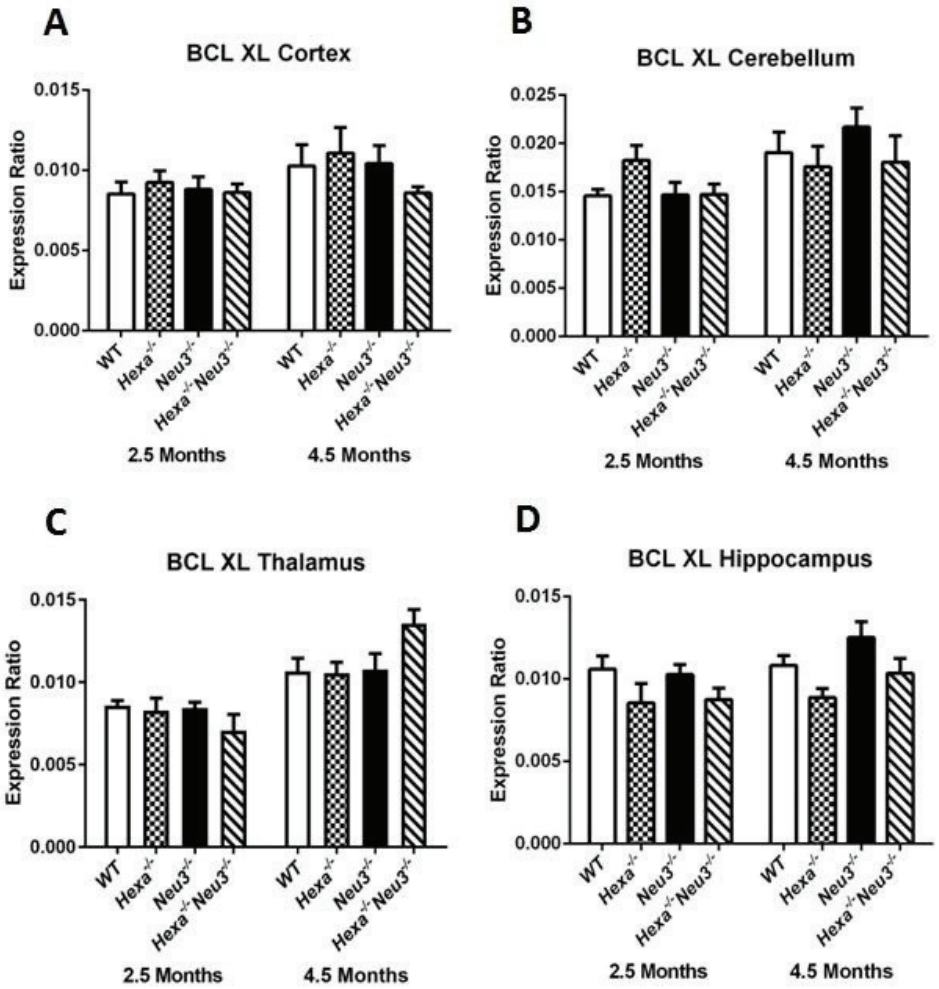

Figure 3.21. BCL XL gene expression levels of cortex (A), cerebellum(B), thalamus(C) and hippocampus (D) tissues of 2.5- and 4.5-month-old *WT, Hexa*$^{-/-}$*, Neu3*$^{-/-}$ and *Hexa*$^{-/-}$*Neu3*$^{-/-}$ mice. (n=3). Expression ratios were calculated by ΔCT method and 2-way-ANOVA analysis was used to determine p-values via GraphPad.

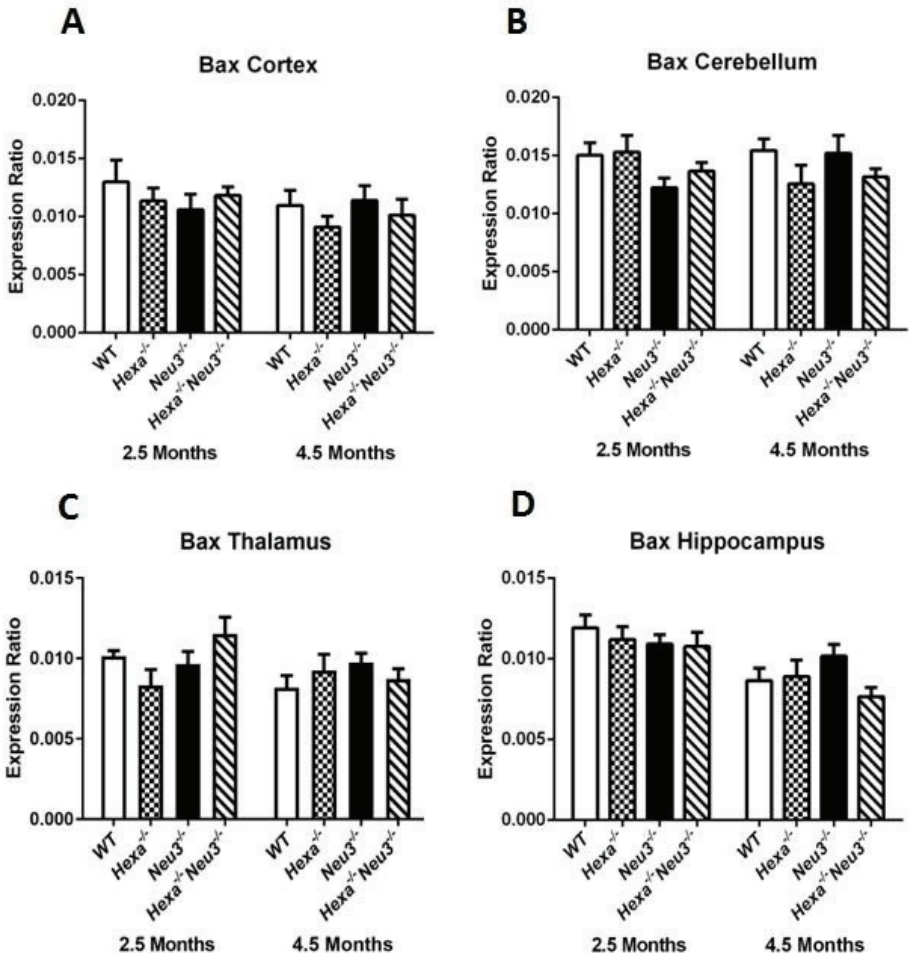

Figure 3.22. Bax gene expression levels of cortex (A), cerebellum(B), thalamus(C) and hippocampus of 2.5- and 4.5-month-old *WT, Hexa*$^{-/-}$*, Neu3*$^{-/-}$ and *Hexa*$^{-/-}$ *Neu3*$^{-/-}$ mice. (n=3) Expression ratios were calculated by ΔCT method and 2-way-ANOVA analysis was used to determine p-values via GraphPad.

3.3.2. Flow Cytometry

Intracellular ROS level was measured applying flow cytometric analysis by using nonflurometric dye H_2DCFDA which is oxidized to fluorimetric DCF in the presence of ROS. Negative control samples which were not treated with H_2DCFDA did not exhibit any fluorescence accordingly. In positive control group hydrogen peroxide treatment provided increased ROS level for each genotype however the one for *Hexa*$^{-/-}$ *Neu3*$^{-/-}$ fibroblast was significantly higher compared to *WT* and *Hexa*$^{-/-}$ fibroblasts. In sample group which were only treated with H_2DCFDA, significantly increased intracellular ROS level was demonstrated for *Hexa*$^{-/-}$*Neu3*$^{-/-}$ fibroblasts when compared to that of *Hexa*$^{-/-}$ and *Neu3*$^{-/-}$ fibroblast samples. (Figure 3.26)

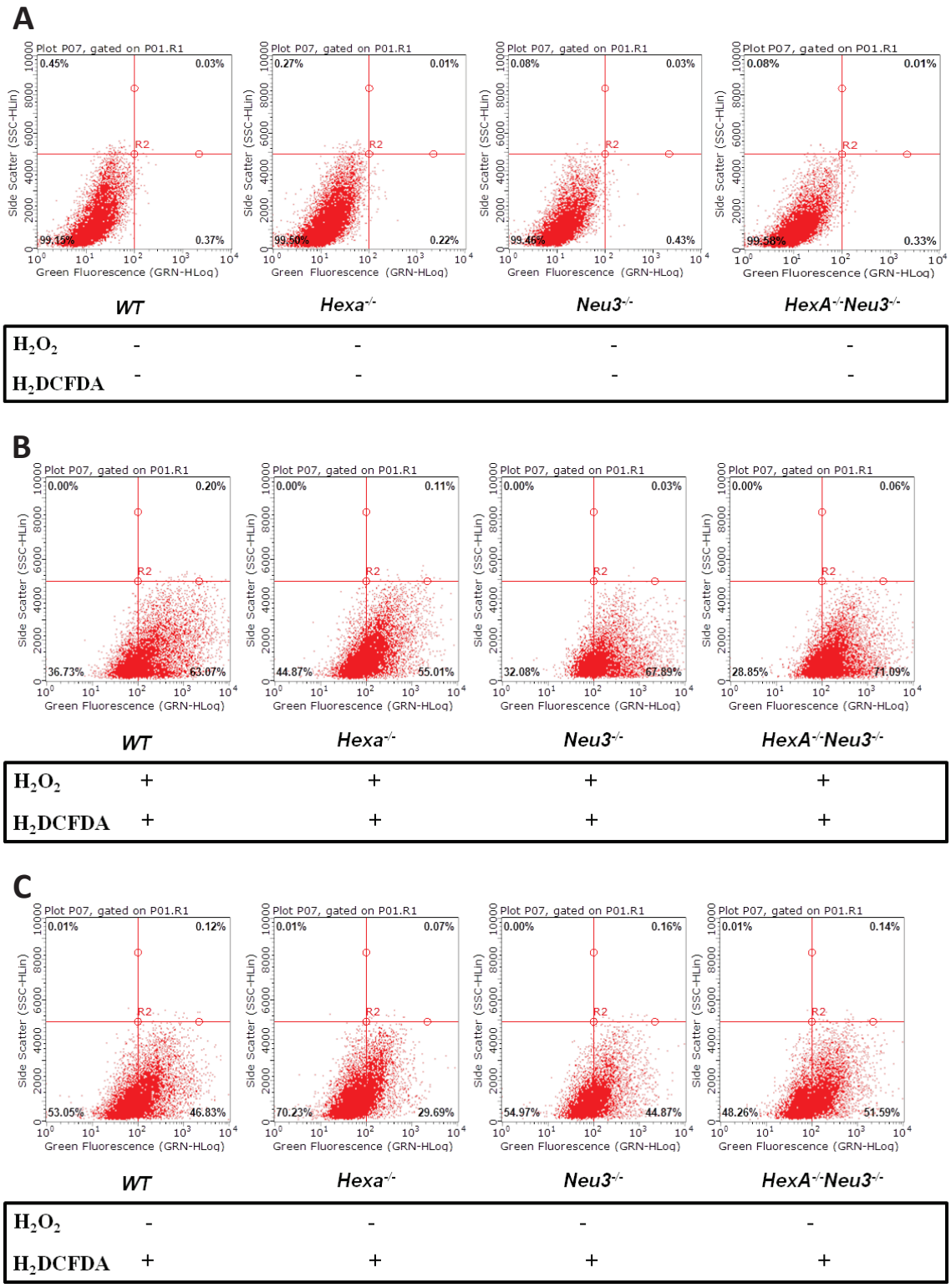

Figure 3.23. Intracellular ROS level measurement of fibroblasts of *WT, Hexa*$^{-/-}$*, Neu3*$^{-/-}$ and *Hexa*$^{-/-}$*Neu3*$^{-/-}$ mice. Flow cytometric analysis of H_2DCFDA for negative control (A), positive control (B) and sample group (C) also oxidized DCF percentages were plotted (D). (*p<0,05, **p<0,01, ***p<0,001, ****p<0,0001)

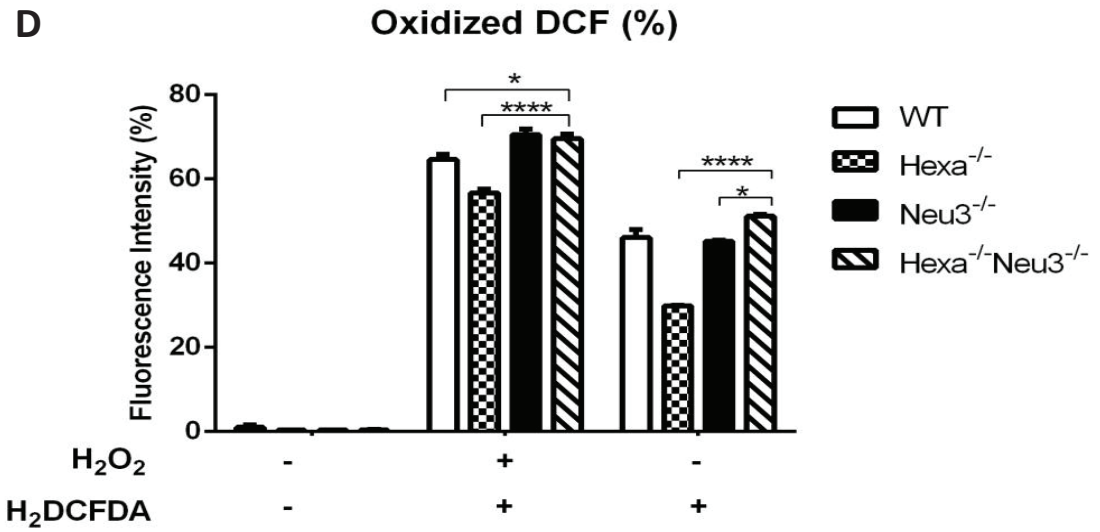

Figure 3.23 (cont.)

3.3.3. Western Blot

Western blot analysis for APE1/Ref-1 protein was performed by using cortex,cerebellum, thalamus and hippocampus regions and also fibroblasts of *WT, Hexa*$^{-/-}$*, Neu3*$^{-/-}$ and *Hexa*$^{-/-}$*Neu3*$^{-/-}$ mice.

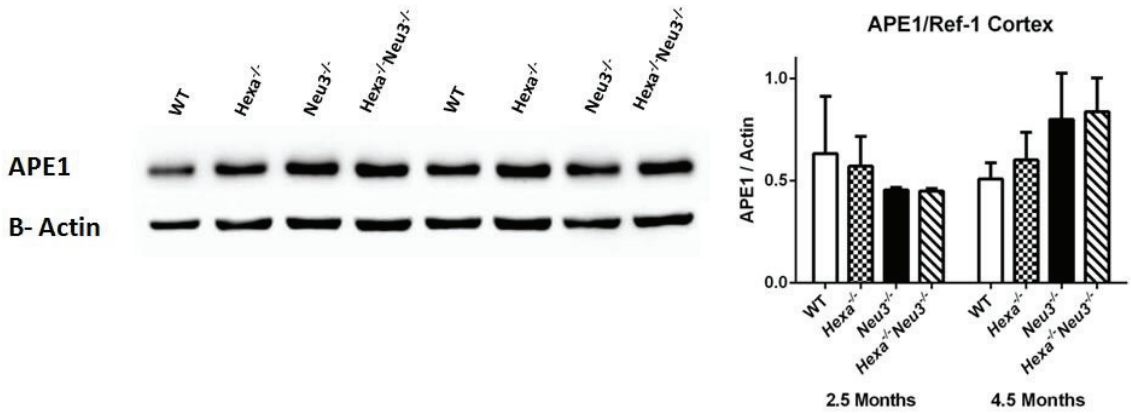

Figure 3.24. Western blot analysis of APE1/Ref-1 in cortex region of 2.5 and 4.5-month-,old *WT, Hexa*$^{-/-}$*, Neu3*$^{-/-}$ and *Hexa*$^{-/-}$*Neu3*$^{-/-}$ mice (n=3;*p<0,05,**p<0,01,***p<0,001,****p<0,0001)

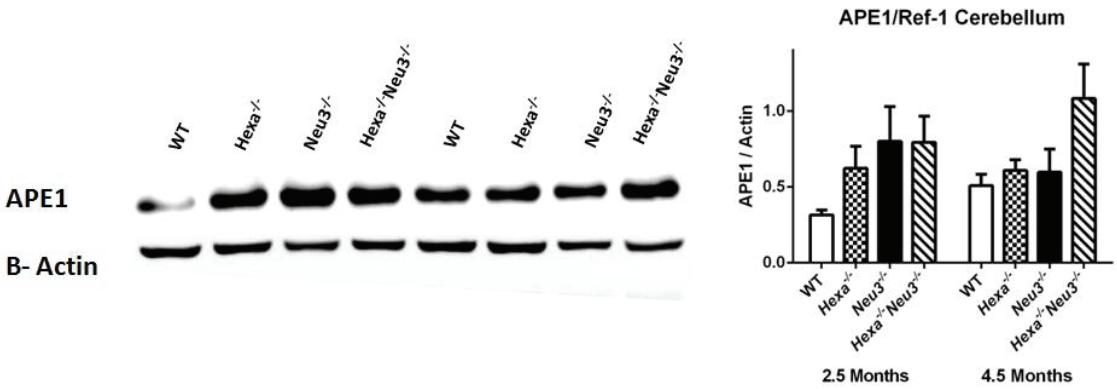

Figure 3.25. Western blot analysis of APE1/Ref-1 in cerebellum region of 2.5 and 4.5-month-,old *WT, Hexa*$^{-/-}$*, Neu3*$^{-/-}$ and *Hexa*$^{-/-}$*Neu3*$^{-/-}$ mice (n=3;*p<0,05,**p<0,01,***p<0,001,****p<0,0001)

Expression analysis of APE-1/Ref1 in cortex region showed no significant change however a slight increase in 4.5-month-old *Hexa*$^{-/-}$*Neu3*$^{-/-}$ was observable compared to its *WT* littermates (Figure 3.24). For cerebellum same trait was observed but the increase in 4.5-month-old *Hexa*$^{-/-}$*Neu3*$^{-/-}$mice comparing to its other littermates was more noticeable than that of cortex. Moreover slight increase was also detected in cerebellum of 2.5-month-old *Hexa*$^{-/-}$*Neu3*$^{-/-}$ mice comparing to its *WT* counterparts (Figure 3.25).

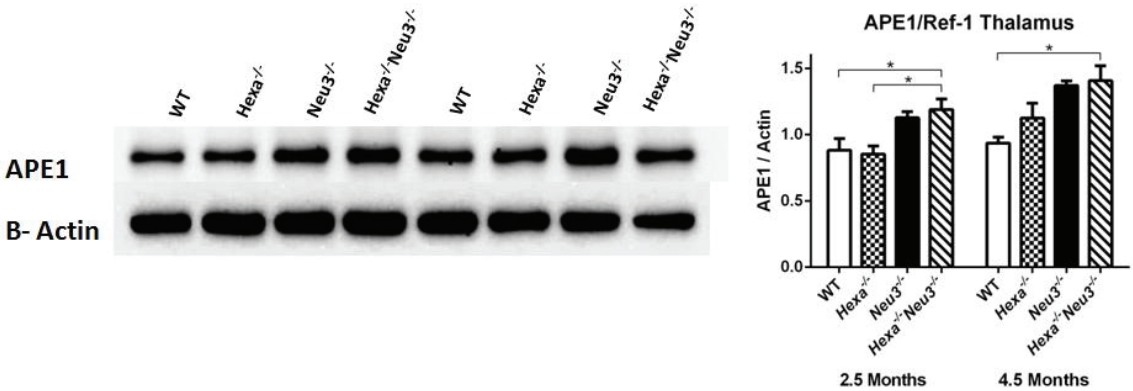

Figure 3.26. Western blot analysis of APE1/Ref-1 in thalamus region of 2.5- and 4.5-month-,old *WT, Hexa*$^{-/-}$*, Neu3*$^{-/-}$ and *Hexa*$^{-/-}$*Neu3*$^{-/-}$ mice (n=3;*p<0,05,**p<0,01,***p<0,001,****p<0,0001)

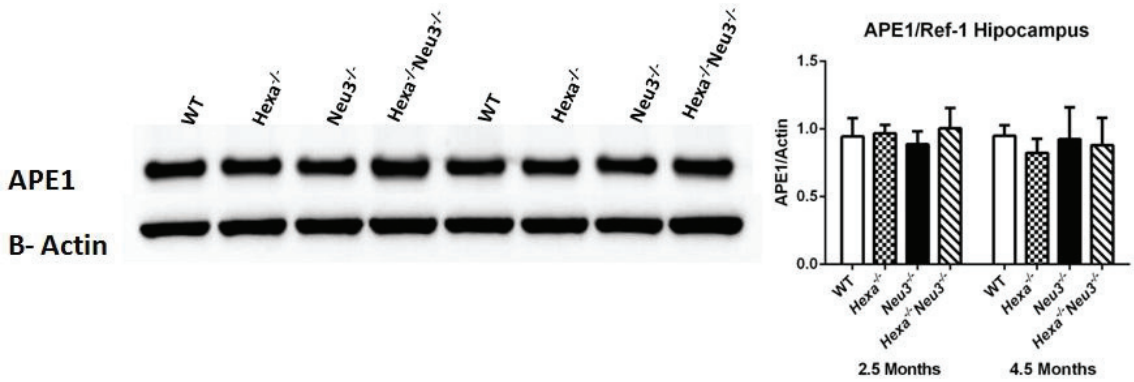

Figure 3.27. Western blot analysis of APE1/Ref-1 in hippocampus region of 2.5 and 4.5-month-,old *WT, Hexa*$^{-/-}$*, Neu3*$^{-/-}$ and *Hexa*$^{-/-}$*Neu3*$^{-/-}$ mice (n=3; *p<0,05, **p<0,01, ***p<0,001,****p<0,0001).

In thalamus region, significantly increased APE1/Ref-1 expression was observed in 2,5-month-old *Hexa*$^{-/-}$*Neu3*$^{-/-}$ mice when compared to its both *WT* and *Neu3*$^{-/-}$ littermates. In 4.5-month-old group, expression of APE1/Ref-1 was detected to be significantly increased in *Hexa*$^{-/-}$*Neu3*$^{-/-}$ mice compared to that of *WT* (Figure 3.26).

APE1/Ref-1 expression did not exhibit detectable change in hippocampus region of *WT, Hexa*$^{-/-}$*, Neu3*$^{-/-}$ and *Hexa*$^{-/-}$*Neu3*$^{-/-}$ mice (Figure 3.27).

In western blot analysis performed on fibroblast samples, APE1/Ref-1 expression did not exhibit any significant change for any genotype (Figure 3.28).

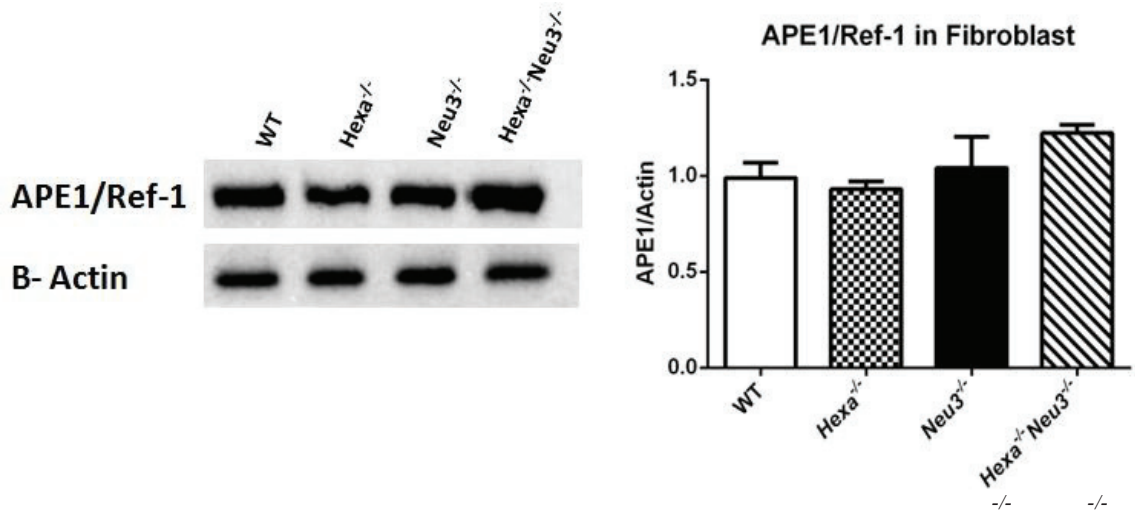

Figure 3.28. Western blot analysis of APE1/Ref-1 in fibroblasts of *WT, Hexa*$^{-/-}$*,Neu3*$^{-/-}$ and *Hexa*$^{-/-}$ *Neu3*$^{-/-}$ mice.

3.3.4. Immunocytochemistry

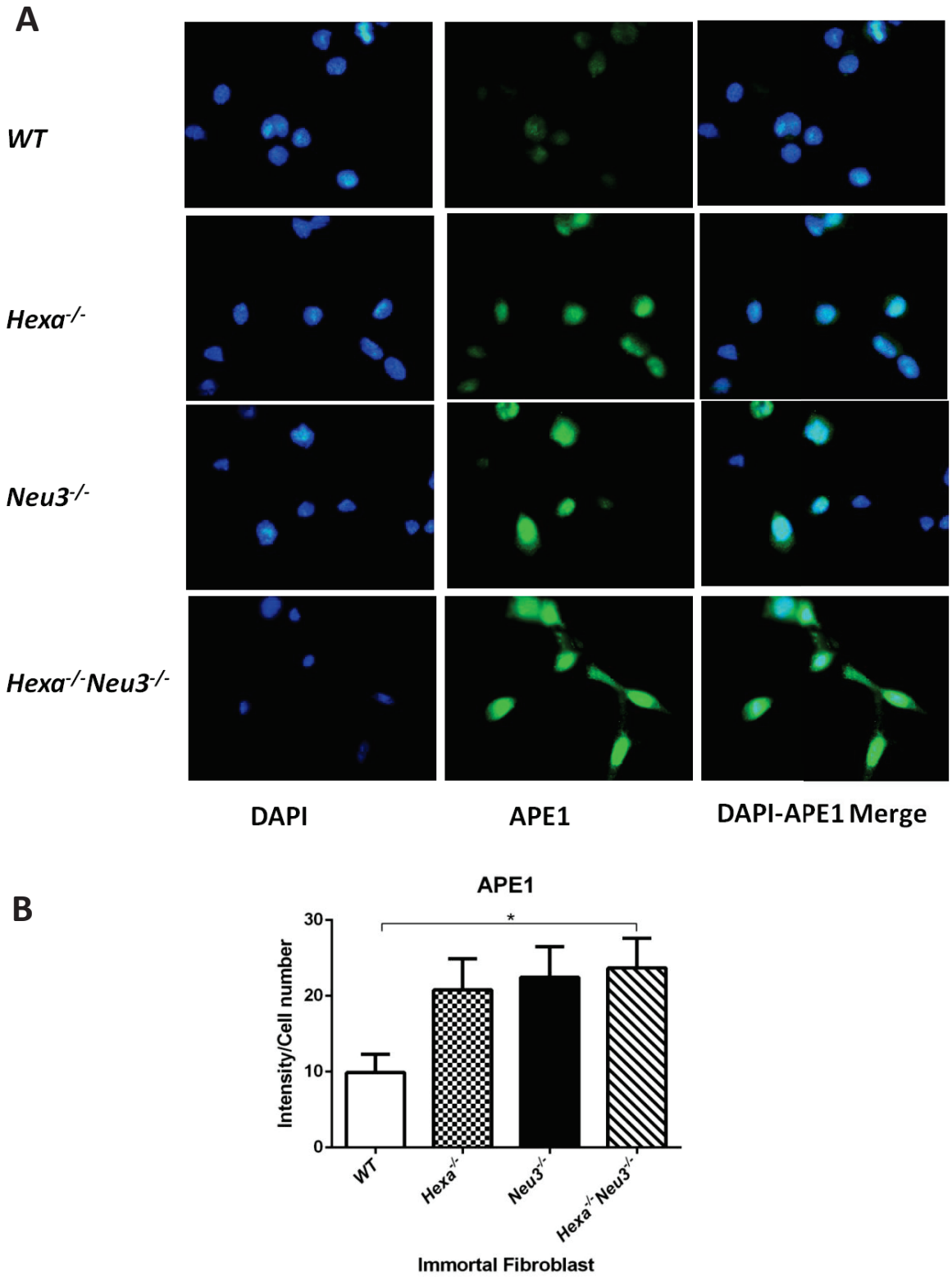

Figure 3.29. Immunostaining of APE1/Ref-1 in *WT, Hexa*$^{-/-}$*, Neu3*$^{-/-}$ and *Hexa*$^{-/-}$*Neu3*$^{-/-}$ fibroblasts. Magnification is 10X, scale bar is for 100μm. Images for each genotype were taken under same light intensity differing only for filter type.

The expression and the localization of APE1/Ref-1, which are known to be mainly regulated by ROS levels were measured by immunocytochemical analysis and significantly increased cytoplasmic APE1/Ref-1 expression was demonstrated in fibroblasts of *Hexa*$^{-/-}$*Neu3*$^{-/-}$ mice when compared to its other counterparts (Figure 3.29. A and B).

CHAPTER 4

DISCUSSION

Tay - Sachs disease is an autosomal recessively inherited severe lysosomal storage disorder that mainly affects the central nervous system. It is caused by mutations on the HEXA gene encoding α-subunit of β-Hexosaminidase A enzyme. The enzyme normally catalyzes GM2 to GM3 conversion but when it is absent or dysfunctional the GM2 degradation is interrupted. The undegraded GM2 ganglioside is progressively accumulated especially in neurons and causes neurodegeneration at the end. The babies with the disease are healthy at birth however progressive accumulation of GM2 results in increasing death of neurons, disruption in mental and motor functions and eventually death at 2-4 years of age. There has not been a treatment developed yet. The *Hexa*$^{-/-}$ mice generated as Tay-Sachs model was nearly normal and a bypass mechanism mediated by a sialidase was discovered. It was recently determined that Neu3 sialidase involves in ganglioside degradation in the Tay-Sachs disease pathology and the *Hexa*$^{-/-}$*Neu3*$^{-/-}$ mice was observed to mimic the neuropathologic and clinical phenotype of the disease. As it exhibits abnormal GM2 accumulation in the brain, progressive neurodegeneration, slow growth and neurobehavioral abnormalities like tremors and ataxia. Therefore it is used as early-onset Tay-Sachs disease mouse model. (Seyrantepe et al. 2018)

Autophagy is a lysosome-dependent pathway which is important for degradation of cytoplasmic components like damaged organelles, waste products or misfolded proteins in order to maintain cellular homeostasis. Autophagic flux (the rate at which autophagic vacuoles are processed by lysosomes) is reported to be impaired in most lysosomal storage diseases. Impairment of autophagic flux is demonstrated to result in secondary accumulation of autophagic substrates like cargo molecules, proteins mediating autophagy or autophagosome itself (Lieberman et al. 2012). In lysosomal storage disorders deficiency in lysosomal enzymes causes undegraded substance accumulation in lysosomes and impairs autophagosome-lysosome fusion or completion of autophagy (Settembre et al. 2008). In order to understand whether this pattern is also applicable for early-onset Tay-Sachs disease mouse model, autophagic markers were analyzed by RT-PCR, immunohistochemistry and immunocytochemistry. p62 is an

autophagic marker which in volves in selective autophagy by binding to ubiquitinated proteins and when the autophagic flux function smoothly it is degraded at the end of the autophagic pathway with the cargo components. However if the autophagy is impaired and cannot be terminated p62 accumulates in either autophagosomes or autophagolysosomes. Upregulation of transcriptional expression of p62 and Beclin1 was reported for muscle biopsy samples of Pompe disease (Nascimbeni et al. 2012). Expression analysis of p62 showed significant increase in cortex of 4.5-month-old *Hexa*$^{-/-}$*Neu3*$^{-/-}$ mice compared to its *WT* and *Hexa*$^{-/-}$ littermates also in cerebellum of 4.5-month-old *Hexa*$^{-/-}$*Neu3*$^{-/-}$ mice slight increase was observable (Figure 3.3.A and B). Beclin1 is a protein that mediates autophagic induction as mentioned in introduction part. In our data Beclin1 expression did not exhibit significant changes for *Hexa*$^{-/-}$*Neu3*$^{-/-}$ mice except for decreased expression in cerebellum of 4.5-month-old *Hexa*$^{-/-}$*Neu3*$^{-/-}$ mice compared to its *Hexa*$^{-/-}$ littermates. Also significantly increased Beclin1 expression was observed for cortex of 4.5-month-old *Neu3*$^{-/-}$ mice as well (Figure3.2.).

Lamp2 is a lysosome-associated protein and a key mediator of chaperone-mediated autophagy (Rout et al. 2014). Increase in lysosomes in *Hexa*$^{-/-}$*Neu3*$^{-/-}$ mice brain regions was already reported (Seyrantepe et al. 2018). Consistently with that; our results indicates significantly increased LAMP2 expression in all brain regions of 4.5-month-old *Hexa*$^{-/-}$*Neu3*$^{-/-}$ mice compared to their *Hexa*$^{-/-}$ littermates (Figure 3.4). For cortex and thalamus region, significant increase was also observable in 2.5-month-old *Hexa*$^{-/-}$*Neu3*$^{-/-}$ mice when compared to that of *Hexa*$^{-/-}$ (Figure 3.4. A and C). The increase in LAMP2 is whether related to elevated level of lysosomes in *Hexa*$^{-/-}$*Neu3*$^{-/-}$ mice or implies alteration in chaperone mediated autophagy pathway requires further studies.

In order to understand whether there is an impairment in autophagic flux and accumulation of secondary substrates in early-onset Tay-Sachs disease mouse model; immunohistochemical analysis were performed for LC3, LAMP1 and p62 proteins. Our overall data indicates significantly increased co-localization of LC3 and LAMP1 in cortex (Figure3.5), cerebellum (Figure 3.6), thalamus (Figure 3.7) and hippocampus (Figure 3.8 and 3.9) region of *Hexa*$^{-/-}$*Neu3*$^{-/-}$ mice compared to *WT* and/or *Hexa*$^{-/-}$. LC3 itself is a marker for autophagosomes and when its co-localized with LAMP1 they represent autophagolysosome structure (Raben, et.al., 2009). The increased co-localization in *Hexa*$^{-/-}$*Neu3*$^{-/-}$ mice brain can be interpreted as autophagosome and lysosome fusion successfully processed and autophagolysosome accumulation is

observed in this mouse model. However abnormal increase in lysosomes in *Hexa*$^{-/-}$ *Neu3*$^{-/-}$ mice was already reported(Seyrantepe et al. 2018), this may cause inevitable overlapping with LC3 even if the autophagosomes and lysosomes did not fused because of lysosomal dysfunction.

Immunohistochemical analysis for p62 was performed for only brain sections of *Hexa*$^{-/-}$ and *Hexa*$^{-/-}$*Neu3*$^{-/-}$ mice to determine the capability of *Hexa*$^{-/-}$*Neu3*$^{-/-}$ mice to complete the autophagic process, even if the autophagolysosome formation accomplished. As mentioned, p62 is a cargo protein that regulates selective autophagy of many substrates and it is degraded with the autophagic material as the autophagy completes (Ichimura and Komatsu 2010). Our immunostaining data for p62 showed significantly increased p62 accumulation in cortex (Figure 3.10.A and C), cerebellum (Figure 3.10.B and D), hippocampus (Figure 3.11), and pons (Figure 3.12. B and D) regions of *Hexa*$^{-/-}$*Neu3*$^{-/-}$ mice brains compared to that of *Hexa*$^{-/-}$ mice. This data suggests that there is impairment in autophagic degradation of p62.

Overall data about autophagic markers suggest that in *Hexa*$^{-/-}$*Neu3*$^{-/-}$ mice model the autophagic flux is blocked at either autophagosome or autophagolysosome level. Either way the autophagy cannot be completed in this model as the p62 immunostaining data indicates. Moreover, secondary accumulation of autophagic substrates like autophagosomes and undegraded p62 in *Hexa*$^{-/-}$*Neu3*$^{-/-}$ mice model was indicated in this research for the first time.

Autophagy has been reported to have pro-death or pro-survival functions depending on the conditions (Eisenberg-Lerner et al. 2009). The pro-survival effect of the autophagy is provided by the clearance of damaged components and energy recycling function of autophagy; however autophagy itself was also reported to mediate caspase mechanism and apoptosis-independent cell death (Kroemer and Levine 2008). In the neurodegenerative or lysosomal storage disorders autophagy has not been directly related to apoptosis but its impairment causes increase in cellular stress conditions and increases apoptosis indirectly (Tessitore et al., 2009). As the impairment of the autophagic flux has been shown in this research and involvement of apoptosis has been reported for *Hexa*$^{-/-}$*Neu3*$^{-/-}$ mice (Seyrantepe et al. 2018); we also wanted to investigate the effect of abnormal GM2 and autophagosome accumulation on apoptotic pathway. We quantified mRNA levels of ER stress and oxidative stress markers and apoptotic

regulator genes on brain regions of 2.5- and 4.5-month-old *WT, Hexa*$^{-/-}$*,Neu3*$^{-/-}$ and *Hexa*$^{-/-}$ *Neu3*$^{-/-}$ mice.

ATF6 is one of the ER stress markers and its expression has been shown to elevate in neuronal ceroid lipofuscinoses (NCL) fibroblast samples (Wei et al. 2008). When we checked the ATF6 expression, in cortex of 4.5-month-old *Neu3*$^{-/-}$ a significant increase was observed comparing to *WT* and also for cerebellum of 2.5-month-old *Hexa*$^{-/-}$ significantly increased ATF6 expression was demonstrated (Figure 3.14. A and B). However, no significant change was observed for *Hexa*$^{-/-}$*Neu3*$^{-/-}$ mice brain samples. Under ER-stress conditions, ATF6 undergoes posttranslational modification and act as an upstream effector of CHOP activation (Yoshida et al. 2000), and in GM1 gangliosidosis mouse model the posttranslationally cleaved active form of ATF6 was reported to be elevated (Tessitore et al. 2004). ATF6 mRNA expression seems to not have an effect on *Hexa*$^{-/-}$*Neu3*$^{-/-}$ mice pathology on transcriptional level however the posttranslational modification of ATF6 requires further research.

Calnexin is an ER-associated protein that facilitates protein folding, quality control of protein folding in ER, and withholds misfolded proteins for degradation (Kleizen and Braakman 2004). In Gaucher disease (GD) cells from patients with severe GD, it was reported that glucocerebrosidase (dysfunctional enzyme in GD) co-localizes with calnexin in immunocytochemical results, indicating that most of the protein was retained in the ER and did not reach the lysosomes (Ron and Horowitz 2005). Conversely in another research the mRNA expression of calnexin was remained unchanged in GD cells (Mu at al., 2008). In our data; calnexin expression exhibited significant increase only for cerebellum of 4.5-month-old *Hexa*$^{-/-}$*Neu3*$^{-/-}$ mice compared to that of 2.5-month-old (Figure 3.15. B). This increase may be a consequence of age dependent increase of cellular stress. Unlike Gaucher disease; in *Hexa*$^{-/-}$*Neu3*$^{-/-}$ mice, the pathology is not caused by misfolded proteins; it is caused by deficiency of the HEXA and NEU3 genes. Therefore it is expected to not observe a striking change in mRNA expression of calnexin which provides quality control of protein folding.

X-box binding protein is a transcription factor which is spliced by activated IRE1 upon ER stress (Walter and Ron 2011). The XBP1 mRNA comprises of two overlapping reading frames; under normal conditions only unspliced variant is transcribed without translation and once the UPR is activated the unspliced variant converted to spliced XBP1 which promotes transcription of UPR target genes (Van

Schadewijk et al. 2012). Significantly increased expression of spliced XBP1 was reported in GD derived fibroblasts (Maor et al. 2013), several neurodegenerative disorders including Huntington's disease and ALS (Hetz and Mollereau 2014). In this research expression of unspliced XBP1 was measured and significantly decreased level was demonstrated in all brain regions of 4.5-month-old *Hexa*$^{-/-}$*Neu3*$^{-/-}$ mice when compared to its *Hexa*$^{-/-}$ and *Neu3*$^{-/-}$ littermates. Moreover unspliced XBP1 expression was also significantly decreased in cerebellum and hippocampus regions of 2.5-month-old *Hexa*$^{-/-}$*Neu3*$^{-/-}$ mice compared to their *WT* littermates (Figure 3.16). The decrease in unspliced XBP1 can be caused by that they undergo splicing process however this should be validated with further investigation.

Superoxide Dismutase 2 is a mitochondrial antioxidant enzyme required for protecting the cells from reactive oxygen species and maintains cellular and mitochondrial redox balance. In some LSDs; the balance between ROS production and antioxidant defence mechanism was reported to be disrupted (Plotegher and Duchen 2017). In NPC human fibroblasts, it was demonstrated that SOD2 has decreased protein expression (Woš et al. 2016). Also in *Hexb*$^{-/-}$ GM2 gangliosidosis mouse brains decreased SOD2 mRNA and protein expression was reported (K. Suzuki et al. 2016). In our results, SOD2 expression was only significantly increased in cortex of 4.5-month-old *Hexa*$^{-/-}$ and *Neu3*$^{-/-}$ single knockout mice compared to their *WT* littermates. In other regions no significant change was observed, expression in *Hexa*$^{-/-}$*Neu3*$^{-/-}$ mice was similar to that of *WT* for both age groups (Figure 3.17).

Catalase is another oxidative stress marker which involves in antioxidant defence mechanism. It catalyzes degradation of hydrogen peroxide into water and oxygen molecules. While increased Catalase activity was reported in blood samples of GD patients (Mello et al. 2015), in NCL human fibroblast this activity was reported to be decreased (Vidal-Donet et al. 2013). In *Hexa*$^{-/-}$*Neu3*$^{-/-}$ mice brain regions Catalase expression did not exhibit significant changes except for significant increase in 2.5-month-old *Hexa*$^{-/-}$*Neu3*$^{-/-}$ mice compared to *WT* littermates (Figure 3.18.).

Thioltransferase-1 (Ttase1) is a member of glutaredoxin family proteins and involves in antioxidant defence mechanism, as well. Its transcriptional expression reported to be increased in fibroblasts from human NCLs, GM1 gangliosidosis, Tay-Sachs disease and GD patients(Wei et al. 2008). However, in this research no significant change was observed in Ttase1 expression except for significantly decreased level in hippocampus of 2.5-month-old *Hexa*$^{-/-}$*Neu3*$^{-/-}$ mice compared to its *WT*

littermates (Figure 3.19). Even if it is not significant slightly decreased Ttase-1 expression in cortex and cerebellum of 4.5-month-old *Hexa*$^{-/-}$*Neu3*$^{-/-}$ mice may be related to decreased antioxidant defence in this model.

Bcl-2, Bcl XL and Bax are members of Bcl2 family and are components of intrinsic pathway of apoptosis as mentioned in introduction part. Bax mediates opening of mitochondrial voltage-dependent anion channel hence causes loss of membrane potential and release of cytochrome c. Released cytochrome c activates caspase-9 and leads to apoptosis. Bcl-2 and Bcl XL involves in inhibition of pro-apoptotic genes like Bax and Bak hence acts in antiapoptotic role(Mrschtik and Ryan 2015). In this research for *Hexa*$^{-/-}$*Neu3*$^{-/-}$ mice model, no significant change was observed in Bcl2, Bcl XL and Bax expression in transcriptional level (Figure 3.20, 3.21 and 3.22). Bcl2 was significantly decreased in cerebellum of 2.5-month-old *Neu3*$^{-/-}$ mice and increased in cerebellum of 4.5-month-old *Neu3*$^{-/-}$ mice when compared to their *WT* littermates (Figure 3.20).

Overall RT-PCR results for apoptosis markers are inconclusive and require further research on translational level.

Reactive oxygen species are inevitable by-product of oxidative phosphorylation and they recycled by antioxidant defence mechanisms. The balance between ROS production and antioxidant defence mechanism provides redox homeostasis. If the net ROS generation is increased above the capacity of antioxidant defence mechanism, oxidative stress is increased and increased ROS causes lipid peroxidation, oxidation of proteins and DNA damage (Plotegher and Duchen 2017). Alterations in rate of ROS generation have been reported in several LSDs. In NPC fibroblasts derived from human patients, decreased ROS generation was reported (Woš et al. 2016). On the other hand in human Krabbe disease cell line and Pompe disease mouse model increased ROS level was demonstrated (Voccoli et al. 2014; Lim et al. 2015). Moreover in Fabry disease the intracellular ROS level was measured to be higher in Gb_3 accumulated cultured Fabry endothelial cells(Shen et al. 2008) and in GD fibroblasts increased intracellular ROS level was also reported (Deganuto et al. 2007). In order to measure intracellular ROS level in fibroblasts of *Hexa*$^{-/-}$*Neu3*$^{-/-}$ mice for the first time; we used flow cytometric analysis of H_2DCFDA in which oxidation of nonfluorimetric H_2DCFDA to fluorimetric DCF by excessive ROS. Our results indicated significantly increased ROS level in *Hexa*$^{-/-}$*Neu3*$^{-/-}$ fibroblasts compared to *Hexa*$^{-/-}$ ones for both positive control and sample group (Figure 3.23).

APE1/Ref-1 is a DNA repair enzyme promoting base excision repair mechanism in nucleus. Besides the involvement in DNA repair mechanism, APE1/Ref-1 is also able to control nuclear redox activity by providing redox-dependent mechanism for regulation of target gene expression. It is major regulator of the cellular response to increased oxidative stress(Tell et al. 2005). The protein expression level of APE1/Ref-1 was analyzed in brain regions and fibroblasts of *WT, Hexa*$^{-/-}$*, Neu3*$^{-/-}$ and *Hexa*$^{-/-}$*Neu3*$^{-/-}$ mice to determine the cellular response to oxidative stress. For cortex and cerebellum slight increase and for thalamus significant increase in APE1/Ref-1 protein expression was observed in 4.5-month-old *Hexa*$^{-/-}$*Neu3*$^{-/-}$ mice when compared to their *WT* and *Hexa*$^{-/-}$ littermates (Figure 3.24 and 3.25). For thalamus significantly increased expression was also demonstrated in 2.5-month-old *Hexa*$^{-/-}$*Neu3*$^{-/-}$ mice compared to its *WT* and *Hexa*$^{-/-}$ counterparts (Figure 3.26). In fibroblast samples, no significant change was observed by western blot analysis (Figure 3.28).

Besides the nuclear functions; APE1/Ref-1 has been reported to have functions in cytoplasmic compartment within mitochondria (Frossi et al. 2002) and ER (Fan et al. 2003). However, detailed mechanism of cytoplasmic functions of APE1/Ref-1 has not been understood yet. In fibroblasts of GD increased cytoplasmic expression was reported (Deganuto et al. 2007). We also analyzed the expression and localization of APE1/Ref-1 in fibroblasts of *WT, Hexa*$^{-/-}$*, Neu3*$^{-/-}$ and *Hexa*$^{-/-}$*Neu3*$^{-/-}$ mice by immunocytochemical analysis and our results showed that increased cytoplasmic APE1/Ref-1 expression in fibroblast of *Hexa*$^{-/-}$*Neu3*$^{-/-}$ mice compared to that of *WT* (Figure 3.29).

4.1. Conclusion

In this thesis study, autophagic and apoptotic mechanism were investigated in *WT, Hexa*$^{-/-}$*, Neu3*$^{-/-}$ and *Hexa*$^{-/-}$*Neu3*$^{-/-}$ mice. Investigation of autophagic markers by RT-PCR and immunostaining indicated that there is impairment in autophagic flux in early-onset-Tay-Sachs disease mouse model. The immunohistochemical analysis of LC3 and p62 indicated that the impairment of autophagic flux results in secondary accumulation of autophagic components, which may add up the neurodegeneration, observed in disease pathology.

Even if the apoptosis has already been reported for early-onset Tay-Sachs disease mouse model, specific regulators and trigger factors leading to apoptosis were analyzed in this study for the first time. Our RT-PCR results for apoptotic markers were generally inconclusive except for the decreased expression of unspliced XBP1 in *Hexa*$^{-/-}$ *Neu3*$^{-/-}$ mice model which indicates ER-stress increment. We also analyzed the oxidative stress involvement in the pathology of *Hexa*$^{-/-}$*Neu3*$^{-/-}$ mouse model. The intracellular ROS level was measured and it was elevated in fibroblasts of *Hexa*$^{-/-}$*Neu3*$^{-/-}$ mouse model. The cellular response to increased oxidative stress was also measured by analyzing APE1/Ref-1 protein expression and higher expression in *Hexa*$^{-/-}$*Neu3*$^{-/-}$ mouse model was also demonstrated for this marker as well. The increase in ROS production can be associated to the increase in APE1/Ref-1 expression. Both ROS and APE1/Ref-1 increases may be occurred as a consequence of the abnormal GM2 and secondary accumulation of autophagic components in early-onset Tay-Sachs disease mouse model.

4.2. Future Directions

A detailed investigation about functionality of lysosomes in *Hexa*$^{-/-}$*Neu3*$^{-/-}$ mouse model may further elucidate the mechanism of the autophagic impairment as it is not clear that whether autophagosomes are able to fuse with lysosomes or not. Moreover; as LAMP2 is both a lysosome marker and a key regulator of chaperone-mediated autophagy, the chaperone mediated autophagy mechanism can be further studied to determine whether the elevated level of LAMP2 is only related to increased lysosome number or it also actively regulates chaperone-mediated autophagy in pathology of early-onset-Tay-Sachs disease mouse model. As a therapeutic approach, induction of autophagy might be promising way to reduce the accumulated molecules and cellular stress level.

Analysis of apoptotic markers on translational level might provide better understanding for their role in regulation of increased neurodegeneration as the posttranslational modifications of the proteins can be detected as well. As increase in oxidative stress in early-onset Tay-Sachs mouse model has been shown in this study, functionality of mitochondria and iron metabolism can be investigated to have a better understanding of the effect of the pathology on the cellular and mitochondrial homeostasis.

REFERENCES

Americo, Jose, Fernandes Filho, and Barbara E Shapiro. 2010. "Tay-Sachs Disease." *Arch Neurol* 61 (11):1466–68. https://doi.org/10.1001/archneur.61.9.1466.

Ashkenazi, Avi, and Vishva M. Dixit. 1998. "Death Receptors: Signaling and Modulation." *Science*. https://doi.org/10.1126/science.281.5381.1305.

B'Chir, Wafa, Anne Catherine Maurin, Valérie Carraro, Julien Averous, Céline Jousse, Yuki Muranishi, Laurent Parry, Georges Stepien, Pierre Fafournoux, and Alain Bruhat. 2013. "The EIF2α/ATF4 Pathway Is Essential for Stress-Induced Autophagy Gene Expression." *Nucleic Acids Research* 41 (16):7683–99. https://doi.org/10.1093/nar/gkt563.

Bellettato, Cinzia Maria, and Maurizio Scarpa. 2010. "Pathophysiology of Neuropathic Lysosomal Storage Disorders." *Journal of Inherited Metabolic Disease*. https://doi.org/10.1007/s10545-010-9075-9.

Cory, Suzanne, and Jerry M. Adams. 2002. "The BCL2 Family: Regulators of the Cellular Life-or-Death Switch." *Nature Reviews Cancer*. https://doi.org/10.1038/nrc883.

Cox, Timothy, Robin Lachmann, Carla Hollak, Johannes Aerts, Sonja Van Weely, Martin Hrebícek, Frances Platt, et al. 2000. "Novel Oral Treatment of Gaucher's Disease with N-Butyldeoxynojirimycin (OGT 918) to Decrease Substrate Biosynthesis." *Lancet* 355 (9214):1481–85. https://doi.org/10.1016/S0140-6736(00)02161-9.

Deganuto, Marta, Maria Gabriela Pittis, Alex Pines, Silvia Dominissini, Mark R. Kelley, Rodolfo Garcia, Franco Quadrifoglio, Bruno Bembi, and Gianluca Tell. 2007. "Altered Intracellular Redox Status in Gaucher Disease Fibroblasts and Impairment of Adaptive Response against Oxidative Stress." *Journal of Cellular Physiology* 212 (1):223–35. https://doi.org/10.1002/jcp.21023.

Donida, Bruna, Carlos Eduardo Diaz Jacques, Caroline Paula Mescka, Daiane Grigolo Bardemaker Rodrigues, Desirèe Padilha Marchetti, Graziela Ribas, Roberto Giugliani, and Carmen Regla Vargas. 2017. "Oxidative Damage and Redox in Lysosomal Storage Disorders: Biochemical Markers." *Clinica Chimica Acta*. https://doi.org/10.1016/j.cca.2017.01.007.

Du, Y., Z. Ma, S. Lin, R. C. Dodel, F. Gao, K. R. Bales, L. C. Triarhou, et al. 2001. "Minocycline Prevents Nigrostriatal Dopaminergic Neurodegeneration in the MPTP Model of Parkinson's Disease." *Proceedings of the National Academy of Sciences* 98 (25):14669–74. https://doi.org/10.1073/pnas.251341998.

Eisenberg-Lerner, A., S. Bialik, H. U. Simon, and A. Kimchi. 2009. "Life and Death Partners: Apoptosis, Autophagy and the Cross-Talk between Them." *Cell Death and Differentiation*. https://doi.org/10.1038/cdd.2009.33.

Elmore, Susan. 2007. "Apoptosis: A Review of Programmed Cell Death." *Toxicologic*

Pathology 35 (4):495–516. https://doi.org/10.1080/01926230701320337.

Fan, Zusen, Paul J. Beresford, Dong Zhang, Zhan Xu, Carl D. Novina, Akira Yoshida, Yves Pommier, and Judy Lieberman. 2003. "Cleaving the Oxidative Repair Protein Ape I Enhances Cell Death Mediated by Granzyme A." *Nature Immunology* 4 (2):145–53. https://doi.org/10.1038/ni885.

Feng, Yuchen, Ding He, Zhiyuan Yao, and Daniel J. Klionsky. 2014. "The Machinery of Macroautophagy." *Cell Research*. https://doi.org/10.1038/cr.2013.168

Frossi, Barbara, Gianluca Tell, Paola Spessotto, Alfonso Colombatti, Gaetano Vitale, and Carlo Pucillo. 2002. "H2O2 Induces Translocation of APE/Ref-1 to Mitochondria in the Raji B-Cell Line." *Journal of Cellular Physiology* 193 (2):180–86. https://doi.org/10.1002/jcp.10159.

Fuller, Maria, Peter J Meikle, and John J Hopwood. 2006. *Epidemiology of Lysosomal Storage Diseases: An Overview*. *Fabry Disease: Perspectives from 5 Years of FOS*. http://www.ncbi.nlm.nih.gov/pubmed/21290699.

Gardner, Brooke M., and Peter Walter. 2011. "Unfolded Proteins Are Ire1-Activating Ligands That Directly Induce the Unfolded Protein Response." *Science* 333 (6051):1891–94. https://doi.org/10.1126/science.1209126.

Gravel, Roy A., Michael M. Kaback, Richard L. Proia, Konrad Sandhoff, Kinuko Suzuki, and Kunihiko Suzuki. 2014. "The GM2 Gangliosidoses." In *The Online Metabolic and Molecular Bases of Inherited Diseases*, 3827–76. https://doi.org/10.1036/ommbid.184.

Gump, Jacob M., and Andrew Thorburn. 2011. "Autophagy and Apoptosis: What Is the Connection?" *Trends in Cell Biology*. https://doi.org/10.1016/j.tcb.2011.03.007.

Haddad, Saria El, Marwan Khoury, Mohammad Daoud, Rami Kantar, Hayat Harati, Talal Mousallem, Oscar Alzate, Brian Meyer, and Rose Mary Boustany. 2012. "CLN5 and CLN8 Protein Association with Ceramide Synthase: Biochemical and Proteomic Approaches." *Electrophoresis* 33 (24):3798–3809. https://doi.org/10.1002/elps.201200472.

Hengartner, M. O. 2000. "The Biochemistry of Apoptosis." *Nature*. https://doi.org/10.1038/35037710.

Hetz, Claudio, and Bertrand Mollereau. 2014. "Disturbance of Endoplasmic Reticulum Proteostasis in Neurodegenerative Diseases." *Nature Reviews Neuroscience*. https://doi.org/10.1038/nrn3689.

Huizing, Marjan, Amanda Helip-Wooley, Wendy Westbroek, Meral Gunay-Aygun, and William A. Gahl. 2008. "Disorders of Lysosome-Related Organelle Biogenesis: Clinical and Molecular Genetics." *Annual Review of Genomics and Human Genetics* 9 (1):359–86. https://doi.org/10.1146/annurev.genom.9.081307.164303.

Ichimura, Yoshinobu, and Masaaki Komatsu. 2010. "Selective Degradation of P62 by

Autophagy." *Seminars in Immunopathology* 32 (4):431–36. https://doi.org/10.1007/s00281-010-0220-1.

Igdoura, Suleiman A., Carmen Mertineit, Jacquetta M. Trasler, and Roy A. Gravel. 1999. "Sialidase-Mediated Depletion of G(M2) Ganglioside in Tay-Sachs Neuroglia Cells." *Human Molecular Genetics* 8 (6):1111–16. https://doi.org/10.1093/hmg/8.6.1111.

Igney, Frederik H., and Peter H. Krammer. 2002. "Death And Antı-Death: Tumour Resıstance To Apoptosıs." *Nature Reviews Cancer* 2 (4):277–88. https://doi.org/10.1038/nrc776.

Kaback, Michael M. 2001. *Tay-Sachs Disease*. *Advances in Genetics*. Vol. 44. https://doi.org/10.1016/S0065-2660(01)44084-3.

Kannan, Krishnaswamy, and Sushil K. Jain. 2000. "Oxidative Stress and Apoptosis." *Pathophysiology: The Official Journal of the International Society for Pathophysiology (ISP)* 7 (27):153–63. https://doi.org/http://dx.doi.org/10.1016/S0928-4680(00)00053-5.

Keilani, Serene, Yi Lun, Anthony C. Stevens, Hadis N. Williams, Eric R. Sjoberg, Richie Khanna, Kenneth J. Valenzano et al. "Lysosomal dysfunction in a mouse model of Sandhoff disease leads to accumulation of ganglioside-bound amyloid-β peptide." Journal of Neuroscience 32, no. 15 (2012): 5223-5236.

Kleizen, Bertrand, and Ineke Braakman. 2004. "Protein Folding and Quality Control in the Endoplasmic Reticulum." *Current Opinion in Cell Biology*. https://doi.org/10.1016/j.ceb.2004.06.012.

Kolter, Thomas, and Konrad Sandhoff. 1999. "Sphingolipids - Their Metabolic Pathways and the Pathobiochemistry of Neurodegenerative Diseases." *Angewandte Chemie - International Edition*. https://doi.org/10.1002/(SICI)1521-3773(19990601)38:11<1532::AID-ANIE1532>3.0.CO;2-U.

Kose, Melis, Secil Akyildiz Demir, Gulcin Akinci, Cenk Eraslan, Unsal Yilmaz, Serdar Ceylaner, Eser Sozmen Yildirim, and Volkan Seyrantepe. "The second case of saposin a deficiency and altered autophagy." (2018): 1-12.

Kroemer, Guido, and Beth Levine. 2008. "Autophagic Cell Death: The Story of a Misnomer." *Nature Reviews Molecular Cell Biology*. https://doi.org/10.1038/nrm2529.

Lee, W. S., W. H. Yoo, and Han-Jung Chae. 2015. "ER Stress and Autophagy." *Current Molecular Medicine* 15 (8):735–45. https://doi.org/10.2174/1566524015666150921105453.

Lieberman, Andrew P., Rosa Puertollano, Nina Raben, Susan Slaugenhaupt, Steven U. Walkley, and Andrea Ballabio. 2012. "Autophagy in Lysosomal Storage Disorders." *Autophagy*. https://doi.org/10.4161/auto.19469.

Lim, Jeong A., Lishu Li, Or Kakhlon, Rachel Myerowitz, and Nina Raben. 2015. "Defects in Calcium Homeostasis and Mitochondria Can Be Reversed in Pompe Disease." *Autophagy* 11 (2):385–402. https://doi.org/10.1080/15548627.2015.1009779.

Locksley, Richard M., Nigel Killeen, and Michael J. Lenardo. 2001. "The TNF and TNF Receptor Superfamilies: Integrating Mammalian Biology." *Cell*. https://doi.org/10.1016/S0092-8674(01)00237-9.

Maiuri, M. Chiara, Einat Zalckvar, Adi Kimchi, and Guido Kroemer. 2007. "Self-Eating and Self-Killing: Crosstalk between Autophagy and Apoptosis." *Nature Reviews Molecular Cell Biology*. https://doi.org/10.1038/nrm2239.

Maor, Gali, Sigal Rencus-Lazar, Mirella Filocamo, Hermann Steller, Daniel Segal, and Mia Horowitz. 2013. "Unfolded Protein Response in Gaucher Disease: From Human to Drosophila." *Orphanet Journal of Rare Diseases* 8 (1). https://doi.org/10.1186/1750-1172-8-140.

McGowan, A. J., R. S. Fernandes, A. Samali, and T. G. Cotter. 1996. "Anti-Oxidants and Apoptosis." *Biochemical Society Transactions* 24 (1):229–33. https://doi.org/10.1042/bst0240229.

Mello, Alexandre Silva, Cristina Da Silva Garcia, Fernanda De Souza Machado, Niara Da Silva Medeiros, Mariane Farias Wohlenberg, Jéssica Pereira Marinho, Caroline Dani, Cláudia Funchal, and Janice Carneiro Coelho. 2015. "Oxidative Stress Parameters of Gaucher Disease Type I Patients." *Molecular Genetics and Metabolism Reports* 4:1–5. https://doi.org/10.1016/j.ymgmr.2015.05.001.

Mizushima, Noboru, Yoshinori Ohsumi, and Tamotsu Yoshimori. 2002. "Autophagosome Formation in Mammalian Cells." *Cell Structure and Function* 27 (6):421–29. https://doi.org/10.1247/csf.27.421.

Monti, Eugenio, Erik Bonten, Alessandra D'Azzo, Roberto Bresciani, Bruno Venerando, Giuseppe Borsani, Roland Schauer, and Guido Tettamanti. 2010. "Sialidases in Vertebrates. A Family Of Enzymes Tailored For Several Cell Functions." *Advances in Carbohydrate Chemistry and Biochemistry* 64 (C):404–79. https://doi.org/10.1016/S0065-2318(10)64007-3.

Moscat, Jorge, and Maria T. Diaz-Meco. 2009. "P62 at the Crossroads of Autophagy, Apoptosis, and Cancer." *Cell*. https://doi.org/10.1016/j.cell.2009.05.023.

Mrschtik, Michaela, and Kevin M. Ryan. 2015. "Lysosomal Proteins in Cell Death and Autophagy." *FEBS Journal*. https://doi.org/10.1111/febs.13253.

Mu, Ting Wei, Douglas M. Fowler, and Jeffery W. Kelly. 2008. "Partial Restoration of Mutant Enzyme Homeostasis in Three Distinct Lysosomal Storage Disease Cell Lines by Altering Calcium Homeostasis." *PLoS Biology* 6 (2):0253–65. https://doi.org/10.1371/journal.pbio.0060026.

Müller, Sabrina, Julia Dennemärker, and Thomas Reinheckel. 2012. "Specific

Functions of Lysosomal Proteases in Endocytic and Autophagic Pathways." *Biochimica et Biophysica Acta - Proteins and Proteomics*. https://doi.org/10.1016/j.bbapap.2011.07.003.

Nascimbeni, A. C., M. Fanin, E. Masiero, C. Angelini, and M. Sandri. 2012. "The Role of Autophagy in the Pathogenesis of Glycogen Storage Disease Type II (GSDII)." *Cell Death and Differentiation* 19 (10):1698–1708. https://doi.org/10.1038/cdd.2012.52.

Norbury, Chris J, and Ian D Hickson. 2001. "C r Dna D," 367–401.

Ohmi, Yuhsuke, Yuki Ohkawa, Yoshio Yamauchi, Orie Tajima, Keiko Furukawa, and Koichi Furukawa. 2012. "Essential Roles of Gangliosides in the Formation and Maintenance of Membrane Microdomains in Brain Tissues." *Neurochemical Research*. https://doi.org/10.1007/s11064-012-0764-7.

Pacheco, Christopher D., and Andrew P. Lieberman. 2007. "Lipid Trafficking Defects Increase Beclin-1 and Activate Autophagy in Niemann-Pick Type C Disease." *Autophagy*. https://doi.org/10.4161/auto.4586.

Palmano, Kate, Angela Rowan, Rozey Guillermo, Jian Guan, and Paul McJarrow. 2015. "The Role of Gangliosides in Neurodevelopment." *Nutrients*. https://doi.org/10.3390/nu7053891.

Pan, Chendong, Matthew S. Nelson, Morayma Reyes, Lisa Koodie, Joseph J. Brazil, Elliot J. Stephenson, Robert C. Zhao, et al. 2005. "Functional Abnormalities of Heparan Sulfate in Mucopolysaccharidosis-I Are Associated with Defective Biologic Activity of FGF-2 on Human Multipotent Progenitor Cells." *Blood* 106 (6):1956–64. https://doi.org/10.1182/blood-2005-02-0657.

Persaud-Sawin, Dixie-Ann, Antonius VanDongen, and Rose-Mary Naaman Boustany. 2002. "Motifs within the CLN3 Protein: Modulation of Cell Growth Rates and Apoptosis." *Human Molecular Genetics* 11 (18):2129–42. https://doi.org/10.2196/jmir.1581.

Phaneuf, Daniel, Nobuaki Wakamatsu, Jing Qi Huang, Anita Borowski, Alan C. Peterson, Sheila R. Fortunato, Gerd Ritter, et al. 1996. "Dramatically Different Phenotypes in Mouse Models of Human Tay-Sachs and Sandhoff Diseases." *Human Molecular Genetics* 5 (1):1–14. https://doi.org/10.1093/hmg/5.1.1.

Platt, Frances M., Barry Boland, and Aarnoud C. van der Spoel. 2012. "Lysosomal Storage Disorders: The Cellular Impact of Lysosomal Dysfunction." *Journal of Cell Biology* 199 (5):723–34. https://doi.org/10.1083/jcb.201208152.

Platt, Frances M., and Terry D. Butters. 2000. "Substrate Deprivation: A New Therapeutic Approach for the Glycosphingolipid Lysosomal Storage Diseases." *Expert Reviews in Molecular Medicine* 2 (1):1–17. https://doi.org/10.1017/S1462399400001484.

Plotegher, Nicoletta, and Michael R. Duchen. 2017. "Mitochondrial Dysfunction and

Neurodegeneration in Lysosomal Storage Disorders." *Trends in Molecular Medicine*. https://doi.org/10.1016/j.molmed.2016.12.003.

Publication, Online, and Rose-Mary Naaman Boustany. 2013. "Lysosomal Storage Diseases-The Horizon Expands NATURE REVIEWS | NEUROLOGY Lysosomal Storage Diseases-the Horizon Expands." *Nat. Rev. Neurol. Advance Online Publication*. https://doi.org/10.1038/nrneurol.

Raben, Nina, A. Roberts, and R. H. Plotz. 2007. "Role of Autophagy in the Pathogenesis of Pompe Disease." *Acta Myologica* 26 (1):45–48. https://doi.org/10.3906/sag-1407-75.

Raben, Nina, Lauren Shea, Victoria Hill, and Paul Plotz. n.d. *Monitoring Autophagy in Lysosomal Storage Disorders*. *Autophagy in Disease and Clinical Applications, Part C*. 1st ed. Vol. 453. Elsevier Inc. https://doi.org/10.1016/S0076-6879(08)04021-4.

Risher, W. Christopher, Sagar Patel, Il H wan Kim, Akiyoshi Uezu, Srishti Bhagat, Daniel K. Wilton, Louis Jan Pilaz, et al. 2014. "Astrocytes Refine Cortical Connectivity at Dendritic Spines." *ELife* 3:1–24. https://doi.org/10.7554/eLife.04047.

Rizzuto, Rosario, Paolo Pinton, Walter Carrington, Frederic S. Fay, Kevin E. Fogarty, Lawrence M. Lifshitz, Richard A. Tuft, and Tullio Pozzan. 1998. "Close Contacts with the Endoplasmic Reticulum as Determinants of Mitochondrial Ca2+ Responses." *Science* 280 (5370):1763–66. https://doi.org/10.1126/science.280.5370.1763.

Ron, Idit, and Mia Horowitz. 2005. "ER Retention and Degradation as the Molecular Basis Underlying Gaucher Disease Heterogeneity." *Human Molecular Genetics* 14 (16):2387–98. https://doi.org/10.1093/hmg/ddi240.

Rout, Ashok K., Marie Paule Strub, Grzegorz Piszczek, and Nico Tjandra. 2014. "Structure of Transmembrane Domain of Lysosome-Associated Membrane Protein Type 2a (LAMP-2A) Reveals Key Features for Substrate Specificity in Chaperone-Mediated Autophagy." *Journal of Biological Chemistry* 289 (51):35111–23. https://doi.org/10.1074/jbc.M114.609446.

Rozenberg, R., and L. V. Pereira. 2001. "The Frequency of Tay-Sachs Disease Causing Mutations in the Brazilian Jewish Population Justifies a Carrier Screening Program." *São Paulo Medical Journal = Revista Paulista de Medicina* 119 (4):146–49. https://doi.org/10.1590/S1516-31802001000400007.

Saelens, Xavier, Nele Festjens, Lieselotte Vande Walle, Maria Van Gurp, Geert Van Loo, and Peter Vandenabeele. 2004. "Toxic Proteins Released from Mitochondria in Cell Death." *Oncogene*. https://doi.org/10.1038/sj.onc.1207523.

Sandhoff, K, and E Conzelmann. 1983. "The Biochemical Basis of Gangliosidoses."

Sango, Kazunori, Shoji Yamanaka, Alexander Hoffmann, Yasuharu Okuda, Alexander

Grinberg, Heiner Westphal, Michael P. McDonald, et al. 1995. “Mouse Models of Tay–Sachs and Sandhoff Diseases Differ in Neurologic Phenotype and Ganglioside Metabolism.” *Nature Genetics* 11 (2):170–76. https://doi.org/10.1038/ng1095-170.

Sano, Renata, and John C. Reed. 2013. “ER Stress-Induced Cell Death Mechanisms.” *Biochimica et Biophysica Acta - Molecular Cell Research*. https://doi.org/10.1016/j.bbamcr.2013.06.028.

Sarkar, Sovan, Bernadette Carroll, Yosef Buganim, Dorothea Maetzel, Alex HM Ng, John P. Cassady, Malkiel A. Cohen et al. "Impaired autophagy in the lipid-storage disorder Niemann-Pick type C1 disease." Cell reports 5, no. 5 (2013): 1302-1315.

Schadewijk, Annemarie Van, Emily F A Van'T Wout, Jan Stolk, and Pieter S. Hiemstra. 2012. “A Quantitative Method for Detection of Spliced X-Box Binding Protein-1 (XBP1) MRNA as a Measure of Endoplasmic Reticulum (ER) Stress.” *Cell Stress and Chaperones* 17 (2):275–79. https://doi.org/10.1007/s12192-011-0306-2.

Schnaar, Ronald L. 2010. “Brain Gangliosides in Axon-Myelin Stability and Axon Regeneration.” *FEBS Letters*. https://doi.org/10.1016/j.febslet.2009.10.011.

Schneider Gasser, Edith M, Carolin J Straub, Patrizia Panzanelli, Oliver Weinmann, Marco Sassoè-Pognetto, and Jean-Marc Fritschy. 2006. “Immunofluorescence in Brain Sections: Simultaneous Detection of Presynaptic and Postsynaptic Proteins in Identified Neurons.” *Nature Protocols* 1 (4):1887–97. https://doi.org/10.1038/nprot.2006.265.

Schneider, Jaime L., and Ana Maria Cuervo. 2014. “Autophagy and Human Disease: Emerging Themes.” *Current Opinion in Genetics and Development*. https://doi.org/10.1016/j.gde.2014.04.003.

Settembre, Carmine, Alessandro Fraldi, David C. Rubinsztein, and Andrea Ballabio. 2008. “Lysosomal Storage Diseases as Disorders of Autophagy.” *Autophagy* 4 (1):113–14. https://doi.org/10.4161/auto.5227.

Seyrantepe, Volkan, Secil Akyildiz Demir, Zehra Kevser Timur, Johanna Von Gerichten, Christian Marsching, Esra Erdemli, Emin Oztas, et al. 2018. “Murine Sialidase Neu3 Facilitates GM2 Degradation and Bypass in Mouse Model of Tay-Sachs Disease.” *Experimental Neurology* 299 (July 2017):26–41. https://doi.org/10.1016/j.expneurol.2017.09.012.

Seyrantepe, Volkan, Pablo Lema, Aurore Caqueret, Larbi Dridi, Samar Bel Hadj, Stephane Carpentier, Francine Boucher, et al. 2010. “Mice Doubly-Deficient in Lysosomal Hexosaminidase a and Neuraminidase 4 Show Epileptic Crises and Rapid Neuronal Loss.” *PLoS Genetics* 6 (9). https://doi.org/10.1371/journal.pgen.1001118.

Shen, Jin-Song, Xing-Li Meng, David F Moore, Jane M Quirk, James A Shayman, Raphael Schiffmann, and Christine R Kaneski. 2008. “Globotriaosylceramide

Induces Oxidative Stress and Up-Regulates Cell Adhesion Molecule Expression in Fabry Disease Endothelial Cells." *Molecular Genetics and Metabolism* 95 (3):163–68. https://doi.org/10.1016/j.ymgme.2008.06.016.

Simonaro, C. M., Y. Ge, E. Eliyahu, X. He, K. J. Jepsen, and E. H. Schuchman. 2010. "Involvement of the Toll-like Receptor 4 Pathway and Use of TNF- Antagonists for Treatment of the Mucopolysaccharidoses." *Proceedings of the National Academy of Sciences* 107 (1):222–27. https://doi.org/10.1073/pnas.0912937107.

Sonnino, Sandro, Laura Mauri, Vanna Chigorno, and Alessandro Prinetti. 2007. "Gangliosides as Components of Lipid Membrane Domains." *Glycobiology*. https://doi.org/10.1093/glycob/cwl052.

Su, Minfei, Yang Mei, and Sangita Sinha. 2013. "Role of the Crosstalk between Autophagy and Apoptosis in Cancer." *Journal of Oncology*. https://doi.org/10.1155/2013/102735.

Sun, Ying, and Gregory A. Grabowski. "Altered autophagy in the mice with a deficiency of saposin A and saposin B." Autophagy 9, no. 7 (2013): 1115-1116.

Suzuki, Kyoko, Akira Yamaguchi, Shoji Yamanaka, Seiichi Kanzaki, Masato Kawashima, Takashi Togo, Omi Katsuse, et al. 2016. "Accumulated α-Synuclein Affects the Progression of GM2 Gangliosidoses." *Experimental Neurology* 284:38–49. https://doi.org/10.1016/j.expneurol.2016.07.011.

Suzuki, Yuichiro Justin, Henry Jay Forman, and Alex Sevanian. 1996. "Oxidants as Stimulators of Signal Transduction." *Free Radical Biology and Medicine*. https://doi.org/10.1016/S0891-5849(96)00275-4.

Tatti, Massimo, Marialetizia Motta, and Rosa Salvioli. "Autophagy in Gaucher disease due to saposin C deficiency." Autophagy 7, no. 1 (2011): 94-95.

Tell, Gianluca, Giuseppe Damante, David Caldwell, and Mark R. Kelley. 2005. "The Intracellular Localization of APE1/Ref-1: More than a Passive Phenomenon?" *Antioxidants & Redox Signaling* 7 (3–4):367–84. https://doi.org/10.1089/ars.2005.7.367.

Tessitore, Alessandra, Maria Del P. Martin, Renata Sano, Yanjun Ma, Linda Mann, Angela Ingrassia, Eric D. Laywell, Dennis A. Steindler, Linda M. Hendershot, and Alessandra D'Azzo. 2004. "GM1-Ganglioside-Mediated Activation of the Unfolded Protein Response Causes Neuronal Death in a Neurodegenerative Gangliosidosis." *Molecular Cell* 15 (5):753–66. https://doi.org/10.1016/j.molcel.2004.08.029.

Tessitore, Alessandra, Marinella Pirozzi, and Alberto Auricchio. 2009. "Abnormal Autophagy, Ubiquitination, Inflammation and Apoptosis Are Dependent upon Lysosomal Storage and Are Useful Biomarkers of Mucopolysaccharidosis VI." *PathoGenetics* 2 (1):4. https://doi.org/10.1186/1755-8417-2-4.

Vidal-Donet, José Manuel, Jaime Cárcel-Trullols, Bonaventura Casanova, Carmen

Aguado, and Erwin Knecht. 2013. “Alterations in ROS Activity and Lysosomal PH Account for Distinct Patterns of Macroautophagy in LINCL and JNCL Fibroblasts.” *PLoS ONE* 8 (2). https://doi.org/10.1371/journal.pone.0055526.

Voccoli, V., I. Tonazzini, G. Signore, M. Caleo, and M. Cecchini. 2014. “Role of Extracellular Calcium and Mitochondrial Oxygen Species in Psychosine-Induced Oligodendrocyte Cell Death.” *Cell Death and Disease* 5 (11). https://doi.org/10.1038/cddis.2014.483.

Walter, Peter, and David Ron. 2011. “The Unfolded Protein Response: From Stress Pathway to Homeostatic Regulation.” *Science*. https://doi.org/10.1126/science.1209038.

Wei, Hui, Sung Jo Kim, Zhongjian Zhang, Pei Chih Tsai, Krystyna R. Wisniewski, and Anil B. Mukherjee. 2008. “ER and Oxidative Stresses Are Common Mediators of Apoptosis in Both Neurodegenerative and Non-Neurodegenerative Lysosomal Storage Disorders and Are Alleviated by Chemical Chaperones.” *Human Molecular Genetics* 17 (4):469–77. https://doi.org/10.1093/hmg/ddm324.

Woš, Marcin, Joanna Szczepanowska, Sławomir Pikuła, Anna Tylki-Szymańska, Krzysztof Zabłocki, and Joanna Bandorowicz-Pikuła. 2016. “Mitochondrial Dysfunction in Fibroblasts Derived from Patients with Niemann-Pick Type C Disease.” *Archives of Biochemistry and Biophysics* 593:50–59. https://doi.org/10.1016/j.abb.2016.02.012.

Yamanaka, Shoji, Mark D Johnsont, Alex Grinbergt, Heiner Westphalt, Jacqueline N Crawleyt, Masako Taniike, Kinuko Suzuki, and Richard L Proia. 1994. “Targeted Disruption of the Hexa Gene Results in Mice with Biochemical and Pathologic Features of Tay-Sachs Disease (Animal Model/GM2 Ganglioudosis/Homologous Recombination/Lysosomal Storage Disease).” *Medical Sciences* 91:9975–79. https://doi.org/10.1073/pnas.91.21.9975.

Yang, Zhifen, and Daniel J. Klionsky. 2010a. “Eaten Alive: A History of Macroautophagy.” *Nature Cell Biology*. https://doi.org/10.1038/ncb0910-814.

Yang, Zhifen, and Daniel J. Klionsky. 2010b. “Mammalian Autophagy: Core Molecular Machinery and Signaling Regulation.” *Current Opinion in Cell Biology*. https://doi.org/10.1016/j.ceb.2009.11.014.

Yoshida, H., T. Okada, K. Haze, H. Yanagi, T. Yura, M. Negishi, and K. Mori. 2000. “ATF6 Activated by Proteolysis Binds in the Presence of NF-Y (CBF) Directly to the Cis-Acting Element Responsible for the Mammalian Unfolded Protein Response.” *Molecular and Cellular Biology* 20 (18):6755–67. https://doi.org/10.1128/MCB.20.18.6755-6767.2000.

Yu, Li, Christina K. McPhee, Lixin Zheng, Gonzalo A. Mardones, Yueguang Rong, Junya Peng, Na Mi, et al. 2010. “Termination of Autophagy and Reformation of Lysosomes Regulated by MTOR.” *Nature* 465 (7300):942–46. https://doi.org/10.1038/nature09076.

Yu, Robert K., Yi-Tzang Tsai, Toshio Ariga, and Makoto Yanagisawa. 2011. "Structures, Biosynthesis, and Functions of Gangliosides-an Overview." *Journal of Oleo Science* 60 (10):537–44. https://doi.org/10.5650/jos.60.537.

Yuziuk, Jeffrey A., Carmen Bertoni, Tommaso Beccari, Aldo Orlacchio, Yan Yun Wu, Su Chen Li, and Yu Teh Li. 1998. "Specificity of Mouse G(M2) Activator Protein and β-N- Acetylhexosaminidases A and B. Similarities and Differences with Their Human Counterparts in the Catabolism of G(M2)." *Journal of Biological Chemistry* 273 (1):66–72. https://doi.org/10.1074/jbc.273.1.66.